UNIVERSITY OF LONDON

Imperial College of Science and Technology
Blackett Laboratory
Optics Section

PASSIVE MODE-LOCKING THEORY FOR CONVENTIONAL AND COLLIDING-PULSE LASERS

By

ROBERT DOLPH ETTINGER

Thesis submitted in part fulfillment of the requirements for the Ph.D. degree of the University of London, and the Diploma of Imperial College of Science and Technology.

APRIL 1986

A B S T R A C T

The thesis contributes to the theory of passive mode-locking, the technique by which ultrashort optical pulses are generated in lasers containing a saturable absorber. It contains extensive discussion of the conditions under which dye lasers produce extremely short pulses.

A study of the steady state pulses compares various analytic treatments with results of numerical simulation. Evolutions are followed from the perturbed stationary field solution but the ultimate pulse duration is shorter than the recovery times of the saturable absorber dye and the laser dye. The effects of limited bandwidth and of noise are covered.

The shortest pulses generated experimentally (= 10^{-13} s duration) use the colliding-pulse mode-locking technique (CPML) in which two trains of pulses propagate in opposite senses within a ring laser. The theory of the saturable absorber where the pulses collide is discussed. A two-way absorber theory is developed that overcomes previous approximations concerning the saturation grating that the standing-wave field produces. Formulae are given for a number of special cases.

The limitations of existing analyses of colliding-pulse mode-locking are discussed and the improved two-way absorber theory is used within a computer model of the CPML effect. Extensions to the model are considered.

T H I S

T H E S I S

I S D E D I C A T E D T O A L L T H E F A M I L Y

C O N T E N T S

Chapter 1

INTRODUCTION

1.1 Mode-locking

Instabilities in the output from lasers [1] were found as soon as the ruby laser was invented. Stability criteria still remain the subject of current research [2]. Noise provides a statistical character to the spiking phenomena in the solid state lasers: only by active means may the non-linear dynamics in these systems be made to produce well defined transient responses [3,4]. Even if noise is irrelevant, we note that there are many situations in nonlinear optics where the evolution is so complicated that the apparent contradiction of "deterministic chaos" occurs. No matter how finely we might adjust the initial conditions the same evolution will never be seen again.

Passive mode-locking is the technique that has allowed light to be assembled into a pulse only 1 cycle* long. In homogenously broadened lasers (usually dye as opposed to solid state systems but colour centre and semiconductor lasers too) the dynamics of this successful passive mode-locking embody the absolute reversal of optical chaos. The initial conditions, whether organised or noisy, always give way to a completely organised pulse. The ancestral distribution of electromagnetic radiation within the cavity unavoidably reshapes (self-organisation) into that pulse. This process requires hundreds of cavity transits.

We introduce passive mode-locking without immediately speaking of the modes which, in the frequency domain, get "locked". (The frequency domain turns out to make mode-locking theory less convenient than the time domain if many modes are involved). A continuously operating mode-locked

---

*We are referring to a far-infrared transient [5] generated from the mode-locked laser pulse. The shortest reported laser pulse [6] lasts 4 cycles in the visible.

laser (CW mode-locking) holds a "bouncing" pulse inside the cavity. Similar to a nonlinear optical soliton in a fibre, this special pulse is self-reproducing because the nonlinear influences upon it cancel out periodically. The period for passive mode-locking is very close to the small-signal cavity round trip time, because the nonlinear effects do not make much difference in a cavity that is mostly free space. However, the slight difference that can occur is important in order to understand fully a self-reproducing pulse. This effective temporal slip is one chosen by the complete nonlinear system.

Inside the cavity of a passively mode-locked dye laser there are two free-flowing dye jets placed at Brewster's angle. For simplicity we shall assume that the cavity is a ring with 100% reflecting mirrors except for the output mirror. If in some way unidirectional lasing is forced, then the output mirror transmits a fraction of the trapped pulse when it periodically completes a round trip in the cavity. The active jet is pumped by a CW laser (Ar^+ gas laser usually) and laser amplification must replenish the energy lost at the output mirror. By itself, amplifier saturation fixes the CW power of a single-frequency laser pumped above threshold. The additional passive dye jet for mode-locking is unpumped and therefore exhibits saturable absorption. The self-reproducing pulse covers a wide frequency bandwidth determined by the chemistry of the dye solutions or by the filtering properties of narrow band mirrors. Every round trip follows the same pattern: the special pulse transmitted by each jet is very different from the pulse that enters - but the correct pulse will reach the output mirror to continue the mode-locked pulse train and at the same time begin an IDENTICAL round trip.

The conditions for passive mode-locking involve the cavity transit time (T_{RT}) and the recovery time of the amplifying molecules (T_{1a}) even though the pulses are shorter than these times by a factor of order 10^4. There is feedback, upon entry of a pulse into the amplifier, from the time when a pulse saturated the amplifier on the previous transit. The

incomplete amplifier recovery involved here arises when $T_{RT} \approx T_{1a}$. If a rate equation model [7] is used instead of the self-reproducing pulse model, then to every $\xi = T_{RT}/T_{1a}$ there corresponds a pulse energy such that amplifier saturation and subsequent recovery settle so as to cancel out. In this model the absorber recovery is complete: there is no feedback via that route. Saturation is as a function of pulse energy (and not pulse shape) when the pulse duration is short compared with both amplifier and absorber recovery time. Before the model's introduction it had not been understood how short mode-locked pulses could exist without equally short absorber recovery time.

Quantitative pulse-width predictions are not possible in the rate equation model. Either the self-reproducing pulse theory introduced by Haus [8] or the use of computer simulation is necessary in order to get this information. The mathematical problems increase when, to treat the case of colliding-pulse mode-locking, we drop the assumption that the ring laser operation is unidirectional.

Finally in this introduction the modes will be discussed. The finite output coupling means that strictly the modes should be calculated in a volume of which the laser cavity is but a part. However, for high Q cavities the quasi-modes discussed in [9] behave like ideal confined modes. Ignoring higher order transverse modes, the travelling-wave longitudinal nodes of an empty ring (or the Fabry Perot modes of linear cavities) are separated in frequency by c/T_{RT}. Phase slip near the waist (where diffraction is important) of a Gaussian beam, and in the nonlinear media, both lead to complications that we leave aside entirely. The high Q ensures that the fields circulating inside an empty cavity change insignificantly from one round trip to the next. This is why the output pulse-repetition frequency matches the mode spacing above. The Fourier series expansion will express any periodic output as a sum over the discrete modes. It is well known that a "comb" of modes, locked to be in phase at $t = 0$, add to give a train of pulses whose widths decrease as more modes are excited. Without the nonlinear absorber, the

homogeneously broadened laser would ideally oscillate in the single mode which achieves threshold. On its inclusion, however, we obtain parametric amplification of the neighbouring modes through nonlinear coupling by the time dependent saturation. Thousands of modes finally oscillate with phases locked. The same description applies in the case of active mode-locking except that the modulation (of gain or loss) required to produce sidebands is externally generated.

The theory of mode-locking is extensively reviewed elsewhere [10] and a recent textbook by Haus [11] also introduces the most basic concepts. Within the present thesis we specialise to one area of this enormous field.

1.2 Recent Progress in Ultrashort Pulse Generation (1978-1985)

To complement the theoretical material of the remainder of the thesis, we outline below the recent technological advances. We concentrate on work carried out since 1977 and rely on the excellent review article by Bradley [12] for earlier background to the generation and measurement of picosecond pulses

At the start of our survey period, the shortest pulses were produced reliably by passively mode-locked dye lasers of the flashlamp pumped and continuous wave varieties. There were also suggestions that CW dye lasers synchronously pumped by actively mode-locked lasers had potential advantages (see below) but it is now known that the pulse-trains produced lack the stability associated with passive mode-locking.

The best results quoted by Bradley were obtained in two types of experiment. Figure 1 shows the passively mode-locked CW dye laser arrangement with a free-flowing gain jet and a 200μm contacted flow cell for the absorber dye. Subpicosecond pulses could be tuned from 598-615 nm by rotating the tuning prism. The alternative flashlamp pumped systems produced longer pulses but permitted peak powers to reach 25MW (as opposed to 1kW for CW laser pump). Apart from these dye systems, semiconductor diode mode-locking was in an early stage and mode-locking (by synchronous pumping) of colour centre lasers was already under development [13].

In the system of figure 1, the rhodamine6G-DODCI dye combination produced 0.3ps pulses : in that laser these particular dyes optimise the parameters needed for efficient mode-locking in passive mode-locking theory. However the tunability of passive mode-locking arises from the wide choice of saturable absorbers which, unlike those employed in Nd:Glass lasers, need not have a rapid recovery time. Thus, at the right concentration, cresyl violet absorber also produced sub-picosecond pulses [14]. It was established that

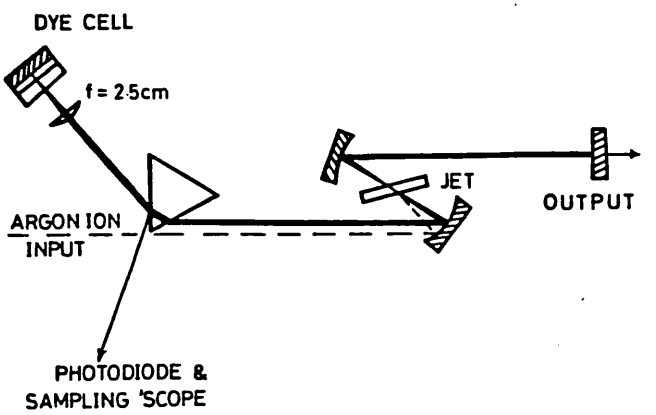

Passively mode-locked cw dye laser cavity configuration.

Figure 1 Conventional Mode-Locked Dye Laser [15]

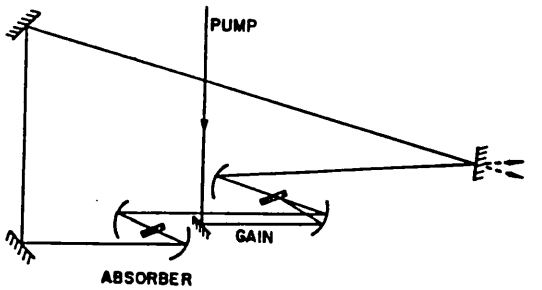

Schematic diagram of ring laser used for CPM. The focusing mirrors for the gain region have a 10-cm radius and those for the absorber have a 5-cm radius. Cavity roung-trip time was 10 nsec.

Figure 2 Colliding-Pulse Mode-Locked Dye Laser [19]

the autocorrelations showed no evidence of substructure in the pulses measured. Double jet-stream systems had not been optimised in this regard: this showed that use of a contacted absorber was beneficial.

Diels et al. [16] removed the intracavity prism (sacrificing experimental tunability) and relied on a "square" multilayer coating reflectance to prevent disorganised oscillation of modes outside the spectral range taken up by the 0.2ps mode-locked pulse. In this experiment both dyes were mixed in a single jet (instead of using a contacted absorber). As a result the mode-locking stability was very poor.

Mode-locking by synchronous pumping was turned to again because the absorber could be dispensed with. Second harmonic generation is most efficient for short pulses and therefore the doubled pulses (at 532nm) from an actively mode-locked CW Nd:YAG laser provided a more powerful pump than the Ar^+ laser. Sizer et al. [17] found that there was sufficient power left over, after pumping the slave cavity, to drive a pulsed regenerative amplifier which in turn synchronously pumped a chain of dye amplifiers. The shortest pulses that were produced by this technique were 0.5ps long [18].

Another leap was taken in 1981 when Fork, Greene and Shank produced 90fs pulses in a ring laser using the technique of colliding-pulse mode-locking, a special version of passive mode-locking [19]. The stability was as good as that of the pump Ar^+ laser even though a double jet-stream cavity was used. The result only happened when the distance between the two jets was close to one quarter of the ring perimeter, as shown in figure 2. In the colliding-pulse mode-locking technique (CPML) the absorber performs a very similar function to the contacted absorber in figure 1 (- the focussing mirrors also added around the absorber jet play the same role as the concentrating lens). The difference is that instead of facilitating a single stable pulse-train the ring system synchronises two counterpropagating trains of pulses that collide inside the absorber. When the jets are

correctly positioned this is the steady state because the total energy loss in saturating the absorber is minimised. A specially thin absorber jet (10 μm) was used in the experiment.

CPML was demonstrated as well [19] using a linear cavity in which the pair of jet-streams was precisely placed to put the absorber jet half way between the cavity mirrors. Although pulsewidths were not as short as in the ring, the performance was better than had been obtained from the contacted configuration described before.

It is certainly the case that (symmetric and identical) counter-propagating pulses only make a pure standing wave everywhere in a cell or jet at the stage when their peaks superimpose perfectly. At this instant the edges of the two pulses are outside the jet. When the stage arrives when the "mirror-image" trailing edges are exiting from the two-way absorber it is not possible to achieve the ideal standing wave. Fork et al. therefore believed that, although the total energy loss would go up, the two-way absorber in CPML performed pulse shortening even when the pulse was already compressed towards the absorber jet thickness. The mechanism was the enhancement of the peaks relative to the trailing edges occuring since the latter were exposed to the greater loss in the spatially inhomogeneous absorber, (a saturation-induced grating) only "resonant" for pure standing-wave fields. There was speculation that phase conjugation effects would come into a CPML explanation along these lines.

The generation of two output pulse-trains from the ring laser is a disadvantage. Methods exist to convert a ring laser into a travelling wave system [20] but then the benefits of colliding pulses would be lost. The solution to this problem is to use a linear cavity with the contacted absorber replaced by an antiresonant ring [21,22] that encloses the absorber jet, as carried out in the case of a Nd:Glass laser by Buchert et al. [23].

Dye lasers ceased to be the only reliable source of ultrashort pulses when progress was reported in extracavity compression of longer pulses from mode-locked solid state

lasers. This was achieved by Johnson et al. [24,25] who generated 0.41ps pulses at 532nm. However the significance of "ultrashort" had already changed because the CPML dye laser pulses had been compressed already to 30fs [26]. In the case of synchronously pumped mode-locked dye lasers, extracavity compression also solved stability problems and Nikolaus et al. [27] reported exceptionally clean pulse shapes.

The fibre compression results suggested that similar processes could take place inside a laser cavity. Chirp had already been observed in the 70fs pulses generated from a synchronously pumped dye laser with saturable absorber mixed into the gain jet [28] and in the pulses from colliding-pulse systems [29,30]. Compensating for a downchirp by use of the positive (normal) group velocity dispersion of an intracavity prism, Dietel et al. [31] found that there was an optimum glass thickness for the colliding-pulse cavity. The chirp was attributed to self-phase modulation in the saturable absorber. However, the most favourable regime for mode-locking occurs when the saturable absorber is strongly saturated by the leading edge of the pulse [32]: the remaining self-phase modulation [33] due to the intensity dependent refractive index of the solvent used in the jets will cause up-chirp instead of down-chirp.

More effective intracavity pulse compression is carried out by soliton pulse shaping [34]. The up-chirp effect is compensated for by anomalous group velocity dispersion, just as in the colour-centre soliton laser [35] based on an extracavity fibre. The technique has produced 27fs pulses directly from a colliding-pulse mode-locked laser incorporating an arrangement of prisms that provides adjustable negative dispersion [36,37]. Very recently high-order soliton-like pulses were directly generated by a similar system [38]: the pulses performed a characteristic high-order soliton evolution with a period of 2400 cavity round trips and the change could be seen in the autocorrelations and spectra taken "stroboscopically" using a sampler averager. High-order solitons may allow enhanced

intracavity compression. (Already the shortest pulses produced using extracavity fibre compression are only 4 optical cycles long [6]).

The special benefit of colliding-pulse absorber saturation still remains important in the femtosecond passively mode-locked lasers that utilise soliton shaping. The extension to synchronously pumped colliding-pulse ring lasers has also been accomplished [39]. Clearly the motivation to develop a model of colliding pulses is now very strong indeed.

CHAPTER 2

PASSIVE MODE-LOCKING THEORY

2.1 Self-reproducing laser pulses

Mode-locking theory was first studied using a frequency domain approach. The aim was to show how the mutual phases of a small number of oscillating modes attain a fixed relationship that results in pulsed output from the laser. However, as explained in the introduction, the temporal approach to mode-locking provides the more natural description - particularly when the number of modes concerned is large.

Cutler [40] laid the foundations of the time-domain approach to active mode-locking [3] some years before the laser, let alone laser mode-locking, was thought of! The context was a microwave device known as a regenerative pulse generator. The circuit consisted of a feedback loop around which the pulse re-circulates indefinitely, at each traversal giving response at the output terminals. The re-circulating pulse is not degraded if, in addition to a loop gain of unity at its peak, the effects of noise are counteracted. The passive "expandor" plays the required role in the loop by providing less attenuation for a high field amplitude than a low one. A self-reproducing pulse is generated, resulting from the competition between sharpening in the expandor and broadening in a filter. The filter represents the limited frequency response of the circuit that prevents an evolving pulse from indefinite shortening.

Laser mode-locking has recently been reviewed by New [10]. From the enormous field that has developed, only the passively mode-locked CW lasers are our concern here. The dye laser, in particular, is able to operate continuously (i.e. without Q-switching) because the system has an amplifier recovery time (T_{1a}) commensurate with a single cavity transit period (T_{CAV}), therefore damping out relaxation oscillations. We describe this type of behaviour as "soft" because when short laser pulses saturate the population inversion the recovery within a single round trip is sufficient for every pulse to control its own gain modulation.

In the dye laser a small number of dye molecules must be pumped to the upper laser level, owing to a large cross section for stimulated emission from the upper level compared with the reabsorption from the ground state (happening at shorter wavelengths). In the "soft" system this small population readily undergoes deep saturation and a strong recovery all in the space of one transit. The theory of passive mode-locking must take this into account, as well as the absorber saturation. The aim is to predict the self-reproducing pulse.

Laser systems with "hard" saturation ($T_{1a} >> T_{CAV}$) are unreliable at producing passively mode-locked pulses because the random initial conditions control the outcome of any shot (The stored energy, proportional to T_{1a}, is released in a time less than T_{1a} as a giant pulse: mode-locking occurs "underneath" this giant pulse envelope). Active mode-locking is attractive in the solid state lasers because it overcomes the stability problems otherwise associated with a "hard" laser system. Instead of relying on survival of a single peak from the intra-cavity flux acted upon by the passive saturable absorber, the stable active modulation is there to provide the (round trip) synchronised "shutter" from the outset.

In the case of dye lasers, active modulation is produced by pumping using a mode-locked laser. Recent research [10] on mode-locking by synchronous pumping has shown that the self-reproducing pulses are rather different to those in "hard" laser systems. In particular, the mismatch between master and slave laser transit times is very important in determining pulse widths. However, no such problem applies in the case of passive mode-locking in a dye laser which is very much closer to Cutler's early device where the self-reproducing pulse concept originated.

Cutler's device was explained in language very similar to the modern concept [41] of "pulse shortening rate", which we shall discuss later on. Note, however, that the pulse stability in the microwave device was brought about by an automatic gain control for the nonlinear element in the

circuit and not from the "soft" saturation dynamics as in the optics case.

2.2 The "bouncing ball" model [7]

The "bouncing ball" model applies to the pulse re-circulating in a passively mode-locked dye laser if the pulse length is already short in comparison with the recovery times of both absorber and amplifier, but not so short as to be affected by the filter. It is a model based simply on energy conservation and this section explains how zones of stability (in a parameter space representing experimental adjustments) for the ultrashort pulses may be deduced [7].

The equations describing the saturable amplification are derived in Appendix B. The population inversion density and the laser intensity (normalised for the amplifier) obey the following coupled rate equations:

$$\frac{\partial n_a}{\partial t} = \frac{n_{ao} - n_a}{T_{1a}} - n_a \lambda_a \qquad (1)$$

$$\frac{\partial \lambda_a}{\partial z} + \frac{1}{c}\frac{\partial \lambda_a}{\partial t} = n_a \sigma \lambda_a \qquad (2)$$

In the "bouncing ball" model we neglect the first term on the right hand side of equation (1) during the ultrashort pulse (the SLOW AMPLIFIER approximation) and neglect the second (saturation) term during the remaining time ($\lambda_a \approx 0$) in order to allow for gain recovery. The assumption is that the recovery term plays no role on the right hand side of (1) on a timescale short compared with T_{1a}. Since in a dye laser $T_{1a} > 1ns$ and $T_{pulse} < 1ps$ this is an excellent approximation.

The same argument will be used (shortly) for the saturable absorber, making it clear that a fast absorber is not necessary in passively mode-locked dye lasers. Note, however, that $T_{1b} << T_{RT}$ so that there is full absorber recovery between round trips (in summary: $T_{pulse} << T_{1b} < T_{1a} \approx T_{RT}$).

In the local time co-ordinates $x = z$ and $\tau = t - z/c$, the governing equations equations during the ultrashort pulse are:

$$\left.\begin{aligned} \frac{\partial n_a}{\partial \tau} &= -n_a \lambda_a \\ \frac{\partial \lambda_a}{\partial x} &= n_a \sigma_a \lambda_a \end{aligned}\right\} \quad x\text{: pulse being amplified} \qquad (1a), (2a)$$

and during the recovery period:

$$\left.\begin{aligned} \frac{\partial n_a}{\partial \tau} &= \frac{n_{ao} - n_a}{T_{1a}} \\ \frac{\partial \lambda_a}{\partial x} &= 0 \end{aligned}\right\} \quad x: \text{ amplifier recovering} \qquad (1b), (2b)$$

The exact solution of the coupled equations (1a) and (2a) will be quoted in Chapter 2; it is only the growth in energy of the pulse which is required here. Define the normalised energy "dose",

$$j = \int_{-\infty}^{\infty} \lambda_a d\tau$$

In terms of j, the slow amplifier performs the operation

$$j_{out} = \ln \left\{ 1 + e^{n_{ao}\sigma_a l} \left[e^{j_{in}} - 1 \right] \right\} \qquad (3)$$

where l is the amplifier length and j_{out} and j_{in} are the values of j at the output and input respectively.

The proof of (3) is given implicitly by several authors [42-46] and we shall give a derivation towards the end of this section only in order to make more explicit the unique characteristics of "slow" absorption and amplification.

Introducing the gain coefficient (Appendix B) we write (3) in the abbreviated form

$$j_{out} = \ln \left\{ 1 + e^{A_u} \left[e^{j_{in}} - 1 \right] \right\} \qquad (4a)$$

where the factor of e^{A_u} is also known as α_u. (The u reminds us that the coefficient or factor containing n_{ao} is for the unsaturated gain).

The slow saturable absorber obeys a similar law

$$sj_{out} = \ln\left\{1 + e^{-B_u}\left[e^{sj_{in}} - 1\right]\right\} \qquad (5)$$

where $sj = \int_{-\infty}^{\infty} \lambda_b d\tau$ is the absorber "dose" and $e^{-B_u} = \beta_u$.

In the "bouncing ball" model the initial gain is not the full amount A_u (= $n_{ao}\sigma l$) but the incompletely recovered coefficient

$$A_L = \int_o^l n_a^{INITIAL}(x)\ \sigma_a\ dx$$

which means that a more general amplifier law (see section 2.3) replaces equation (4a), namely:

$$j_{out} = \ln\left\{1 + e^{A_L}\left[e^{j_{in}} - 1\right]\right\} \qquad (4b)$$

By integrating the pure recovery equation (1b) for the amplifier population we may write down a gain "feedback" condition covering the period from the end of saturation by the energy j until just before the next saturation a round trip later. Specifically,

$$A_L = \Xi\, A_T + (1 - \Xi)A_u \qquad (6)$$

where $\Xi = \exp(-T_{RT} / T_{1a})$ has to be non-zero because incomplete amplifier recovery is essential for stability: this is the sign of a "soft" nonlinearity for timescales that exceed T_{RT}.

Experimental details might lead to complications in the equations assembled above. For example, unless the cavity geometry is an idealized unidirectional ring, the location of the nonlinear elements in the laser cavity (Fabry Perot) is also important. The amplifier might be placed away from the centre of the cavity, in which case unequal recovery

parameters Ξ must be allowed in two parts of the round trip double saturation cycle. Absorber recovery is so rapid that the same effect only matters when the absorber is close to a mirror; the more important case is when there is no gap whatsoever and the two-way slow absorber theory (chapter 4) is needed. Colliding pulse mode-locking exhibits the same dependence on absorber jet positioning that the Fabry Perot has upon absorber cell contacting.

An approximation that applies when the changes to the pulse and to the saturable elements are small is:

$$A_T = A_L \, e^{-j_{in}} \tag{7a}$$

$$B_T = B_L \, e^{-sj_{in}} \tag{7b}$$

However, we can obtain the exact results by writing (4) and (5) in differential form

$$dj_{out} = e^{A_u} \, e^{j_{in} - j_{out}} \, dj_{in}$$

$$dj_{out} = e^{-B_u} \, e^{s(j_{in} - j_{out})} \, dj_{in}$$

from which the true coefficients are seen to be as follows

$$A_T = A_L - (j_{out} - j_{in}) \tag{8a}$$

$$B_T = B_L - s(j_{out} - j_{in}) \tag{8b}$$

Equations (8) can be regarded as energy conservation laws. (Equations (7) do apply exactly in a composite cavity model in which A and B are distributed coefficients per unit length, but the discrete model is normally closer to experiment.)

The proof of (3) makes use of the energy conservation condition. Integrating the equality $\sigma_a \partial n_a/\partial \tau + \partial \lambda_a/\partial x = 0$ we obtain an equation for the variation of j with x,

$dj/dx = \sigma_a(n_{aL} - n_{aT})$. We obtain (3) if we use $n_{aL} = n_{ao}$ and $n_{aT} = n_{ao}e^{-j}$ and integrate over a thickness 1.

As an example of the "bouncing ball" treatment of a mode-locked ring laser, values of $s = 5$, $\alpha_u = 25$, $\beta_u = 0.2$, $\gamma = 0.4$ were taken together with an amplifier incomplete recovery $\Xi_a = \exp(-0.8)$. An effectively complete absorber recovery was used: $\Xi_b = \exp(-4)$. The result, when an initial starting energy was taken through sequential amplification, absorption and linear loss (γ) followed by the same processes on the next round trips taking incomplete recovery into account, was convergence to a stable cycle. With the parameter values above, the prediction was:

AMPLIFIER	$-\ \alpha_L = 7.4$	$j_{in} = .787$	$\alpha_T = 1.6$
ABSORBER	$-\ \beta_L = 0.21$	$j_{in} = 2.3$	$\beta_T = 0.999$
LINEAR LOSS	$-$	$j_{in} = 2,\ j_{out} = 0.787$	

The point is that as well as the stable pulse energy being repeated, the recovery of α_T and β_T reproduces the same leading edge conditions for the recirculating pulse. This is the "bouncing ball"!

Once the energy of an evolving pulse is stable, the pulse shape may still change. The study of the effect requires numerical simulation of the pulse evolution, as outlined in the next section. However, it is well known in practice that the pulse compression rate (the term "pulse compression velocity" is used in [41]) is only sufficiently large to allow ultrashort pulses to be achieved if there is loss on the leading and trailing edges of the pulse. In the end the pulse will become so short that the rate equations (1) and (2) break down.

In (1) and (2) the limited bandwidth of the amplifying (absorbing) molecules is entirely ignored. This is valid as long as collisions between dye and solvent molecules are so frequent that the microscopic polarisations are "thermalised" much more quickly than the photon flux is changing.

Statistically this means that the recovery rate (T_2^{-1}) of the off-diagonal density matrix element must be large, as assumed in Appendix B. There are no steady state pulses in numerical simulations unless bandwidth limitation is also put in. There is, however, a correlation between rapid unrestrained pulse compression and finding short stable pulses when the filter limits the process.

The regime where $g_L \equiv \alpha_L \beta_L \gamma$ and $g_T \equiv \alpha_T \beta_T \gamma$ are simultaneously less than one (i.e. where there is net loss on both the leading and trailing edges of the pulse) is called the static pulse compression regime. To find the boundaries of this regime one simply searches for the values of α_L which (keeping β_L and γ as above) result in $\alpha_L \beta_L \gamma = 1$ or $\alpha_T \beta_T \gamma = 1$. A particular α_L value may be obtained either by adjusting the cavity length (Ξ_a, Ξ_b) or the laser pumping (A_u) and the two boundaries are therefore lines of constant pulse energy in this parameter space. For the parameter values used above, the extreme input energies at the amplifier are given by $0.293 < j_{in} < 1.269$ so that the chosen parameters should lead to strong compression of the pulse with energy 0.787. What actually happens in the presence of bandwidth limitation is shown in the next section. From the numbers already given, the net gain factors must be $g_L \approx 0.6$ and $g_T \approx 0.65$ whilst in the rate equation regime. In this case the peak (static in local time) <u>has</u> to sharpen if the pulse energy remains conserved.

2.3 Computer model including bandwidth limitation

This section describes the numerical method used to simulate passive mode-locking. As well as demonstrating the features predicted by the "bouncing ball" model, simulation reveals to us how a steady state is attained when bandwidth limitation is included. The remaining sections in this chapter contain the results of numerical evolutions carried out by the method described here.

The entire cavity is represented by a mesh of equally spaced samples of the electric field. Only a small fraction of these meshpoints ultimately convey the ultrashort pulse - elsewhere the flux is close to zero. Although this is inefficient (in computing terms), the advantage is that evolutions may be started from a smooth initial disturbance so that the onset of mode-locking can be traced before the "bouncing ball" stage ($T_{PULSE} << T_{1a}, T_{1b}$). Since we do not assume that an ultrashort pulse will be produced, both the assumptions and the quantitative predictions of analytic theories are tested.

In the computer program used to study the evolution in time of the mode-locked emission, the entire gain at the amplifier is applied in one step. Hence the physical thickness of the amplifying jet is not one of the inputs to the program. The same applies in the case of the absorber, which may be treated in the equivalent 'lumped' manner.

We shall now integrate over the amplifying medium rate equation in order to obtain the results used for the computer simulation. These results are amenable to a modified Runge-Kutta numerical approximation scheme.

The amplifier is described locally by n_a, the population-difference density, obeying

$$\frac{\partial n_a}{\partial t} = \frac{n_u}{T_1} - \frac{n_a}{T_1}(1 + \lambda) \qquad (1)$$

where n_u is the long-time steady state value of $n_a(z)$ which is achieved by the pumping mechanism in the absence of any laser action ($\lambda = 0$). The normalised flux λ has an interpretation as photons per molecule and it follows that stimulated emission and absorption enhance the total decay rate to $T_1^{-1}(1 + \lambda)$ compared with the purely spontaneous rate, T_1^{-1}.

The action of the lumped amplifier on the flux at the input ($z = 0$) is (after propagating z)

$$\lambda(z,t) = \lambda(0, t - \frac{z}{c})\ e^{A(z,t)}$$

where $A(z,t)$ is referred to as a gain coefficient. The total gain in the amplifier of thickness ξ will be abbreviated $A(\xi,t) = A(t)$.

From Beer's law an expression for $A(z,t)$ which links up with (1) may be written down at once, namely

$$A(z,t) = \sigma \int_0^z n(\xi', t - \frac{z - \xi'}{c})\ d\xi'$$

where σ is, by definition, the gain cross section. An integrated version of (1) is obtained by applying the operation $\sigma \int_0^{\xi} d\xi'$ to both sides:

$$\frac{\partial}{\partial t} A(t) = \frac{A_0}{T_1} - \frac{A(t)}{T_1} - \frac{\sigma}{T_1} \int_0^{\xi} n(z, t - \frac{z}{c}) \lambda(z,t)\, dz \qquad (2)$$

where $A_0 = \sigma n_u \xi$.

The integrand is the same as the 'lumped' quantity:

$$\lambda(0, t - \frac{z}{c}) \frac{\partial}{\partial z} (e^{A(z,t)}) = \sigma n(z, t - \frac{z}{c})\, e^{A(z,t)}\, \lambda(0, t - \frac{z}{c})$$

$$= \sigma n(z, t - \frac{z}{c})\, \lambda(z,t)$$

Therefore:

$$\frac{\partial}{\partial t} A(t) = \frac{A_0}{T_1} - \frac{A(t)}{T_1} - \frac{1}{T_1} \lambda(0,t) \int_0^{\xi} \frac{\partial}{\partial z} (e^{A(z,t)})\, dz$$

$$= \frac{A_0}{T_1} - \frac{A(t)}{T_1} - \frac{1}{T_1} \lambda(0,t)\, [e^{A(t)} - 1] \qquad (3)$$

The Runge-Kutta method was used to evaluate this result* for A(t). In terms of the mesh step δt the fourth-order calculation of $A(t + \delta t)$ is as follows [90]:

---

*Yasa and Teschke ([47],1975) employ a formula similar to (3) in work on synchronous pumping.

$$C1 = \tilde{R}(\, A(t),\, \lambda(0,t)) \;.\; \delta t$$

$$C2 = \tilde{R}(\, A(t) + \tfrac{1}{2}\, C1,\, \lambda(0,t + \tfrac{\delta t}{2})) \;.\; \delta t$$

$$C3 = \tilde{R}(\, A(t) + \tfrac{1}{2}\, C2,\, \lambda(0,t + \tfrac{\delta t}{2})) \;.\; \delta t$$

$$C4 = \tilde{R}(\, A(t) + C3,\, \lambda(0,t + \delta t)) \;.\; \delta t$$

We used $\tilde{R}$ to denote the right hand side of (3) and it is now the average of C2, C3 and $\frac{C1 + C4}{2}$ that is used to step $A(t + \delta t) - A(t)$. In this form, however, this Runge-Kutta method can not be used because the input field $\lambda(o)$ is defined only at the meshpoints: if known at t and $t + \delta t$, then $\lambda(0,t + \frac{\delta t}{2})$ is absent. In order to calculate C2 and C3, however, it was decided to use linear interpolation to provide an estimate of the required flux value. Results show improved convergence, when using this method, over results obtained using $\tilde{R}(\lambda(0,t))$ everywhere.

The evolution of a flux pattern known initially at all meshpoints (typically M = 1024) of a ring cavity is now simple to follow. For each meshpoint the flux value is multiplied by $e^{A(t)}e^{-B(t)}e^{-\Gamma}$ to represent passage through the saturable gain, saturable absorption and constant loss of the cavity components. Before proceeding to the next meshpoint the saturation of A(t) is evaluated as described above, and that of B(t) follows from a result analagous to (3):

$$\frac{\partial}{\partial t} B(t) = \frac{1}{T_{1b}} (B_0 - B + s\lambda(0,t)[e^{-B(t)} - 1])$$

where T_{1b} is now the lifetime of the absorber and the factor $s = \sigma_b/\sigma_a$ allows for the fact that λ was defined in terms of the amplification cross-section σ_a rather than that of the absorber. The process is repeated for many circuits of the whole-cavity mesh.

Steady state pulses do not exist in the absence of a filter. The filter algorithm, based on a model Fabry-Perot etalon was placed after the linear loss in the simulations. It performs the following mathematical function:

$$E(t) \leftarrow R\,E(t - \delta t) + TE(t)$$

The phase delay in the filter has been assumed equal to the mesh spacing used in the program (etalon thickness $\delta t/2$) and the optical carrier frequency coincides with an Airy transmission maximum so that R is real. Notice that $E(t - \delta t)$ is the previous OUTPUT field from the etalon as set by the preceding application of this reassignment rule. Since the transmission ($T = 1 - R$) of the etalon is therefore included implicitly it is only R which multiplies this filter memory term. Whilst phase information is completely ignored when stepping the rate-equations for A(t) and B(t) - these contain $\lambda = |E|^2$ driving terms - it is essential to the correct operation of the filter. With E(t) replacing $\lambda(t)$ for this reason, the amplitude gains $e^{A(t)/2}e^{-B(t)/2}e^{-\Gamma/2}$ were used for the calculations described above. One advantage of treating fields directly was that a complex random number might be added to the fields upon every step to simulate incoherent noise (possibly arising from spontaneous emission).

Note that the filter removes energy from a rapidly varying pulse by reflecting the portion that is not transmitted. In a two-level medium with finite bandwidth, however, the energy 'loss' is simply associated in the frequency domain with reduced utilisation of the inversion by off-resonant stimulating photons: the idea of reflection has then no place. We deliberately avoid the complications (saturation) of that nonlinear filter by using the separate Fabry-Perot. It is interesting to note, however, that finite absorber bandwidth also contributes an opposing energy 'gain' so that the overall behaviour would be of some interest.

10 ns is a typical cavity round-trip time in a ring dye laser. Therefore in order to resolve well a 1 ps optical pulse the number of meshpoints in the whole cavity must be about 5×10^4. This type of accuracy is impractical and therefore we restrict the number of points to 1024 so that our model will only be capable of making qualitative predictions. By specifying a filter memory time of about 5 meshpoints the pulse was prevented from narrowing below, typically, 20 meshpoints. Mode-locked pulses from the cw dye laser were recognised [48] early on to have durations far shorter than the saturable absorber lifetime (300 ps in the case of the dye DODCI). We mentioned this in connection with the compression zone theory of New [49]. For the numerical simulation it was decided to compress slightly the 'space' between the T_{1b} value and the expected pulsewidths in meshpoints. For example, the settings

$$m = 1024 \qquad t = \frac{T_{1b}}{T_{1a}} = 0.2 \qquad \xi = \frac{T_{CAV}}{T_{1a}} = 1.3$$

were often used, meaning that $T_{CAV} = 1024$, $T_{1a} = 788$ and $T_{1b} = 158$ meshpoints.

Confidence in the model was enhanced when the filter strength was varied: behaviour was always unchanged except for the expected scaling. The filter memory time is controlled in the program by the transmission of the Fabry Perot etalon.

2.4 Computed behaviour

Figure 1 shows the evolution of the intra-cavity flux over twenty five transits, in a simulation begun from a constant flux (defined by the unstable equilibrium solution to the model equations with time derivatives set to zero) with a small added sinusoidal perturbation which grows exponentially in the first stages of mode-locking. The horizontal coordinate is local time: the observer is at the input side of the amplifier. After the initial growth (which agrees with the perturbative description of New and Rea [50]) saturates, the next stage where we can simplify the analysis comes once a single pulse short compared with T_{1a} and T_{1b} circulates in the laser. The slow absorber and slow amplifier approximations made in section 2.2 are then valid, until the filter finally limits the indefinite pulse compression of the "bouncing ball" theory.

The limit to the pulse compression when the filter was excluded from the computer model was found only to arise from the coarseness of the numerical mesh. The compression occurs without the pulse slipping in local time and is known as static pulse compression. It was verified that the net gain factors on the edges of the pulse were less than unity and that they were the same all through the later evolution. The energy in the pulse also became stable. This is what the "bouncing ball" model predicted.

The most interesting information was obtained when the filter was made effective. Instead of indefinite compression, the pulse width stabilised. At the same time the gain factors and pulse energy settled at stable values different from those earlier on. This indicated that a self-reproducing pulse was forming.

In figure 2 we measure the logarithm of the minimum flux between the filter-limited pulses on every round trip. The computational cost of obtaining a true self-reproducing flux profile is high because the "trough" continues to deepen long after the pulse compression ceases. The evolution was

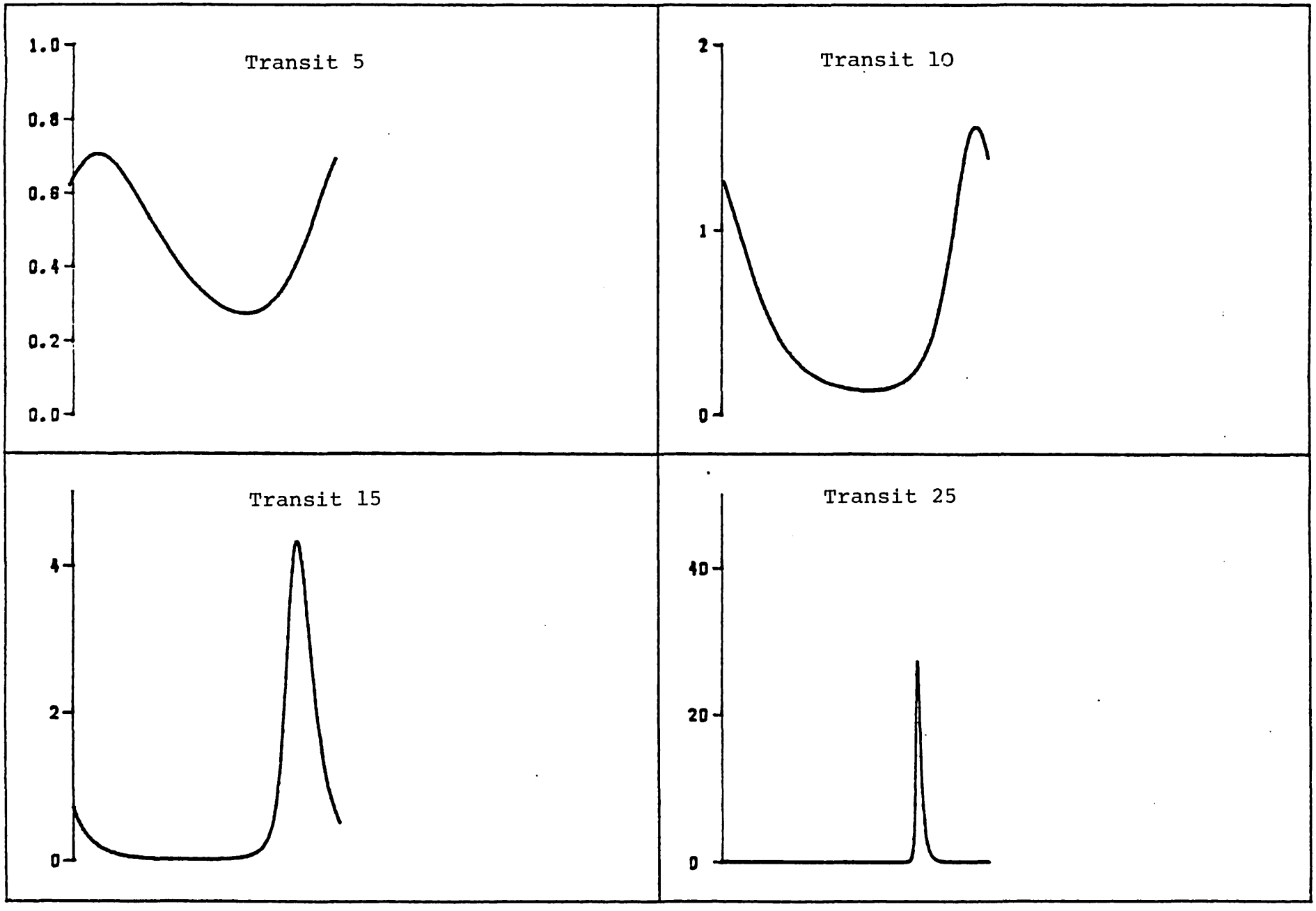

FIGURE 1 STATIC COMPRESSION - no filter.

followed to completion in this particular example - 140 round trips were required. This state would not be reached in practice in the presence of noise, when the (smoothed) pattern becomes stable much earlier.

For the same run as in figure 2, the pulse energy is plotted in figure 3 to show how large a drop in energy is caused by the filter. This also accounts for the changes in net gains on the leading and trailing edges of the pulse. The change is as important whatever the strength of the filter. Only the timescales of the whole evolution and of the pulse change; not the energy balance. We take this up in section 2.6.

When the pulse shortens to the point where the filter starts to have an effect, the pulse starts to drift in local time. This observation leads us to consider how the steady state pulse is determined by the filter in the computer model: drift in local time must play a role.

Haus' model [8] of the stationary state achieved in passive mode-locking with a slow saturable absorber takes the filter into account. The main result (see section 2.6) states:

$$(1) \quad \tau_p = \frac{\tau_{FWHM}}{1.76} = \left(\frac{4}{s}\right) t_F \frac{/\Gamma}{j/B_L}$$

Here τ_{FWHM} is the width of the intensity formula $\mathrm{sech}^2(t/\tau_p)$ and $B_L = -\ln\beta_u$ and $\Gamma = -\ln\gamma$ mean the same as in section 2.2. The main conclusion is simply that the pulses are shorter (relative to t_F) when absorber saturation sj is big.

The meaning of t_F must be considered. In the present computer model the etalon, implemented in the time domain, operates on the discrete mesh of field values to provide a dispersive effect. The theoretical approach used by Haus (introduced in the next two sections) augments the (intensity) loss coefficient $\Gamma = -\ln\gamma$ by an amount $\Gamma t_F^2 (\omega - \omega_0)^2$ in the frequency domain or $\Gamma t_F^2 d^2/dt^2$ in the time domain. It is only possible to use equation (1) when these responses are an adequate description of the filter used. As the

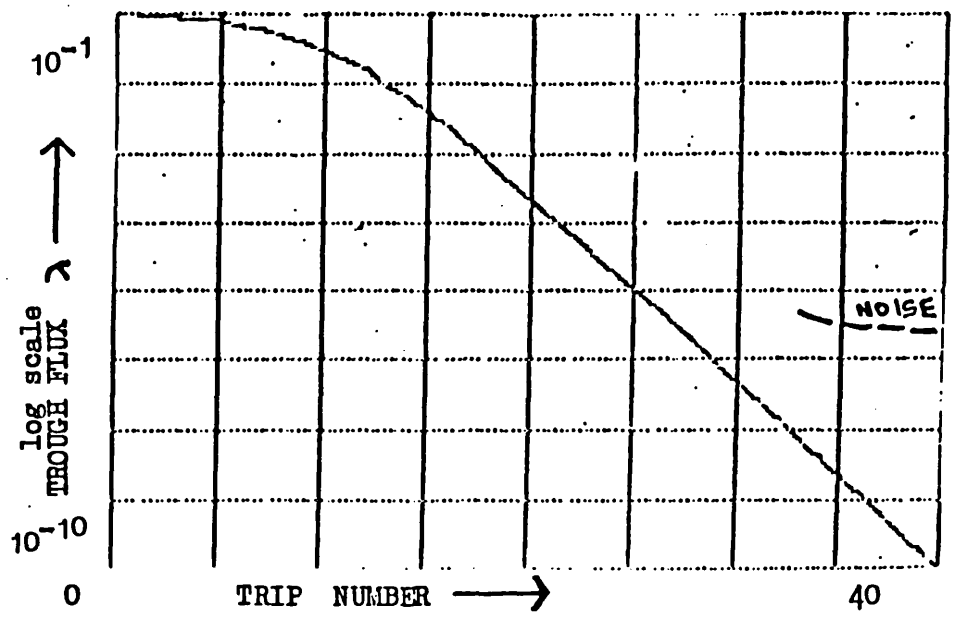

FIGURE 2 THE EVOLUTION OF THE MINIMUM FLUX

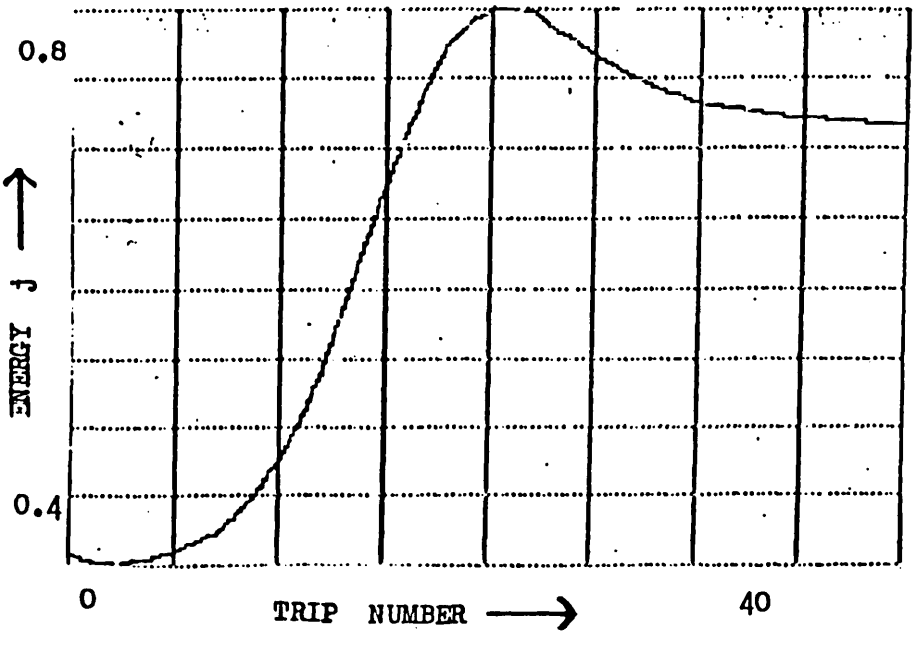

FIGURE 3 PULSE ENERGY EVOLUTION

etalon thickness (half t_M the mesh spacing) in the program is reduced to zero the required transmittance (TRANS) becomes small for a given filter strength. We assume that this limit applies, in which case Haus' filter description holds where $\Gamma t_F = t_M/\text{TRANS}$. In the simulations TRANS = 0.181 so $t_F/t_M \approx 5$. Note that the computer program measures τ_{FWHM} to the nearest integer.

Despite the fact that (1) may be derived only under severe approximations, the literature contains no test of the prediction for real operating parameters. Our simulations produced a stable pulsewidth τ_{FWHM} of 19 meshpoints. On the basis of (1), then, j should be ≈ 0.3. This is not far outside the results of the simulation which gave $j_{in} = 0.58$, 2.0 and 1.7 at the three measuring locations. All energies are lower than in section 2.2 because of an extra energy loss from bandwidth limitation.

In the next sections it will become clear how equation (1) is connected with the drift of the pulse. Then in section 2.8 we will study the system in a way that is more applicable to the Fabry Perot filter actually used in the simulations.

2.5 Haus' parabolic g(j) theory of slow-absorber mode-locking.

It must be stressed that the "bouncing ball" theory discussed earlier is of no help in predicting the pulse-widths a particular amount of bandwidth limitation produces. This problem was first overcome by Haus, as described below.

Haus included the competing effects of the gain dynamics and a generalised filter term in the defining equation for a steady state pulse:

$$\left[\ G(t) - \delta T\ d/dt + \Gamma t_F^2\ d^2/dt^2\ \right]\ V(t) \ = \ 0$$

The middle term in this equation removes the slip from the small modifications made to a pulse by the other two terms on every round trip. The equation states that the field V(t) reproduces exactly after a round trip. A solution consists of a function V(t) and an "eigenvalue" δT. The change to the pulse from each term must be small to justify the use of V(t) and its derivatives instead of several functions, one for each place in the cavity. The filter is represented by the $\Gamma t_F^2\ d^2/dt^2$ temporal spreading operator, the equivalent of a spatial diffusion operator. The filter term shows there to be a characteristic diffusion time $t_F' = /\Gamma\ t_F$ depending on the amount of linear loss Γ and the actual filter time t_F. The possibility of group delay in the filter is not relevant because it would only lead to a d/dt term, which has the same effect as a redefined slip eigenvalue.

In Haus' equation discussed above, as in our numerical calculations, the (limited) bandwidth potentially available enters solely via the curvature at the centre of the frequency-domain filter response. This applies to present dye lasers because the rate of static pulse compression is only sufficient to generate pulses which utilise a small proportion of the CW lasing bandwidth. (Frequency tuning of picosecond pulses - by changing absorber dyes - is feasible

for this very reason.) Stix and Ippen [41] quantified the pulse compression rate, showing that an added filter provides a cancelling pulse broadening rate in the time-domain. This means that the solution for the steady state pulse should be "elastic", making it always possible to obtain shorter pulses by increasing the effectiveness of the "bouncing ball" shortening or by providing extra bandwidth.

We finally explain the essential feature of Haus' theory [8,51] which reduces the problem of solving the equation above to simple algebra. The "bouncing ball" physics is simplified so as to represent saturation by a parabolic law:

$$G(U) = x + \sqrt{q}\, yU - \frac{1}{2} qU^2$$

where the variables $U(t) = \int_0^\infty |V|^2 \, dt$ and constants x, y and q will be related to the physical parameters in the next section, after the consequences of the parabolic assumption have been explored.

It is remarkable that without any further details being needed one finds the sech^2 intensity solution for the model. The solution of Haus' equation is:

$$V(t) = \sqrt{\frac{z^2}{8\, t_F' \sqrt{q}}} \; \text{sech} \left(\frac{1}{4} z \, \frac{t}{t_F'} \right)$$

where z is the larger root of the quadratic equation $-3/8\ z^2 + yz + 2x = 0$. The solution may be verified by using the definition of G(U) to obtain G(t) for substitution in the steady state pulse equation. The associated eigenvalue is:

$$\delta T = (z - 2y)\, t_F'$$

Even though we have postponed much of the detail of this theory (for example the definition of x, y and q) we may draw the following conclusions: first, the "elasticity" has appeared in terms of the combination z/t_F' for the pulse-width; secondly, the pulse-shape has become fixed (sech^2) and thirdly, the normalised energy [$U(t=\infty) = z/\sqrt{q}$] and the pulse-width are determined by the same derived parameter z.

2.6 Discussion in terms of "bouncing ball" model with extra energy loss in the filter

The equation solved in the last section shows that the parameters of the steady-state ($sech^2$) pulse satisfy a quadratic equation. The physical interpretation of the results is provided here.

Before defining x, y and q we must first decide what normalised measure of electric field V(t) is desirable: there is a choice to be made because Haus' model is a nonlinear model in which we want to end up with no more variables than are necessary.

In the "bouncing ball" model we worked in terms of the normalised flux in the amplifier λ_a. We now choose a field $V(t) = \sqrt{\lambda_a}$, and therefore (7a) and (7b) in section 2.2 become

$$A(t) = A_L e^{-U(t)} \tag{1a}$$

$$B(t) = B_L e^{-sU(t)} \tag{1b}$$

Γ is the linear loss coefficient, A and B are the nonlinear slow-amplification and slow-absorption and U(t) was defined as the integral $U(t) = \int_{-\infty}^{t} |V|^2 dt$ in the previous section.

The complete absorber recovery assumption simplifies the analysis because $B_L = B_u$ in that case. However A_L in (1a) is determined in practice by the recovery law which was quoted in section 2.2 (equation (6)). The net gain coefficient for use in Haus' model is now given by:

$$G = A(t) - (B(t) + \Gamma) \tag{2}$$

Expanding the exponentials in (1) allowing for $s > 1$ but assuming $U << 1$ leads to the parabolic approximation:

$$G = A_L - (B_u + \Gamma) + (sB_u - A_L)U - \frac{s^2}{2} B_u U^2 \tag{3}$$

The definition of $q = s^2 B_u$ leads to the following interpretation of x and y of the previous section:

$$x = A_L - (B_u + \Gamma) \tag{4}$$

$$y = \sqrt{B_u}\left[1 - \frac{A_L}{sB_u}\right] \tag{5}$$

The hyperbolic secant formula that gives V(t) from these parameters has been proved already. Now we shall demonstrate the consistency of the normalised results in section 2.5 with the much simpler energy conservation approach of section 2.2. The total energy in the pulse is given by $U(t = \infty) = z/\sqrt{q}$ and therefore from (3), (4) and (5) the energy that the entire pulse gains from a round trip without including bandwidth limitation is:

$$\Delta U = \int_{-\infty}^{\infty} |V|^2 \, G(t) \, dt$$

$$= \int_{0}^{z/\sqrt{q}} G \, dU$$

$$= \frac{1}{\sqrt{q}} \left(xz + \frac{1}{2} yz^2 - \frac{1}{6} z^3\right) \tag{6}$$

The energy balance is achieved by an equal loss of energy in the filter. The fractional loss depends on the shape of the pulse as well as its duration. The net result must be

$$\Delta U + U_{\text{FILTER OUTPUT}} - U_{\text{FILTER INPUT}} = 0 \tag{7}$$

and this suggests the physical origin of the quadratic equation used by Haus. The first term above comes from (6), the second equals $z/\sqrt{q}$ (because V(t) is a self-reproducing pulse) and the last term is easily calculated using the inverse filter operator method (see [10], equation 5.7):

$$U_{\text{FILTER INPUT}} = \int_{-\infty}^{\infty} |V + t_F' \frac{dV}{dt}|^2 dt$$

$$= \frac{z}{\sqrt{q}} \left[1 + \frac{t_F'^2}{3t_p^2} \right]$$

where the factor 3 comes simply by assuming a pulse shape $\text{sech}(t/t_p)$, where t_p is finally fixed using (7):

$$\frac{1}{\sqrt{q}} \left(xz + \frac{1}{2} yz^2 - \frac{1}{6} z^3 \right) - \frac{z}{\sqrt{q}} \frac{t_F'^2}{3t_p^2} = 0$$

In order to complete the discussion we need to connect t_p with z. This is outside the power of the "bouncing ball" approach, but if we take t/t_p dependence $(1/4)\ z\ (t/t_F')$ found in the last section we obtain:

$$\frac{z}{2\sqrt{q}} \left(2x + yz - \frac{1}{3} z^2 \right) - \frac{z}{\sqrt{q}} \frac{z^2}{48} = 0$$

and duplicate the original definition that z is the root of $\frac{-3}{8} z^2 + yz + 2x = 0$.

Since $t_F' = \sqrt{\Gamma} t_f$, $z/\sqrt{q} = j$ and $q = s^2 B_u$ we find the essential physics of passive mode-locking in the $t_p \rightarrow z$ relationship, written now as:

$$t_p = \left(\frac{4}{s}\right) t_F \frac{\sqrt{\Gamma}}{j\sqrt{B_u}}$$

This result was tested in section 2.4. The effect of the parabolic gain approximation was found to be significant.

The stability zones in the present model are shifted slightly compared with those which occur during the static pulse compression without bandwidth limitation. Following Haus [8] we define the stability condition as a net loss on the leading and trailing edges of the pulse for the noise

which the filter does not remove. With the gain parabola (section 2.5) we find that $G_L = x$ and $G_T = x + yz - \frac{1}{2} z^2$.

If a graph is plotted of j/B_u against y then the stability boundaries appear as straight lines through the origin. One can easily prove that the stability condition is met when $\frac{3}{8} z < y < \frac{5}{8} z$ from which the slopes of the boundary lines are found to be $\frac{8}{3s}$ and $\frac{5}{3s}$. This shows that the stability region is wider when s is made large (for example in colliding-pulse arrangements). Once the parameters allow the system to operate outside the stability zone, the pulses may be seriously perturbed by noise (see section 2.7). Notice that for the laser to attain threshold $A_u > B_u + \Gamma$ is necessary, but for stable passive mode-locking $A_L < B_u + \Gamma$ which (since $y > 0$ in equation (5) gives $s > A_L/B_u$) requires that we choose $s > 1 + \Gamma/B_u$ whatever the amplification may be [49].

We can conclude that a large value of s is beneficial from both the pulse compression and stability points of view. The absorber then very readily saturates.

2.7 Effects of noise for dynamic pulse compression

The "deepening" of the trough between successive mode-locked pulses is prevented from continuing to the steady state limit because of noise. This was introduced into the simulations as an injected constant signal and we thus ignore the stochastic structure of the source. The "filling in" of the trough occurs once the main part of the pulse is established. In figure 2 the dotted curve shows, (for a particular injection level), the disappearance of the trough which would otherwise get deeper* for the next hundred round trips.

For a laser operating outside the static compression zone, the effect of injection is found to depend strongly on the bandwidth of the filter. If the bandwidth is wide then the pulse-width that is achieved from dynamic compression is very sensitive to the level of the noise. This differs markedly from the static pulse compression results where the noise which causes the depth of trough to be limited has no effect upon pulse-width.

Figure 4 shows profiles after 40 round trips when Ξ_a was decreased (e.g. by lengthening T_{RT}) enough to operate with gain on the leading edge in the model of section 2.2. For example (4a) the injection is set at 3×10^{-6} (with the same normalisation as λ) and the bandwidth increases from left to right: t_F = 4.5, 2, 0 meshpoints. Dynamic compression is a slow process and for $t_F = 0$ the pulse was still narrowing after 40 round trips. However the other curves do represent steady states and the widths are very much larger than those of pulses inside the compression zone for these filter memory times.

---

*In the absence of noise the final trough for $\log\lambda$ had reached 6×10^{-33}

The effect of increasing the injected signal by factors of 10 and 100 is shown in figures 4b and 4c. The steady state pulses, now occurring already at 40 transits even in the absense of any bandwidth limitation, are controlled by the strength of the noise.

These results indicate that operation outside the regime where g_L and g_T are simultaneously less than 1 will lead to longer pulses which will not usually be shortened by an increase in available bandwidth if the effects of noise are included.

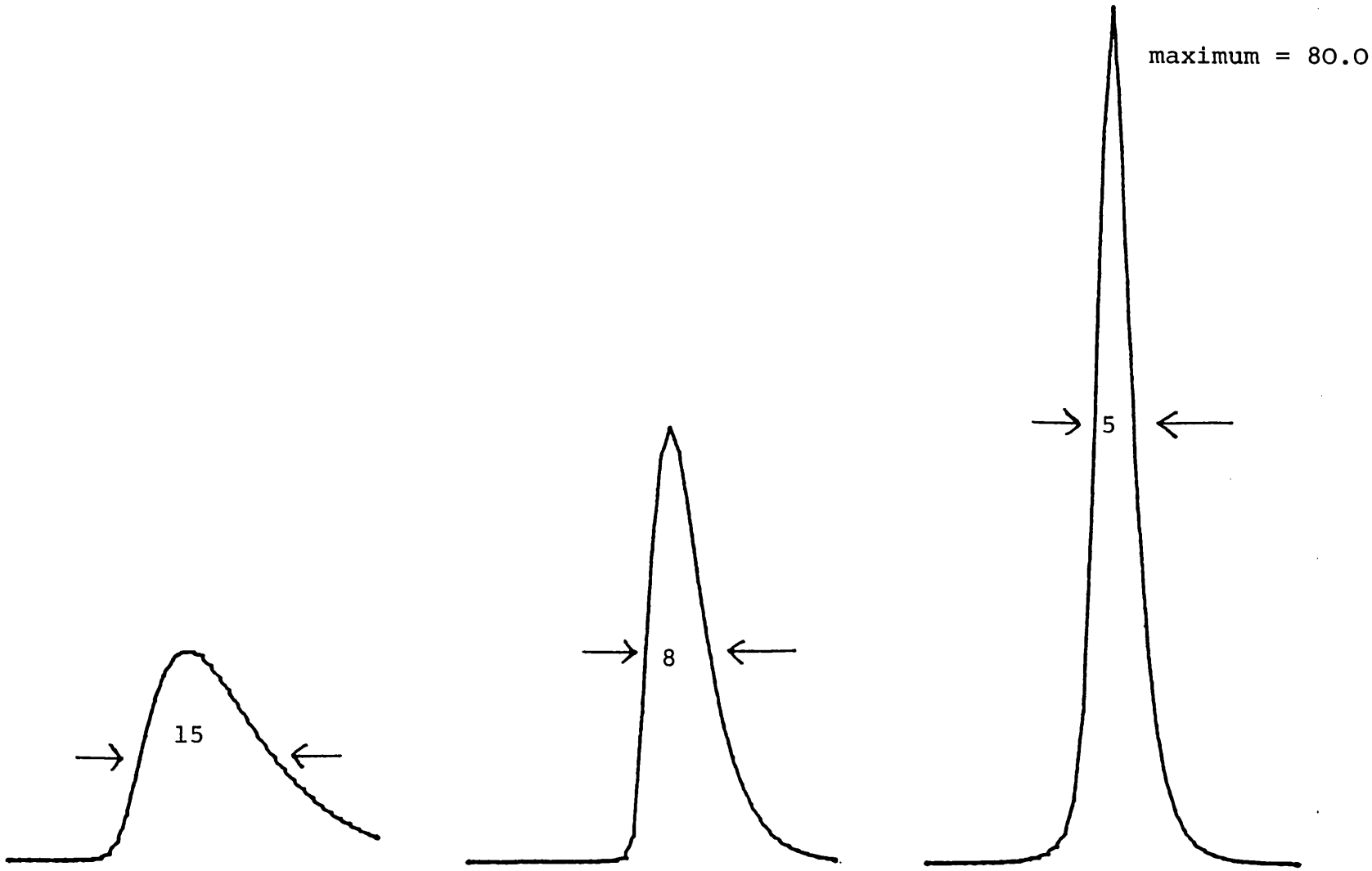

FIGURE 4a DYNAMIC PULSE COMPRESSION INCLUDING INJECTION

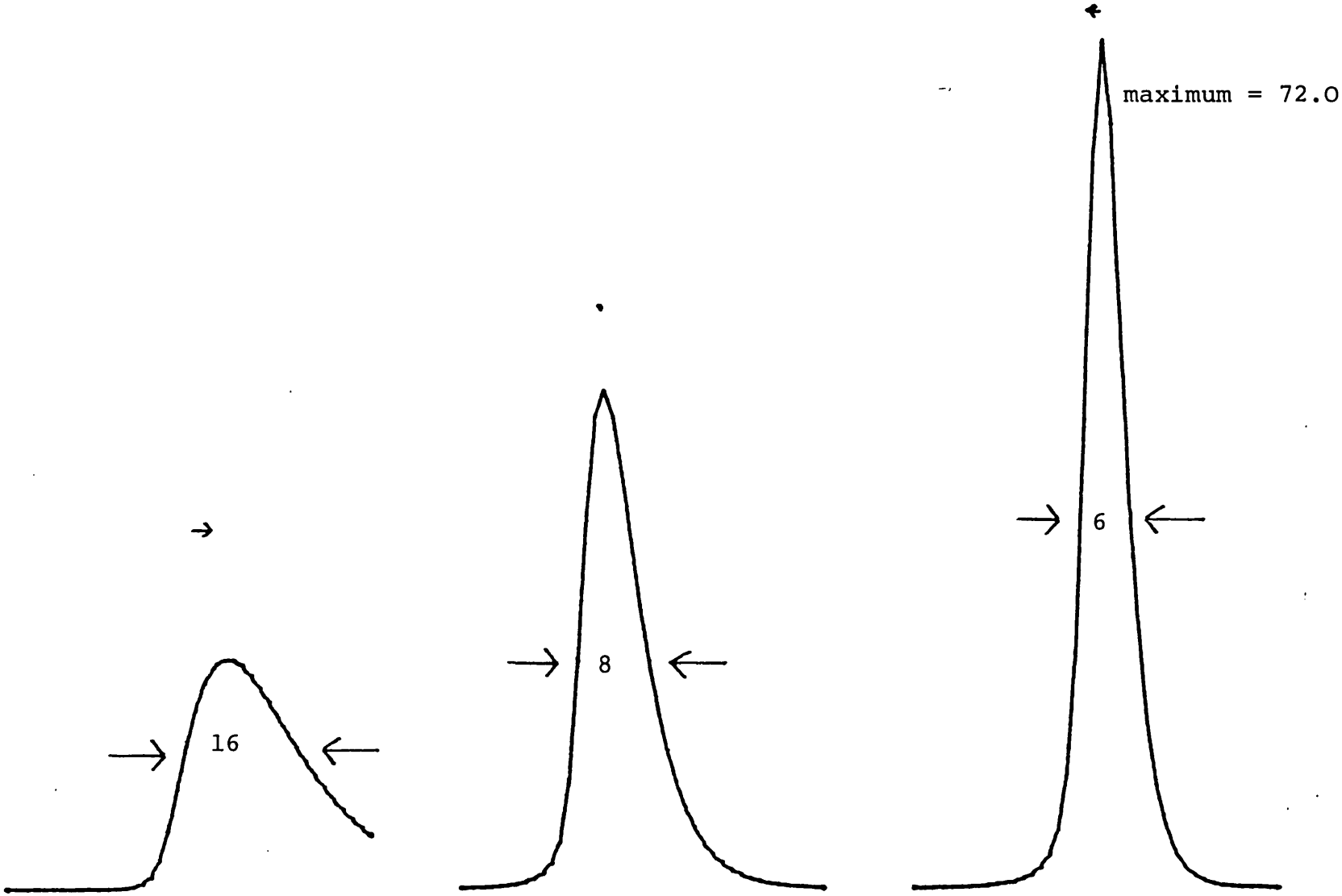

FIGURE 4b INJECTION X 10

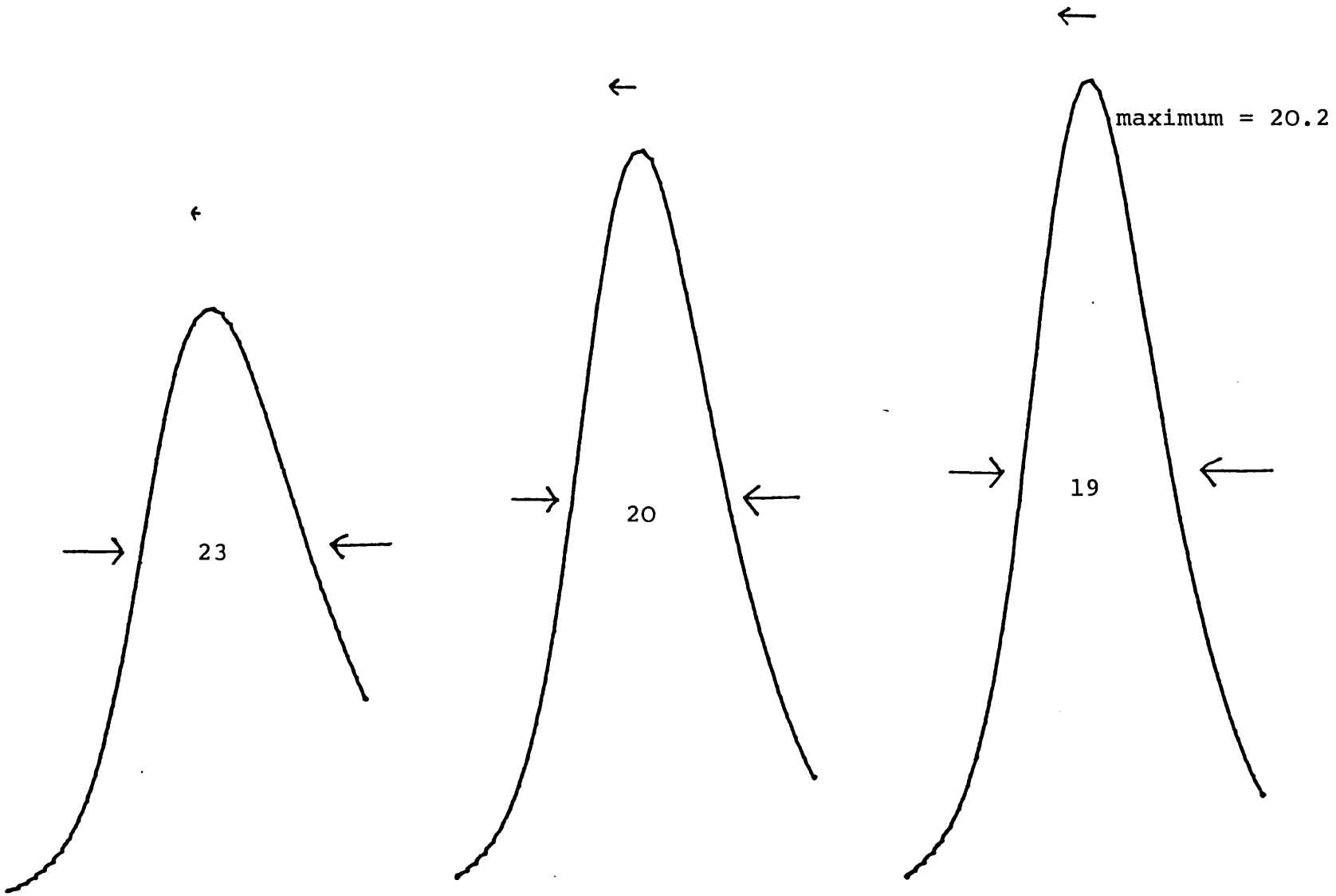

FIGURE 4c INJECTION X 100

2.8 Slipping pulses: relationship between rise and fall times and the net gain.

Steady state pulses in Haus' model have exponential wings. In the original equation in section 2.5 the absense of gain modulation for weak fields always leads to such solutions. Below, we show that the profile of any steady state pulse may be analysed simply everywhere except close to the peak. We allow for the gradual variation of the logarithmic slope in local time.

Taking the flux to consist of a slowly varying exponential exp(kt) where k is locally time-independent, we may assume the electric field to obey

$$E(t-\epsilon) = E(t)\ e^{-(k/2)\epsilon}$$

for small delays (ϵ). The loss in a Fabry Perot filter will simply shift an exponential E(t) in this same fashion, as will a locally constant net gain .

A steady state profile by definition may only suffer a constant slip after a cavity transit. This is true despite the fact that the shifts by the filter and by the net gain depend on k which is time varying. The condition for a steady state pulse is that net gain g(t) and logarithmic slope k(t) must be linked so that the combined effects, just mentioned, supply the constant slip ϵ.

For the steady state pulse obtained after 140 transits figure 5a shows the "theoretical" net gain versus logarithmic slope graph for the measured slip of ϵ= 3.2. The operating parameters are those of section 2.2 (static pulse compression) so that there was no slip at all until the

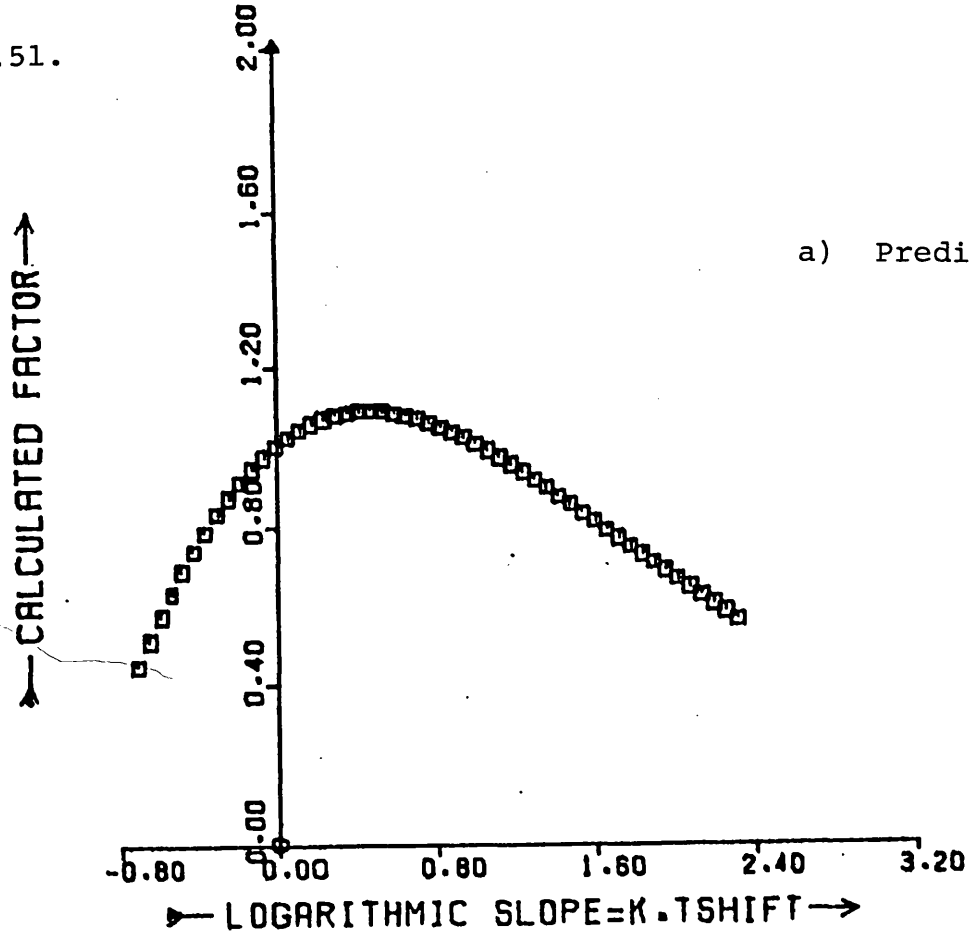

a) Prediction

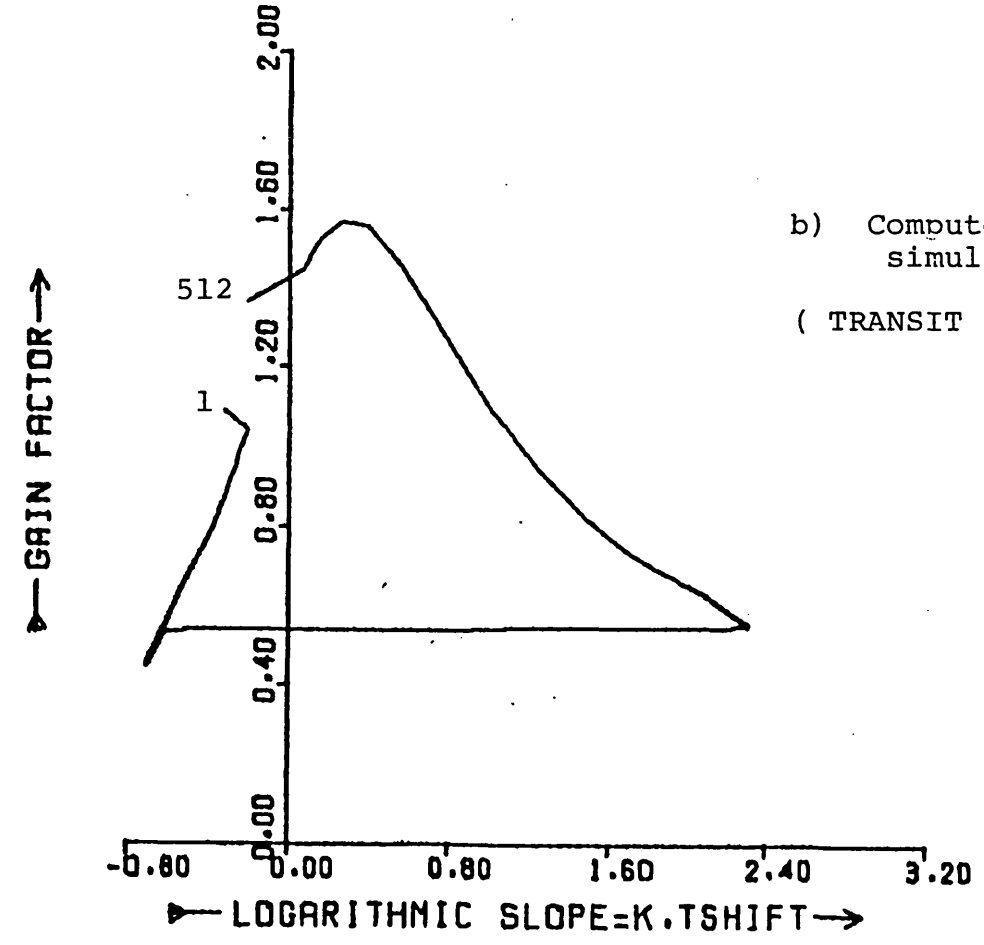

b) Computer simulation

(TRANSIT 140)

FIGURE 5 STEADY STATE PULSE BEHAVIOUR

filter affected the evolution. The theory is dealt with in appendix I. The comparison with simulation (figure 5b) is very good except near the peak of the pulse (where the upper curve cuts the axis).

Figure 5b contains information about the steady state solution, which must now be described. The gap in the plot is where the calculation happened to pass the 140th cavity period from the start of the calculation. The gain is defined as the ratio, with the filter imagined switched off, of the fluxes on the 141st and 140th transits measured at the same local time modulo TCAV. The slope could not easily be measured at the end points and the distortion is an artefact. However, the gap is real: more than 512 meshpoints (1 cavity snapshot) are needed to complete the figure - because the slip (ϵ=3.2) delays the repetition. If the figure was displayed in "real-time" as an evolution approached the steady state from the earlier static pulse compression phase, the gap would grow on each round trip as the filter introduced the slip. Thereafter the gap travels in a clockwise direction around the figure, which develops the sharp "corners" predicted by figure 5a as time goes on.

Figure 5b records the sequence of events during the 140th transit if the curve is traced in a counter-clockwise sense. The horizontal line, traced over at the foot of the trough, separates the trailing and leading edges (on the left and the right). Most of the 512 points are densely gathered close to the ends of this line, confirming that the wings are exponential and that the leading edge of the pulse is steeper than the trailing edge. From the leading edge, continuing amplifier recovery first raises the gain factor gradually ; the exponential rising edge continues almost without saturating whilst this happens. The gain begins to increase

more rapidly when the absorber saturates, reaching a peak before the flux has reached the peak of the ultrafast pulse (the slope of log{flux} is still positive in the figure). Gain saturation dominates the fast descent on the left hand half of the figure, but in the trailing edge of the pulse absorber recovery causes a further drop, which is slowly reversed when amplifier recovery is the only remaining force.

The agreement with theory at the slowly traced out regions in the space of figure 5b indicates that the computer simulation is reliable. The portion of the plot where there is disagreement could be studied in order to improve the test. Haus' approximate theory, though not able to improve the agreement, does indicate a parabolic shape for the entire figure (section 2.5 and appendix I). This is approximately what we have in figure 5b.

CHAPTER 3

TWO-WAY ABSORBER SATURATION

3.1 Introduction

The description of a two-way absorber which can be applied to the study of passive mode-locking must include the following three processes: transient buildup and decay of fields in time and space, highly non-linear saturation by the concentrated mode-locked laser pulses and self-phase modulation (chirping). It is the purpose of this chapter to see how these requirements may be met.

It is not necessary to include relaxation processes in detail because the pulse durations occurring are far shorter than T_1 (longitudinal relaxation time) and far longer than T_2 (transverse relaxation time) for many of the dye solutions used. This makes it possible to ignore T_1 processes (and to treat T_2 processes in a rate-equation approximation). For the sake of completeness, however, comparison will be drawn between the present 'slow absorber' and the other extreme case of a 'fast absorber' with T_1 and T_2 both small compared with the pulse durations.

The first two processes mentioned above are greatly affected by the population grating which arises in the absorber from spatial hole-burning, and which is not present when only a single beam is involved at once. Experimentally, one finds for the conventional passively mode-locked dye laser (unidirectional travelling wave saturation of the absorber) little dependence upon the thickness of the dye cell or jet. However when there is two-beam saturation (as in colliding-pulse systems) one finds that the shortest pulses obtained are determined by the absorber thickness. This is due to the grating; the mechanism responsible is the prime concern of this thesis.

Self-phase modulation is responsible for the chirp sometimes measured in the pulses from mode-locked lasers, as we discussed in section 1.2. The fact that such pulses are

not bandwidth limited can be used to advantage by using linear dispersion inside or outside the cavity to compress the pulses further. Colliding-pulse lasers may well owe their success partly to fortuitous linear dispersion of the correct sign in the dielectrically coated mirrors of the cavity.

The plan for this chapter is to review first the unidirectional absorber and finally tackle the two-way absorber. The inclusion of self-phase modulation is left for future work.

3.2 The conventional absorber

In the appendix the rate equations describing a homogeneously broadened two level system are derived from basic principles. The equations also describe three-level and four-level systems in which rapid thermalisation means that only two levels are important: both a dye amplifier and a saturable absorber dye are in this category.

Taking the case of the absorber (but a change of sign in the population difference leads to all the results for the amplifier) we have:

$$\frac{\partial n}{\partial t'} = - n\sigma I \qquad (1)$$

$$\frac{\partial I}{\partial z'} = - n\sigma I \qquad (2)$$

where, at this stage, no account is taken of population recovery in equation 1. The meanings of the symbols are: $t' = t - (z/c)$ and $z' = z$, local time transformed coordinates; I - normalised intensity in photons/m^2/s (photon flux) travelling in the +z direction; σ - stimulated transition cross section and n is the population density difference between the lower and upper levels.

In this slow absorber limit, there is an analytic solution for the transmitted pulse which was originally used in the case of high energy amplifiers in the 1960's. Standard techniques lead to the following results [42,43]:

$$n(z,t) = \frac{n(z,-\infty)\ e^{\sigma\int_0^z n(z',-\infty)dz'}}{\left\{e^{\sigma\int_{-\infty}^{t'} I(0,t)dt} - 1\right\} + e^{\sigma\int_0^z n(z',-\infty)dz'}}$$

$$I(z,t) = \frac{I(0,t')}{1 - \left\{1 - e^{\sigma\int_0^z n(z',-\infty)dz'}\right\} e^{-\sigma\int_{-\infty}^{t'} I(0,t)dt}}$$

To help make these results plausible note that letting the pulse energy $\sigma\int_{-\infty}^{t'} I(0,t)dt$ remain small yields $n(z,t) \approx n(z,-\infty)$ and the degree of saturation is also small; the flux I then obeys Beer's law for linear absorption. Similarly taking L sufficiently short that $I(L,t') \approx I(0,t')$ we find an exponential saturation

$$e^{-\sigma\int_{-\infty}^{t'} I(o,t)dt};$$

propagation effects are absent in this case since the solution is also a formal solution to (1) with z-dependence suppressed ($\partial/\partial t' \to d/dt'$).

These solutions contain some quite surprising physics. Super-luminary propagation of the peak of a pulse travelling in a nonlinear medium caused interest to workers on amplifier theory. In fact, this effect only involves the continuous reshaping of the pulse as its leading edge saturates the gain available later in local time. Even though a new peak may appear on the profile in this process, no information has been transmitted faster than the speed of light.

3.3 Fleck Hierarchy [52]

The slowly varying population density difference in the one-way absorber is replaced by a rapid grating (real time hologram) structure when there is a second saturating field to form interference fringes. The modulation impressed on a two-way absorber has a period of half a wavelength. Therefore we may carry out the Fourier decomposition,

$$(B10) \qquad n(z,t) = \bar{n} + \sum_{p=1}^{\infty} [n_p \exp\{-2pikz\} + c.c.]$$

where $k = 2\pi/\lambda$ and the coefficients $\bar{n}$ and n_p are allowed to vary SLOWLY with z as the local grating "shape" changes after a large number of periods. We find below that fields and not just intensity (used in section 3.2) determine the effect of a two-way absorber.

Gratings in laser physics have been studied extensively and Appendix A refers to the background of our subject.

We show in appendix B that the transport equations for counter-propagating laser fields depend only on the fundamental and first spatial Fourier components of the population difference intensity n(z,t). From (B8)

$$\left[\frac{1}{c}\frac{\partial}{\partial t} + \frac{\partial}{\partial z}\right] E^{+} = -\frac{\sigma}{2}(\bar{n}E^{+} + n_1 E^{-}) \qquad (1a)$$

$$\left[\frac{1}{c}\frac{\partial}{\partial t} - \frac{\partial}{\partial z}\right] E^{-} = -\frac{\sigma}{2}(\bar{n}E^{-} + n_1^{*} E^{+}) \qquad (1b)$$

The reason that the higher Fourier components do not cause scattering is that the Bragg condition is violated (there is a large phase-mismatch). Appendix B provides the rate equation for n whereas it is the specific behaviour just of $\bar{n}$ and n_1 which will now complete our two-way absorber description. Fleck [52] introduced a hierarchy of coupled equations, rederived below, which describe the evolution of all the Fourier components. The coupling means that n_2 appears in the

driving term for n_1, and so on - this fact unfortunately means that a large number of Fourier components, not otherwise required, must all be followed.

We next substitute (B10) into (B7) and equate the slowly-varying coefficients of like exponents coming from n(z,t) and F(z,t). The result is the infinite Fleck hierarchy.

$$\frac{\partial \bar{n}}{\partial t} = \frac{n_u - \bar{n}}{T_1} - 4\sigma[\bar{n}(|E^+|^2 + |E^-|^2) + (n_1 E^{+*} E^- + \text{c.c.})] \quad (2a)$$

$$\frac{\partial n_1}{\partial t} = \frac{-n_1}{T_1} - 4\sigma[\bar{n}(|E^+|^2 + |E^-|^2) + \bar{n}E^{+*}E^- + n_2 E^{+*}E^-] \quad (2b)$$

$$\frac{\partial n_2}{\partial t} = \frac{-n_2}{T_1} - 4\sigma[n_2(|E^+|^2 + |E^-|^2) + n_1 E^+ E^{-*} + n_3 E^{+*}E^-] \quad (2c)$$

. . .

. . .

. . .

The truncation which Fleck employed in order to use this formulation sets $n_2 = 0$ in (2b), thus closing the system of equations (1a), (1b), (2a) and (2b) at the expense of major approximation.

Note that the factor $(\epsilon_0/\bar{n}k)^{1/2}$ which multiplied E^+ and E^- in the appendix has been dropped since it is convenient from now on to work with normalised fields. Since the photon flux becomes $F = 2(|E^+|^2 + |E^-|^2 + E^+E^{-*}e^{-2ikz} + E^{+*}E^-e^{+2ikz})$ the doses with each pulse are

$$j_\pm = 2\int |E^\pm|^2 \, dt.$$

3.4 Perturbation Expansion of the Fleck Equations

When the non-linearity is not too strong, a few terms in a perturbation expansion can be sufficient to approximate the solution to a nonlinear problem. The approach to be presented here makes use of a dimensionless combination of parameters, α, which has to be large for the method to be of use.

The results are not used elsewhere in this thesis because, as we shall soon see, large α is not a correct assumption for the saturable absorber problems of interest. Nevertheless, the method provides some extra insight into the basic physics embodied in the exact equations.

We define

$$\alpha = \frac{\sigma \; c \; T_1 \; |n_u|}{2 \; \eta}$$

Here n_u represents the unsaturated population difference density; that is the negative equilibrium value to which the absorber will return in the absence of any applied light. The relaxation time is denoted as usual by T_1, the "spin-lattice" or longitudinal damping time. The speed of light inside the medium is c/η, and the interaction strength between photons and population is contained in the cross section σ. Using the values in the table, which appear in Fleck's work, we find $\alpha \approx 4$ for the absorber and $\alpha \approx 10^6$ for the case of the amplifier.

	T_1	σ	$\lvert n_u \rvert$
absorber (CRYPTOCYANINE)	1 ns	$8 \times 10^{-16} cm^2$	$0.35 \times 10^{15} cm^{-3}$
amplifier (RUBY)	$3 \times 10^{-3} s$	$2.5 \times 10^{-20} cm^2$	$2.6 \times 10^{18} cm^{-3}$

Table of data used to calculate α [52]

We shall now define normalised variables for the fields, material parameters, timescale and distance scale in which the perturbation expansion is presented.

Normalised Variables

A steady photon flux $|E^+|^2$ in one direction with magnitude $\frac{1}{4\sigma T_1}$ leads to a degree of saturation $\frac{n_u - \bar{n}}{\bar{n}}$ of unity. This is the reason for using the following normalised fields:

$$A = 2 / \sigma T_1 \; E^+$$
$$B = 2 / \sigma T_1 \; E^-$$

In order that all the variables should be dimensionless we make the substitutions

$$a_o = \frac{\sigma \; c \; T_1}{2 \; \eta} \; \bar{n}$$

$$a_p = \frac{\sigma \; c \; T_1}{2 \; \eta} \; n_p \qquad (p = 1, 2, ...)$$

$$X = \frac{\sigma}{2} \; |n_u| \; z$$

$$T = \frac{\sigma}{2} \; |n_u| \; \frac{c}{\eta} \; t$$

Besides A, B, a_o, a_p, X and T the normalised equations contain only one constant, which turns out to be α.

At T=0 we assume the following initial conditions:

$$A = A_0 \; ; \; B = B_0 \; ; \; a_0 = -\alpha \text{ and } a_p = 0 \text{ for all } p > 0$$

Perturbation Expansion

The series expansions,

$$A = A_0 + \frac{1}{\alpha} A_1 + \frac{1}{\alpha^2} A_2 + \ldots.$$

$$B = B_0 + \frac{1}{\alpha} B_1 + \frac{1}{\alpha^2} B_2 + \ldots.$$

$$a_0 = -\alpha + a_{00} + \frac{1}{\alpha} a_{01} + \frac{1}{\alpha^2} a_{02} + \ldots.$$

$$a_p = a_{p0} + \frac{1}{\alpha} a_{p1} + \frac{1}{\alpha^2} a_{p2} + \ldots. \qquad (p = 1,2, \ldots.)$$

are substituted into the normalised Fleck equations:

$$\alpha \left[\frac{\partial A}{\partial T} + \frac{\partial A}{\partial X}\right] = a_0 A + a_1 B$$

$$\alpha \left[\frac{\partial B}{\partial T} - \frac{\partial B}{\partial X}\right] = a_0 B + a_1^* A$$

$$\alpha \frac{\partial a_0}{\partial T} + (a_0 + \alpha) = -\left\{a_0(|A|^2 + |B|^2) + a_1 A^* B + a_1^* A B^*\right\}$$

$$\alpha \frac{\partial a_p}{\partial T} + a_p = -\left\{a_{p-1} A B^* + a_p (|A|^2 + |B|^2) + a_{p+1} A^* B\right\} \qquad (p = 1,2 \ldots.)$$

Referring to Appendix C , where successive powers of α are equated separately in these equations, one finds

$$a_{pq} = 0 \qquad \text{for all } q < p - 1$$

The first non-zero terms in the "a" expansions are found in terms of A_0 and B_0 alone, namely

$$a_{00} = \int_0^T |A_0|^2 + |B_0|^2 \, dT'$$

$$a_{10} = \int_0^T A_0 B_0^* \, dT'$$

$$\frac{1}{\alpha^{p-1}} a_{p,p-1} = \frac{-\alpha}{p!} (a_{10} / -\alpha)^p \qquad (p = 2,3 \ldots.)$$

The approximations to the fields A, B corresponding to A_0 and B_0 turn out to be the fields which would be present if the absorber were transparent, multiplied by a temporal weighting function.

$$A_0 = e^{-T'} f(X - T')$$
$$B_0 = e^{-T'} g(X + T')$$

The next terms in A and B are the first ones which involve the reaction of the absorber back on the fields

$$A_1 = e^{-T} \int_0^T e^{T'} (a_{00} A_0 + a_{10} B_0)_{(X - T + T',\, T')} \, dT'$$

$$B_1 = e^{-T} \int_0^T e^{T'} (a_{00} B_0 + a_{10}^* A_0)_{(X + T - T',\, T')} \, dT'$$

where the subscripts in parenthesis indicate the values of X" and T" at which $a_{00}(X",T")$ etc. have to be evaluated. Although similar formulae may easily be generated for as many terms in the expansions as is desired, these integrals become impossible to perform analytically even for the simplest of input pulse-shapes.

The main objection to the perturbation expansion method is that it can not be valid if successive terms are similar in size. Comparing α with a_{00} leads to the restriction to "large" α . For $\alpha \approx 4$ and pulse energies sufficient to saturate the absorber strongly, the method cannot be used.

Next, we examine the population grating by the methods developed in this section. We showed that $a_p = \frac{-\alpha}{p!} (a_{10}/-\alpha)^p$ + other terms where $a_{10} = \int_0^T A_0 B_0^* dT'$. It is instructive to note $-\alpha I_p(-2a_{10}/\alpha)$ has exactly the same type of expansion in $1/\alpha$. In a later chapter we show that this Bessel Function result arises naturally from a nonperturbative calculation for a "slow" absorber. This means that, for a particular

case, the "other terms" just mentioned are actually known precisely.

A possible interpretation of α is realised by viewing the nonlinear system in terms of coupled "reactions". Photons interact with molecules (stimulated emission or absorption processes) and molecules interact with a reservoir (recovery processes). The ratio of these interaction strengths follows from the Fleck equations of the previous section, as follows:

$$\frac{\text{rate of reaction upon photons}}{\text{rate of recovery}} \approx \frac{\frac{1}{(E^{\pm})^2}\frac{\partial (E^{\pm})^2}{\partial t'}}{T_1^{-1}}$$

$$\approx \alpha$$

A consequence of the interpretation is that steady-state saturation of the transition occurs when the <u>total</u> reaction rates are equal in magnitude. This is consistent with the formal identity:

$$\alpha \equiv \frac{|n_u|}{\left\{\left[\frac{c}{2\eta}\right]\sigma T_1\right\}^{-1}} = \frac{\text{inversion density.}}{\text{photon density at saturation.}}$$

A large value of α would mean that saturation could not be very great and that any population grating formed would be entirely sinusoidal.

3.5 Special Cases

Two special cases can be treated without recourse either to a perturbation expansion or to numerical solution on a computer.

The first case to be discussed is an implicit analytic solution for the "fast" absorber in the presence of standing waves. The solution is well known in closely related work [85], but has not previously been mentioned in the context of the Fleck equations.

The "slow" absorber is the other special case, where an analytic solution would be most valuable to us. Such a solution does not exist so far as is known. For this case, however, a new result will be derived which is exact when the wave in one direction is weak compared with the opposite wave. The new result indicates one characteristic property of the two-way absorber which could effect mode-locking in colliding-pulse ring cavities but not in contacted absorber cavities. Finally (section 3.5c) the situation with two strong waves is considered.

a) The Fast Absorber

The field propagation equations which have to be solved are:

$$\frac{1}{v}\frac{\partial E^+}{\partial t} + \frac{\partial E^+}{\partial z} = -\frac{\sigma}{2}(\bar{n}\,E^+ + n_1 E^-)$$

$$\frac{1}{v}\frac{\partial E^-}{\partial t} - \frac{\partial E^-}{\partial z} = -\frac{\sigma}{2}(\bar{n}\,E^+ + n_1^* E^+)$$

The fast absorber (also known as an inertialess absorber) is defined to reach equilibrium with the applied field so rapidly that $\bar{n}$ and n_1 in these equations are determined by the instantaneous values of E^+ and E^-.

Thus

$$\bar{n}(t) = \bar{n}(E^+(t), E^-(t))$$
$$n_1(t) = n_1(E^+(t), E^-(t)).$$

The form of these function is made explicit below. Note that the arguments $E^{\pm}(t)$ in fact contain a z dependence as a result of propagation effects: for this reason a further approximation is introduced next.

If the absorber is concentrated into a short distance the z-partial derivatives become large in the propagation equations. These terms also become dominant in the limit when the incident fields are made to vary with time very slowly, which corresponds to a long optical pulse. The thin absorber approximation consists of removing the t-partial derivatives altogether and is justified when the pulse-width is much greater than the cell-width.

We now have the differential equations

$$\frac{dE^+}{dz} = -\frac{\sigma}{2}(\bar{n}E^+ + n_1E^-) \tag{1a}$$

$$\frac{dE^-}{dz} = +\frac{\sigma}{2}(\bar{n}E^- + n_1^*E^+) \tag{1b}$$

Even before specifying $\bar{n}(E^+, E^-)$ and $n_1(E^+, E^-)$ some general features are apparent in these nonlinear coupled wave equations.

- E^+ and E^- at any point in the absorber determine each other through a conservation law containing a constant which must be chosen to satisfy the boundary conditions.
- This conservation law is a solution of

$$\frac{dE^+}{dE^-} = -\frac{\bar{n}E^+ + n_1E^-}{\bar{n}E^- + n_1^*E^+}$$

. Only in very rare cases does an analytic solution to the equations (1) result when the conservation law is used to eliminate one of the fields.

The inertialess population equations are,

$$0 = \frac{n_u - \bar{n}}{T_1} - 4\sigma[\bar{n}(|E^+|^2 + |E^-|^2) + (n_1 E^{+*} E^- + c.c)] \quad (2a)$$

$$0 = \frac{-n_1}{T_1} - 4\sigma[n_1(|E^+|^2 + |E^-|^2) + \bar{n}\, E^+ E^{-*} + n_2 E^{+*} E^-] \quad (2b)$$

and an infinite series of similar equations for the higher order population terms.

If we use the Fleck truncation (setting $n_2 = 0$ in 2b) then $\bar{n}$ and n_1 are particularly easily extracted. However, a set of difference equations can be solved without difficulty and therefore we shall retain all the equations - but quote the results of the truncation as well, for comparison.

The phases of $\bar{n}$ and n_1 can be stated without any calculation. $\bar{n}$ is real and positive, by definition, but $-n_1$ has the same phase as the standing wave, namely $\arg(E^+E^{-*})$. This phase is invariant during propagation and so we can take n_1, E^+, E^- as real without loss of generality.

The solution of the difference equations takes the form $n_k = \bar{n}\,(f)^k$ where f is determined from a characteristic equation, and the knowledge that $n_k \to 0$ as $k \to \infty$. From (2a) we have the normalisation $\bar{n} = n_u/(a + 2bf)$, where $a = 1 + 4\sigma T_1(|E^+|^2 + |E^-|^2)$ and $b = 4\sigma T_1 E^+E^-$. The characteristic equation gives $f = \frac{\sqrt{a^2 - 4b^2} - a}{2b}$.

The $\bar{n}$ and n' functions are now known (Table 1), so we may proceed to look for the conservation law.

	$\bar{n}$	$n_1/\bar{n}$
EXACT	$\frac{n_u}{a} \cdot \frac{1}{\sqrt{1 - x^2}}$	$\frac{\sqrt{1 - x^2} - 1}{x}$
FLECK TRUNCATION	$\frac{n_u}{a} \cdot \frac{1}{1 - \frac{1}{2} x^2}$	$-\frac{x}{2}$

Populations as a function of the normalised parameters a and x = 2b/a — Table 1

The conservation law, in the two cases, is:

EXACT	$\frac{\sqrt{1 - x^2} - 1}{x}$	=	$\frac{\text{const}}{E^+E^-}$
FLECK TRUNCATION	x	=	$\frac{\text{const}'}{E^+E^-}$

(3)

The proof is given in appendix (D), but it is possible that equations (3) have a more fundamental status than this mathematical route suggests. Notice the 'coincidence' that both the two cases imply the proportionality

$$n_1 \quad \propto \quad \frac{\bar{n}}{E^+ E^-} \cdot$$

However, recognising that the constant of proportionality depends on the boundary conditions, the physics involved will not be studied here.

The next and final step in solving the fast absorber is to use the conservation laws in either of eqns. 1. As shown in the appendix we need to solve, for example

$$\text{EXACT} \qquad E^{+}\frac{\partial}{\partial z}E^{+} = -\tfrac{1}{2}\sigma n_u \frac{(E^{+2}-d)^2}{E^{+4}+(1-2d)E^{+2}+d^2} \qquad (4)$$

$$\text{FLECK TRUNCATION} \qquad E^{+}\frac{\partial}{\partial z}E^{+} = -\tfrac{1}{2}\sigma n_u \frac{(E^{+2}-c)^2}{E^{+4}+(1-2c)E^{+2}+2c^2}$$

and this turns out to be straightforward. We reiterate that it is not normally the case that a nonlinear propagation problem can be solved analytically. Indeed, Fleck [52] only states in passing the expressions for $\bar{n}$ and n_1, proceeding then to a numerical solution of the differential equations. Note that his program does not assume a fast absorber as we have to, but it employs the truncation ($n_2 = 0$) which we avoid.

From the results in this section it should be possible to compare, for the fast absorber, true behaviour with that obtained for $n_2 = 0$ truncation. Hence the importance of the higher grating harmonics would be tested. This is one level advanced from a test already carried out by Fleck, who compared the above approximation (sinusoidal standing wave) with a truncation giving $n_1 = 0$ and corresponding to neglect of grating coupling altogether. He found that pulse evolution in passive mode-locking was slowed down, which is due to the fact that saturation power goes up when there is no grating.

The Fleck truncation is only truly correct in the limit of vanishingly small grating effects, which is the case when $x \to 0$. For this limit, the equations of this section can be rewritten in the form used by Borisov et Al [54] to plot detailed graphs showing the behaviour of a "phototropic valve" in a standing light wave. Taking the appropriate combination of (1a) and (1b):

$$a\left[\frac{dE^{+}}{dz} - \frac{1}{2}x\frac{dE^{-}}{dz}\right] = -\frac{\sigma}{2}a(\bar{n}E^{+} + n_1E^{-} + \tfrac{1}{2}x\bar{n}E^{-} + \tfrac{1}{2}xn_1E^{+})$$

$$= -\frac{\sigma}{2}n_u E^{+}\frac{1-x^2/4}{1-x^2/2} \approx -\frac{\sigma}{2}n_u E^{+}$$

and we note that the E^- terms on the RHS cancelled on substituting for $\bar{n}$ and n_1 from the table. In terms of normalised intensities $U^{\pm} = 4\sigma T_1 |E^{\pm}|^2$ we obtain the indicated equations:

$$-(1 + U^+ + U^-) \frac{dU^+}{dz} + U^+ \frac{dU^-}{dz} \approx \sigma n_u U^+$$

and, (using a second combination of 1a, 1b)

$$(1 + U^+ + U^-) \frac{dU^+}{dz} - U^- \frac{dU^-}{dz} \approx -\sigma n_u U^+$$

The authors of [54] found that these equations only agreed with their experimental data for x small, as we would expect.

To conclude this section we shall mention some closely related publications concerned with resonant standing wave saturators. Macomber [55] studied a two-way saturable absorber slab with different boundary conditions to those suggested here (appendix D): the backward wave was not provided externally but consisted of the reflection produced at the change in average refractive index at the slab boundary. In that study of saturable reflection, however, the incorrect conclusion was drawn that E^+E^- is z-independent. The source of this discrepancy is that the slowly varying equations derived from Maxwell's equations were found there without proper selection of phase-matched driving terms. In section 3.3, Fleck's results rightly treat by SVEA only terms that actually are phase-matched. More recently Gruneisen et Al [56] used the same exact approach discussed here to calculate in great generality the steady state phase-conjugate reflectivity of saturable absorbers.

In a Fabry-Perot laser a high power CW theory has to take into account the same types of effect which arise in the two-way saturable absorber. This explains the appearance of similar exact averaging methods in a much earlier paper on

laser amplifiers by Ostrovoskii and Yakubovich [57] that is rarely quoted.

b) The Slow Absorber

Under the assumption that ϵ^+ dominates ϵ^-, the Fleck equations reduce to the following four nonlinear equations:

$$\frac{\partial \bar{n}}{\partial t} = -4\sigma \left[\bar{n}\, \epsilon^{+2}\right] \tag{1}$$

$$\frac{\eta}{c}\frac{\partial \epsilon^+}{\partial t} + \frac{\partial \epsilon^+}{\partial z} = -\frac{\sigma}{2}\bar{n}\, \epsilon^+ \tag{2}$$

$$\frac{\partial n_1}{\partial t} = -4\sigma\left[n_1 \epsilon^{+2} + \bar{n}\, \epsilon^+ \epsilon^-\right] \tag{3}$$

$$\frac{\eta}{c}\frac{\partial \epsilon^-}{\partial t} - \frac{\partial \epsilon^-}{\partial z} = -\frac{\sigma}{2}\left[\bar{n}\, \epsilon^- + n_1 \epsilon^+\right] \tag{4}$$

Relaxation terms are absent because the equations apply to a "slow" absorber. Due to the "strong wave/weak wave" assumption ϵ^- and n_1 are very small: this allows all higher order terms involving these quantities to be omitted. Higher order gratings n_2 etc. also play no role under these circumstances.

In order to simplify the calculations, it is being assumed that the fields are real. $\epsilon^\pm$ represent real variables in contrast to $E^\pm$ appearing in section 3.3. This assumption might not be necessary, but that idea is not pursued here.

The method which we now adopt is very simple. Since n_1 and ϵ^- play no role in equations (1) and (2), we have the solutions for $\bar{n}$ and ϵ^+ already from section 3.2. On substituting those results explicity into (3) and (4) we obtain coupled LINEAR equations to solve for n_1 and ϵ^- (admittedly these equations have non-constant coefficients; this particular problem is tractable nonetheless).

In a convenient notation, ϵ^+ and $\bar{n}$ will be written as

$$(\epsilon^+)^2 = \left\{E_0\left(t - \frac{\eta z}{c}\right)\right\}^2 \qquad \frac{\xi\tau}{1 + \xi\,(\tau - 1)}$$

$$\bar{n} = \frac{n_u}{1 + \xi\,(\tau - 1)}$$

in which;

$$\tau = e^{4\sigma \int_0^t (E_0(t' - \frac{\eta z}{c}))^2 \, dt'}$$

$$\xi = e^{-\sigma n_u z}$$

E_0 is the (possibly time-dependent) input amplitude of the strong wave at z=0.

Now we specialise to a thin absorber so that the spatial derivatives in (2) and (4) are extremely large compared with the other term on the left in these equations. In Appendix F this approximation will be lifted.

The trick now needed to make progress with n_1 and ϵ^- is to transform to new variables G and H defined below. The coupled linear equations with which we are faced become:

$$\frac{\partial H}{\partial \tau} = \frac{G}{\tau}$$

$$\frac{\partial G}{\partial \xi} = \frac{1}{2} H \frac{\tau}{[1 + \xi(\tau - 1)]^2}$$

where

$$H = - n_u E_0^2 \frac{n_1}{\bar{n}}$$

$$= - n_1 E_0^2 (1 + \xi(\tau - 1))$$

$$G = n_u \epsilon^+ \epsilon^-$$

$$= \epsilon^- n_u E_0 \frac{\sqrt{\xi \tau}}{[1 + \xi(\tau - 1)]^{1/2}}$$

In appendix E these equations are solved with the appropriate boundary conditions spelt out.

The solution E1 is most interesting when applied to a situation where the total absorption is small ($\xi_R \approx 1$) because a rigorous study of the effect of allowing for n_1 is easily accomplished.

Let

$$\xi_R = 1 - \frac{1}{\Delta}$$

where Δ is a large number.

The appendix gives a solution (equation E2) for $H_{LEFT}(\tau)$ in terms of Δ and p (= ln τ). The subscript on H refers to the side of the absorber where the strong beam enters and the weak beam leaves. Since $G = \tau \frac{\partial H}{\partial \tau} = \frac{\partial H}{\partial p}$ we differentiate E2 to obtain

$$\epsilon^- = \frac{G_{LEFT}}{n_u E_0} = \frac{1}{n_u E_0} \frac{dH_{LEFT}}{dP}$$

$$= \gamma E_0 \left[1 - \frac{1}{2\Delta} (e^{-p} - pe^{-p}) \right]$$

Initially (p=0) absorption means that ϵ^- leaves the two-way absorber with a value smaller than on entry (γE_0). The formula shows that this absorption can be converted into amplification when n_1 has built up (p>1).

This is a dynamic energy transfer from the strong beam to the weak beam via the saturation grating, as discussed in general terms by Vinetskii et al. [58].

When $p \to \infty$,the strong beam has entirely bleached the absorber, energy transfer ceases and consequently $\epsilon^- = \gamma E_0$.

c) The propagation problem

The logical next step is to replace the weak probe ϵ^- by a strong one. Consider the case (ϵ real) of a thin slow absorber with identical step function inputs $\epsilon^+(0) = \epsilon^-(L) = \epsilon$ that reach the absorber on opposite sides at t = 0. The symmetry of this arrangement is expected to result in a time dependence of the transmitted fields which does not change with increasing ϵ, apart from a normalising factor in the time coordinate. In chapter 4 we will show that the accumulated dose $\int \epsilon^{+2} + \epsilon^{-2}\, dt$ and "cross-dose" $\int \epsilon^+ \epsilon^-\, dt$ at positions inside the absorber completely determine the saturated absorption. This results from the slow-absorber's infinite memory and immunity from recovery. Even without taking the symmetric arrangement, a change in ϵ^+ and ϵ^- (by the same factor) in both the above integrals is equivalent to a change in the units used for t. The field equations

$$\frac{\eta}{c}\frac{\partial \epsilon^+}{\partial t} + \frac{\partial \epsilon^+}{\partial z} = -\frac{\sigma}{2}\left[\bar{n}\,\epsilon^+ + n_1\,\epsilon^-\right]$$

$$\frac{\eta}{c}\frac{\partial \epsilon^-}{\partial t} - \frac{\partial \epsilon^-}{\partial z} = -\frac{\sigma}{2}\left[\bar{n}\,\epsilon^- + n_1\,\epsilon^+\right]$$

are linear in ϵ^+ and ϵ^-, but the presence of the temporal partial derivatives unfortunately means that any rescaling of t will totally change the nonlinear problem as a whole. Thus, a doubling of the input fields will not mean that the fields appearing in the integrals double: propagation effects are more complicated than this. Importantly, however, on neglect of the temporal partial derivatives (the argument is: for a thin absorber - which does not at the same time become a weak absorber - the z derivative must dominate) the propagation equations obviously respond to the doubling in a linear and global manner with the temporal renormalisation serving to preserve the coefficients $\bar{n}$ and n_1 without "side-effects".

The conclusion to be drawn from extension of these arguments is that a two-way absorber, very thin in comparison with the symmetrically incident pulses, responds purely to

$\int \epsilon^2 dt$ whatever the pulse shape. This specialized two-way slow-absorber thus shares the one-way slow-absorber attribute (saturation by dose) but only the latter problem permits analytic solution.

Since no simple solutions of the two-way absorber problem allow for the change in shape of the propagating pulses within the material, it is instructive to deal with the problem from a perturbative point of view.

In the limit of a very weak absorber, $\kappa \to 0$ where $\kappa = n_u \sigma L$ and the changes to the pulses are tiny. However it is not required that the change to the absorber molecules be small as well. In fact, we shall now use the Bessel function results of section 4.2 to give the amount of saturation, possibly total, that the weak absorber undergoes.

Invoking energy conservation (i.e. that the energy gain represented by excitation out of absorber ground state must have come from the saturating pulses) we can write the change in pulse energy in the following perturbative manner;

$$j_{out} - j_{in} = 2\kappa \left[1 - e^{-2j_{in}} I_0\left[2j_{in}\right]\right] + O(\kappa^2)$$

and the simplest case where identical symmetric pulses cross the two-way absorber has been selected.

It is also necessary for these pulses to be long compared with the propagation distance. This thin absorber restriction can be circumvented by dividing a thick absorber into the regions where two pulses do and do not respectively overlap for more than half the total timescale: Bradley, New and Caughey [59] have adopted such an approach for square pulses.

CHAPTER 4

A NEW TREATMENT FOR THE SLOW TWO-WAY ABSORBER

4.1 Introduction.

In chapter 3, two-way absorber saturation was analysed in two special cases. In neither case was one important feature of the Fleck equations of section 3.3 manifested: that is, the repeated coupling between higher and higher spatial Fourier components of the population (as described by the infinite Fleck hierarchy). This is connected with the fact that only $\bar{n}$ and n_1 appear in the propagation equations, as we shall now refer to the pair of equations (1a) and (2a) obtained in section 3.3 from Maxwell's equations for the electromagnetic fields, and with a feature of each case chosen for study.

The fast absorber treatment (section 3.5a), culminating in a full solution of the propagation problem when the absorber is thin, or the pulse almost flat, began with the assumption that the population (equally, every component in the Fourier expansion) remains at its equilibrium value with the instantaneous field at all times. In other words, the saturating intensity changes so slowly in comparison with T_1 (the time to reach equilibrium) that the steady state result for the population applies. Although we calculated the values of $\bar{n}$ and n_1 from the hierarchy of difference equations (page 69), this was just another method of finding the zero and first Fourier components of the steady state population.

$$n = \frac{n_u}{1 + 4\,\sigma\, T_1 ([E^+]^2 + [E^-]^2 + 2E^+E^-\cos(2kz))}$$

For the second special case (section 3.5b) matters are more complicated. It would certainly have been impossible to solve the propagation problem if the full Fleck system had been used. However, as it was necessary to assume that one of the two waves was extremely weak (ϵ^-) the effect of n_2 in the rate equation for n_1 was vanishingly small. This meant

that the repeated coupling between components was not featured, as a 'side-effect' of the weak ϵ approximation.

Although the contribution from all the components, for the general case, is known about, they are never all taken into account. Instead, a truncation is often made after n_1 in all cases. Fleck has pointed out that when similar approximations are made in the theory of neutron scattering the consequences of arbitrary truncation are surprisingly small. It is quite usual to make the truncation even in the fast absorber case, where it is unnecessary.

Since it is unsatisfactory to make an assumption which is hard to justify, as is the case whenever the saturation is large, the present work attempts to avoid the truncation entirely. Surprisingly, this is not difficult for the slow absorber. Furthermore, given that with both pulses strong, the propagation problem has to be solved by numerical integration and not as in section 3.5(b), the exact equations for $\bar{n}$ and n_1 are as easy to use as the truncated versions which have previously been used.

4.2 Solution for the slow absorber

The Fleck hierarchy (section 3.3) of equations came about from a spatial Fourier expansion of the population rate equation derived earlier:

$$\frac{\partial n}{\partial t} = \frac{n_u - n}{T_1} - 4\sigma n\left[|E^+|^2 + |E^-|^2 + (E^+E^{-*}e^{-2ikz} + c.c.)\right] \quad (1)$$

Although other authors always apply Fleck's analysis to this equation (since the rapidly varying exponential terms are removed in the resulting equations), we have found the method to be undesirable in the slow absorber case. This is because Fleck's analysis suggests that all the equations in the infinite set matter; in fact, this section shows that they do not. The new result is central to the computer model of CPML which we will develop.

The slow absorber version of (1),

$$\frac{\partial n}{\partial t} = -4\sigma n\left[|E^+|^2 + |E^-|^2 + (E^+E^{-*}e^{-2ikz} + c.c.)\right] \quad (1a)$$

is integrated by inspection, without the rapidly varying terms posing any problem, and gives

$$n(t) = n(0)\ \exp\left\{-4\sigma\left[a + be^{-2ikz} + b^*e^{+2ikz}\right]\right\} \quad (2)$$

where

$$a = \int_0^t |E^+|^2 + |E^-|^2\ dt' \qquad \text{and} \qquad b = \int_0^t E^+E^{-*}\ dt'.$$

$n(0)$ is the population initially ($t = 0$) and could vary rapidly with z if a spatial hole-burning grating was already present at $t = 0$.

Writing $b = |b|\ e^{i\theta}$ we replace (2) by the more convenient expression

$$n(t) = n(0) \exp \{-4\sigma(a + 2|b| \cos(2kz - \theta))\} \qquad (3)$$

Considering the case where n(0) is slowly varying*, a Fourier expansion (B10) of eqn (3) yields

$$n_p = n(0) \exp\{ip\theta - 4\sigma a\} I_p(-8\sigma|b|) \qquad (4)$$

where I_p are modified pth order Bessel functions.

Hence the field-history integrals a(z) and b(z) determine the population, and in particular its Fourier components therefore follow without using the Fleck hierarchy. In our treatment, the change in 'dose' a and 'cross-dose' b determine the motion of any n_p, whereas in the conventional theory, neighbouring Fourier components drive each other's motion according to coupled equations (section 3.3). The latter (coupled equations) approach, though mathematically correct, is clearly a poorer physical description of a saturation process.

---

*Under this assumption, where n(0) hardly varies with z over distances of a few wavelengths we have initially $\bar{n} = n(0)$ and $n_p = 0 \quad (p > 0)$. Expression (4) applies to this case.

More generally, n(0) includes gratings and we have $\bar{n} = \bar{n}|_0$, $n_p = n_p|_0$ initially. From (3) we get

$$n(t) = \left\{\bar{n}|_0 + \sum_{p=1}^{\infty}\left[n_p|_0 e^{-2pikz} + c.c\right]\right\}$$

$$.e^{-4\sigma a}\left\{I_0(-8\sigma|b|) + \sum_{p=1}^{\infty}\left[e^{ip\theta}I_p(-8\sigma|b|)e^{-2pikz} + c.c\right]\right\}$$

If we collect terms of the type $e^{\pm 2mikz}$ and compare with (B10), it follows that

$$\bar{n} = \sum_{p=-\infty}^{\infty} n_{-p|0} \exp(ip\theta - 4\sigma a) I_p(-8\sigma|b|) \qquad (5a)$$

$$n_m = \sum_{p=-\infty}^{\infty} n_{m-p|0} \exp(ip\theta - 4\sigma a) I_p(-8\sigma|b|) \qquad (5b)$$

with $n_{-m|0} = n_{m|0}^{*} (\equiv \bar{n}_{|0}$ for $m = 0)$.

Note that $I_p = I_{-p}$ for all integers p. To check consistency, let us saturate the initially unmodulated absorber in two stages, using eqns (5) for the second step. If the original doses are a_1 and b_1 respectively, we use the values

$$\bar{n}_{|0} = n(0)\, e^{-4\sigma a_1} I_0(-8\sigma|b_1|)$$

$$n_{p|0} = n(0) \exp(ip\theta_1 - 4\sigma a_1)\, I_p(-8\sigma|b_1|)$$

$$a = a_2$$
$$b = b_2 = |b_2|\, e^{i\theta_2}$$

in step 2. If the results reduce to

$$n_p = n(0)\exp\{ip\theta - 4\sigma(a_1 + a_2)\}\, I_p(-8\sigma|b_1 + b_2|)$$

where $\theta = \arg(b_1 + b_2)$ then consistency with (4) is shown.

The above relation is in fact easily demonstrated by applying the sum rule:

$$\sum_{p+q=m} e^{i(p\alpha + q\beta)} I_p(|x|) I_q(|y|) = e^{im\varphi} I_m(|z|)$$

where $|z|e^{i\varphi} = |x|e^{i\alpha} + |y|e^{i\beta}$.

Recognising that the $\bar{n}$ component is obtained by setting p = 0 in eq (4), we use the recurrence relation

$I_{j-1}(z) - I_{j+1}(z) = (2j/z)I_j(z)$ to obtain

$$n_2 = [\ \bar{n} - |n_1/4\sigma b|\ ]\ e^{2i\theta} \qquad (6)$$

This key result allows the hierarchy of section 3.3 to be terminated without approximation. Higher equations do not matter, in modelling the evolution of $\bar{n}$ and n_1, because n_2 appearing on page 60 in (2b) is already determined.

For the purposes of a computer model of a two-way absorber we need only to provide equations governing $\bar{n}$, n_1, E^+ and E^-. First we shall construct these equations using the theory above, taking the opportunity to express them in a form convenient to use. The equations will then be analysed explicitly, for it should not be necessary to involve 'hidden' features such as the Bessel functions when asking what goes on.

The representation chosen for the complex variables will be polar, since (4) shows that the arguments of the n_p can be deduced easily. Whilst $\bar{n}$ is real (as also apparent from eqn. (B10), we can write $n_1 = -|n_1|e^{i\theta}$ where the minus sign allows for the fact that $I_p(-|x|)$ has polarity of $(-)^p$. Setting $E^+ = \epsilon^+ e^{i\varphi_+}$ and $E^- = \epsilon^- e^{i(\varphi_+ - \Delta)} = \epsilon^- e^{i\varphi_-}$ we have from equations (1a) and (1b) on page 59,

$$\frac{1}{v}\frac{\partial \epsilon^{\pm}}{\partial t} \pm \frac{\partial \epsilon^{\pm}}{\partial z} = -\frac{\sigma}{2}\left[\bar{n}\,\epsilon^{\pm} - |n_1|\,\epsilon^{\mp}\cos(\theta - \Delta)\right] \qquad (7a)$$

$$\frac{1}{v}\frac{\partial \varphi_{\pm}}{\partial t} \pm \frac{\partial \varphi_{\pm}}{\partial z} = \pm\frac{\sigma}{2}|n_1|\frac{\epsilon^{\mp}}{\epsilon^{\pm}}\sin(\theta - \Delta) \qquad (7b)$$

where, to recapitulate:

$$\theta = \arg(b) = \arg\int_0^t \epsilon^+\epsilon^- e^{i\Delta}dt$$

$$\Delta = \arg(\dot{b}) = \arg E^+E^{-*} = \varphi_+ - \varphi_-$$

The description is completed with equations for $\bar{n}$, $|n_1|$ and $\cos(\theta - \Delta)$, $\sin(\theta - \Delta)$ appearing on the right hand sides of (7a) and (7b) and for $|b|$, needed in (7g) below. After differentiating $|b|e^{i\theta} = \int \epsilon^+ \epsilon^- e^{i\Delta}\, dt$, we can show that

$$\frac{\partial |b|}{\partial t} = \epsilon^+ \epsilon^- \cos(\theta - \Delta) \tag{7c}$$

and we use $\frac{\partial \theta}{\partial t} = -\frac{\epsilon^+ \epsilon^-}{|b|} \sin(\theta - \Delta)$ where $\Delta = \varphi_+ - \varphi_-$ to write

$$\frac{\partial \cos(\theta - \Delta)}{\partial t} - \sin(\theta - \Delta) \frac{\partial \varphi_+}{\partial t} + \sin(\theta - \Delta) \frac{\partial \varphi_-}{\partial t}$$

$$= |b|^{-1} \epsilon^+ \epsilon^- \sin^2(\theta - \Delta) \tag{7d}$$

$$\frac{\partial \sin(\theta - \Delta)}{\partial t} + \cos(\theta - \Delta) \frac{\partial \varphi_+}{\partial t} - \cos(\theta - \Delta) \frac{\partial \varphi_-}{\partial t}$$

$$= -|b|^{-1} \epsilon^+ \epsilon^- \sin(\theta - \Delta)\cos(\theta - \Delta) \tag{7e}$$

Finally, from the two lowest Fleck equations (for slow absorber) come

$$\frac{\partial \bar{n}}{\partial t} = -4\sigma \left\{ \bar{n} \, (\epsilon^{+2} + \epsilon^{-2}) - 2|n_1| \epsilon^+ \epsilon^- \cos(\theta - \Delta) \right\} \tag{7f}$$

$$\frac{\partial |n_1|}{\partial t} = -4\sigma \left\{ |n_1| (\epsilon^{+2} + \epsilon^{-2}) - \epsilon^+ \epsilon^- \cos(\theta - \Delta) \left[2\bar{n} - |n_1/4\sigma b| \right] \right\} \tag{7g}$$

Note that (6) has been used as promised, in the n_1 equation, which was therefore expressed

$$\frac{\partial}{\partial t} \left[- |n_1| e^{i\theta} \right] = -4\sigma \left\{ - |n_1| e^{i\theta} (\epsilon^{+2} + \epsilon^{-2}) + \bar{n} \epsilon^+ \epsilon^- e^{i\Delta} \right.$$

$$\left. + \left\{ \bar{n} - \left| \frac{n_1}{4\sigma b} \right| \right\} e^{2i\theta} \epsilon^+ \epsilon^- e^{-i\Delta} \right\}$$

leading to the intermediate result,

$$\frac{\partial|n_1|}{\partial t} + i|n_1|\frac{\partial\theta}{\partial t} = -4\sigma\Big\{+|n_1|(\epsilon^{+2} + \epsilon^{-2}) - \bar{n}\epsilon^{+}\epsilon^{-}$$

$$\left[e^{i(\Delta-\theta)} + e^{-i(\Delta-\theta)}\right] + \left|\frac{n_1}{4\sigma b}\right|\epsilon^{+}\epsilon^{-}e^{-i(\Delta-\theta)}\Big\}$$

whose real part was (7g) and imaginary part simply reduced to the formula for $\frac{\partial\theta}{\partial t}$ already obtained.

Equations 7a - 7g were expressed as finite difference equations, taking the first order approximation for all derivatives, when implementing this method on the computer in Pascal. In all, there are 9 separate equations. For the purposes of this section a simpler subset of the equations will be discussed - (7a), (7c), (7f) and (7g) - which results if $\theta = \Delta$ for all z, t.

Consider the case where unchirped pulses collide in the two-way absorber. Since Δ is then constant we may remove $e^{i\Delta}$ from the integral $\int\epsilon^{+}\epsilon^{-}e^{i\Delta}$ so that $\theta = \Delta$ results. Without loss of generality, the subset equations

$$\frac{1}{v}\frac{\partial\epsilon^{\pm}}{\partial t} \pm \frac{\partial\epsilon^{\pm}}{\partial z} = -\frac{\sigma}{2}\left[\bar{n}\,\epsilon^{\pm} - |n_1|\,\epsilon^{\mp}\right] \tag{8}$$

$$\frac{\partial|b|}{\partial t} = \epsilon^{+}\epsilon^{-} \tag{9}$$

$$\frac{\partial\bar{n}}{\partial t} = -4\sigma\left\{\bar{n}\,(\epsilon^{+2} + \epsilon^{-2}) - 2|n_1|\epsilon^{+}\epsilon^{-}\right\} \tag{10}$$

$$\frac{\partial|n_1|}{\partial t} = -4\sigma\left\{|n_1|(\epsilon^{+2} + \epsilon^{-2}) - \epsilon^{+}\epsilon^{-}\left[2\bar{n} - |n_1/4\sigma b|\right]\right\} \tag{11}$$

now apply. It is these equations which we now propose to analyse.

In (8) there is a reflection term which has the opposite effect of the natural absorption, $\bar{n}$, term. The light scattered into one beam from the other by the periodic structure created during the mutual interaction of both beams adds up in phase with the unscattered light in that direction. Hence there appears to be reduced absorption. In an amplifying medium analogous theory would show that the

scattered light has the opposite phase and subtracts intensity from the beams. Both these results depend physically on the fact that energy in the overlapping electric fields is concentrated at the field anti-nodes where, 'fortuitously', the amount of saturation also is larger than average (e.g. population minima, in the case of the absorber). For the region where $\epsilon^+ \approx \epsilon^-$ the largest effect ($|n_1| = \frac{1}{2}\bar{n}$ since population can not go negative in (B10) as there is nothing physically left to saturate at the dips in such an extreme) if n_2 and higher components are ignored is found to be a quartering of intensity absorption coefficient.

With the presence of a growing $|n_1|$ term, it is apparent that the absorber saturates earlier than it does with the same dose-rate ($\epsilon^{+2} + \epsilon^{-2}$) but zero interference term, $\epsilon^+\epsilon^-$. This enhanced saturation, central to CPML, persists only as long as the counterpropagating pulses coincide in the absorber. Equation (11) contains the terms driving the growth of $|n_1|$ and also has a mechanism to prevent the rise from continuing indefinitely. Considering the early stages and noting that $|n_1/4\sigma b| \approx \bar{n}$ while $|n_1|$ itself is still negligible (set $|b| \to 0$ in (4) and use $I_1(x) \approx \frac{1}{2}x$ to first order) this equation becomes

$$\frac{\partial |n_1|}{\partial t} \approx + 4\sigma\bar{n}\epsilon^+\epsilon^-, \quad \text{solution } 4\sigma\bar{n}|b|, \text{ using (9)}$$

but once $|b|$ is significant these approximations break down and $|n_1|$ will significantly exceed $4\sigma\bar{n}|b|$. The term $|n_1/4\sigma b|$ in (11) is then able to prevent a runaway growth from occurring. For $|b| \to \infty$ all $|n_p|$ have equal values (which approach zero), so the right hand sides of (10) and (11) both contain the factor $-4\sigma(\epsilon^{+2}+\epsilon^{-2} - 2\epsilon^+\epsilon^-)$ which is definitely negative showing that the compensation mechanism worked.

The equations which have been developed in this section describe the two-way absorber exactly. We now show how to obtain the approximate rule used by other authors [60,61].

A weak absorber that is thin enough for the saturating pulses (which must be mirror images of each other) to have envelopes that are constant over the thickness L, has $\epsilon^{+} = \epsilon^{-} = \epsilon(t)$ where ϵ is independent of z. For this mathematical limit the effective absorption, before saturation and afterwards is given as:

ABSORPTION BEFORE: $n_u \sigma L$

SATURATED ABSORPTION: $[\bar{n} - |n_l|]\sigma L$

$$= n_u \sigma L \, e^{-2J}\left[I_0(2J) - I_1(2J)\right]$$

where $J = \int_{-\infty}^{t} 4\sigma\epsilon^2(t)$

The rule covers only the case where $J << 1$, so we expand the transcendental functions* obtaining for the saturated absorption $n_u \sigma L.[1 - 3J + 5J^2 \ldots.]$. This will now be compared with the conventional absorber.

Approximating equation 5 (page 23) we have

---

*$e^{-x} = 1 - x + \frac{1}{2}x^2 - \frac{1}{6}x^3 + 0(x^4)$; $I_0(x) = 1 + \frac{1}{4}x^2 + 0(x^4)$;

$I_1(x) = \frac{1}{2}x + \frac{1}{16}x^3 + 0(x^5)$.

$$
\begin{aligned}
j_{out} &= \ln(1 + e^{-n_u\sigma L}(j + \tfrac{1}{2} j^2 + \tfrac{1}{6} j^3 \ldots.)) \\
&= \ln(\, 1 + j(1 - n_u\sigma L)(1 + \tfrac{1}{2} j + \tfrac{1}{6} j^2) \\
&\qquad + 0([n_u\sigma L]^2) + 0(j^4) \\
&= j(1 - n_u\sigma L)(1 + \tfrac{1}{2} j + \tfrac{1}{6} j^2) \\
&\qquad - \tfrac{1}{2} j^2(1 - 2n_u\sigma L)(1 + j) \\
&\qquad + \tfrac{1}{3} j^3(1 - 3n_u\sigma L) + \ldots. \\
&\approx j[1 - n_u\sigma L(1 - \tfrac{1}{2} j + \tfrac{1}{6} j^2)] \qquad (12)
\end{aligned}
$$

This is a special case (slow absorber extreme) of an expansion provided by Bradley, New and Caughey [59] and can be verified by setting $T_p' = 0$ in their eqn. (6). To obtain the instantaneous absorption we must differentiate $(j_{out} - j)$ with respect to j which yields the result $-n_u\sigma L.[1 - j + \frac{1}{2}j^2]$ which was used by Haus [8] and later authors in the study of conventional passive mode-locking. Note that terms $0([n_u\sigma L]^2)$ would allow for the reduction in saturation rate away from the entrance to a strong absorber, as is the case both in practice and with the computations of Ch2 and Ch5. Returning to the two-way absorber theory we find that [59] provides the result from replacing j by $4j\sin^2 kz$ everywhere in (12) and then spatially averaging across this interference pattern: the instantaneous absorption $-n_u\sigma L[1 - 3j + 5j^2]$ is confirmed by that approach.

If we just increase the energy j in Haus' result by a factor of three, the wrong j^2 term for the two-way instantaneous absorption is used. This reveals an error in [62].

4.3 On the general solution.

The very useful equation (6) connecting the population Fourier components can only be extended to include relaxation (see(1)) if special choices for the time-variation of the saturating fields are made.

As an example, consider the case where saturation occurs rapidly compared with T_1 but then we wish to know how the population structure has developed after a further interval, t, without any applied fields but lasting long enough for significant recovery. During the interval t each component relaxes independently since the coupling terms in the Fleck hierarchy are zero, and the result is

$$\bar{n} = \bar{n}_{slow}\, e^{-t/T_1} + n_u(1 - e^{-t/T_1})$$

$$n_p = n_p^{slow}\, e^{-t/T_1} \qquad (p > 0)$$

where $\bar{n}_{slow}$, n_p^{slow} are independent of t and were fixed by the initial rapid saturation that is described by the results of the previous section. From the fact that (6) applied at t=0, we therefore have as our result,

$$n_2 = [\bar{n} - n_u(1 - e^{-t/T_1}) - |n_1/4\sigma b|]e^{2i\theta}.$$

The point which must be recognised is that it is not a general result since there should be no applied fields while this formula applies.

In the rest of this section we give a general solution for $\bar{n}$ and n_p which is free from the above restrictions. It will then become clear that an extension of (6) to cover these answers is impossible. This important conclusion may be interpreted as a 'lack of sufficient information' that $\bar{n}$ and n_1 possess about the saturating fields which existed at past times: n_2 cannot be specified without that missing additional

information, which is absent even in extensions of (6) that one might imagine - e.g. with use of

$$b' = \int_0^t E^+E^{-*}e^{(t'-t)/T_1}\,dt' \text{ instead of } b = \int_0^t E^+E^{-*}\,dt'.$$

As well as proving these observations, the general formula (equation (15) below) will be useful in its own right for those saturation grating calculations, outside mode-locking theory, where the field history is a known quantity from the outset.

As in Section 4.2 and as in an early work on two-way amplifiers [63], we use a solution of (1) as the starting point and find it unnecessary to work from the infinite set of Fleck equations.

Separating off an integrating factor, the trial solution is

$$n(t) = A(t)\exp\{-4\sigma(a + 2|b|\cos(2kz - \theta)) - t/T_1\}. \quad (13)$$

Substituting into (1) and integrating, we obtain

$$A(t) = A(0) + \frac{1}{T_1}\int_0^t n_u\, e^{\frac{t''}{T_1}} \exp\{-4\sigma(a''+2|b''|\cos(2kz-\theta''))\}dt'' \quad (14)$$

where a", b", θ" are now evaluated at t".

We may now combine (13) and (14) to yield

$$n(t) = [n(0)\ \exp\{-4\sigma(a + 2|b|\cos(2kz - \theta)\}]e^{-t/T_1}$$

$$+ \frac{1}{T_1}\int_0^t n_u e^{-(t-t")/T_1}\exp\{-4\sigma(a - a" + (b - b")e^{-2ikz}$$

$$+ (b - b")^* e^{+2ikz})\}$$

after some rearrangement.

It is easy now to evaluate the Fourier components of this solution in a precisely similar manner to the previous section [see (2)-(5)] on the slow absorber, obtaining

$$n_p = n_p^{slow}(t)e^{-t/T_1}$$

$$+ \frac{1}{T_1}\int_0^t C_p(t,t")e^{-(t-t")/T_1}\,dt" \qquad (15)$$

with n_p^{slow} given by the incomplete (because relaxation is now important) results for n_p, (4) or (5) as appropriate for the choice of initial conditions. The second term involves $C_p(t,t")$ which is defined by the right hand side of (4) with the lower limits on the integrals a and b changed to t" and n(0) replaced by n_u.

When the new result is applied to the earlier example of the slow absorber, then $n_p^{slow}(t)$ is obtained by taking the limit of (15) as $T_1 \to \infty$. As T_1 is decreased, we can see how the effects of relaxation gradually set in. Considering the example introduced at the start of this section, where pure recovery is assumed we have $C_p = 0$ for $p > 0$ and $C_0 = n_u$ whereupon (15) with $p = 0$ is seen to account correctly for the more complicated behaviour of $\bar{n}$.

The general solution (15) demonstrates that 'doses' over subintervals t" to t each contribute to the current value of n_p, although the exponential multiplying C_p reduces the

influence of those contributions starting far in the past (compared with T_1).

Consequently the field history long ago does not matter, the first term in (15) also ceasing to be important for $t>>T_1$ even though $n_p^{slow}(t)$ itself never recovers from earlier saturation. Obviously for $t>>T_1$ it is still possible for the absorber, having undergone some recovery, to be saturated again by short pulses and be thought of as a slow absorber again between times t and $t+\Delta t$. In this case the general formula becomes:

$$n_p(t+\Delta t) \approx 0 + \frac{1}{T_1}\int_0^{t+\Delta t} C_p(t+\Delta t,t'')e^{-(t+\Delta t-t'')/T_1}\,dt''$$

$$\approx \frac{1}{T_1}\int_0^{t} C_p(t+\Delta t,t'')e^{-(t-t'')/T_1}\,dt''$$

where $\Delta t << T_1$. Here we have been careful still to include in C_p the extra 'doses' during Δt which cause rapid saturation with $n_p(t)$ turning to $n_p(t+\Delta t)$. From the sum rule in section 4.2 (footnote) we may expand

$$C_p(t+\Delta t,t'') = \sum_{r=-\infty}^{\infty} \frac{1}{n_u} C_{p-r}(t,t'')\, C_r(t+\Delta t,t)$$

so therefore, (exchanging the order of $\int$ and Σ)

$$n_p(t+\Delta t) \approx \sum_{r=-\infty}^{\infty}\left[\frac{1}{T_1}\int_0^{t} C_{p-r}(t,t'')e^{-(t-t'')/T_1}dt''\right]\left[\frac{1}{n_u} C_p(t+\Delta t,t)\right]$$

$$\approx \sum_{r=-\infty}^{\infty} n_{p-r}(t)\cdot\left[\frac{1}{n_u} C_r(t+\Delta t,t)\right]$$

which has exactly the form of the results derived already for the slow absorber (5) except that a and b appearing there

must be integrals over the new period t to t+Δt and not 0 to t.

The purpose of the general solution is of course to treat the more complicated cases where relaxation and saturation occur simultaneously. It is easily shown that (15) in fact constitutes the limit, as $N \to \infty$, of a series of steps each covering a time interval Δt (= t/N) in which a pure saturation (slow absorber description) precedes a 'lumped' recovery using the pure relaxation formulae. Here we shall indicate a typical one of these steps, the final step $t-\Delta t \to t$ which is

$$n_p(t) = \left\{ \sum_{r=-\infty}^{\infty} n_{p-r}\,(t - \Delta t).\left[\frac{1}{n_u}\, C_r\,(t,t-\Delta t)\right]\right\} e^{-\Delta t/T_1} + \delta_{op}\, n_u\, \frac{\Delta t}{T_1} \qquad (16)$$

The term in curly brackets is equivalent to (5b) and the remaining operations then describe the relaxation which occurred. Appendix H makes the connection with (15), using the principle of induction.

The general formula, (15) solves the Fleck equations with recovery included. It is unlikely that this would be 'guessed' if those equations (and not (1)) were our original concern in this section. In the previous section we could at this point simplify the Fleck system (without recovery) using a recursion relation involving $\bar{n}$, n_1, n_2 and b, since only the total doses a and b affected each of the n_p. The specific field history was irrelevant in that case. In general, however, (15) shows that an infinity of instantaneous doses $C_p(t,t")$ is required that covers every starting point (t") in the past. Here, the full details of the field history are involved in n_p behaviour (apart from a limited 'long-term memory' in the system since $e^{-(t-t")/T_1}$ multiplies C_p).

4.4 The example of a step function.

In this example both fields are taken as switched off until t=0. Then both ϵ^+ and ϵ^- have constant equal values for all t>0. The behaviour after a time $\tau \ll T_1$ must follow the slow absorber result; that for $\tau \gg T_1$ becomes the same as a fast absorber. By applying the general solution to this case, the intermediate change-over is clarified.

Solving (1) we have, for the total absorber population,

$$\frac{n(t)}{n_u} = \begin{cases} 1 & t < 0 \\ \dfrac{1 + (I/I_s)\, e^{-\frac{t}{T_1}(I + (I/I_s))}}{1 + (I/I_s)} & t \geq 0 \end{cases}$$

Where $I = (\epsilon^+)^2 + (\epsilon^-)^2 + 2\epsilon^+\epsilon^- \cos 2kz$, $I_s = 1/4\sigma T_1$ and $\epsilon^+ = \epsilon^- = \text{const}$. Since the fields are time independent they have been taken to be real without loss of generality. Note that I independent of time is essential here.

To calculate the Fourier components of this result as a function of time is one way to proceed. Silberberg and Bar-Joseph [64], in work on phase conjugation, essentially carry out such a step when numerically evaluating certain time-dependent spatial averages which arise. The general solution to be applied shortly leads to a time-dependent recursion relation between the required Fourier components, without actually going to the trouble of calculating them.

Unfortunately the following discussion does not readily extend to other pulse shapes, for reasons which will become clear. This is a serious problem because, except when the absorber is optically thin* (i.e. small modifications to the

---

*for example Silberberg and Bar-Joseph used a thin coating on glass of eosin dye dispersed in gelatin [64].

pulses while saturating the matter which they traverse), pulses of width similar to the absorber undergo significant changes in shape: they could not be taken to be square pulses even if it were a good approximation on entry. The calculations later in this thesis for CPML are based on the slow absorber (which is appropriate to practical systems) reduction of the Fleck hierarchy which is not restricted to a particular pulse shape.

From the general solution, the population may be written in the form

$$n_p(t) = n_p^{slow}\, e^{-t/T_1} + F_p \quad ,$$

$$\text{where } F_p = T_1^{-1} \int_0^t e^{-(t-t")/T_1}\, C_p(t,t")dt". \qquad (17)$$

Consider the equation of motion for F_p:

$$\frac{dF_p}{dt} = \frac{d}{dt}\left[n_p - n_p^{slow}\, e^{-t/T_1}\right]$$

$$= \frac{n_p^{slow}\, e^{-t/T_1}}{T_1} + \left[\frac{dn_p}{dt} - e^{-t/T_1}\,\frac{dn_p^{slow}}{dt}\right]$$

$$= \frac{n_p^{slow} e^{-t/T_1}}{T_1} + \left[\frac{\delta_{op} n_u - n_p}{T_1} - 8\sigma\epsilon^2\left[F_p + \frac{F_{p-1} + F_{p+1}}{2}\right]\right]$$

where we have used the equations on page 60 with $\epsilon^+ = \epsilon^- = \epsilon$, and $\delta_{op} = 0$ unless p = o when it is 1 and $n_p = \bar{n}$.

The terms in brackets all cancel for the special case of ϵ = constant considered here, as shown below.

Integrate (17) by parts using

$$\frac{dc_p}{dt"} = 8\sigma\epsilon^2\left[C_p + \frac{C_{p-1} + C_{p+1}}{2}\right] \text{ to obtain}$$

$$F_p = C_p(t,t) - e^{-t/T_1} C_p(t,0) - \int_0^t e^{-(t-t")/T_1} \frac{dC_p}{dt"} dt"$$

$$= \delta_{op} n_u - n_p^{slow} e^{-t/T_1} - 8\sigma\epsilon^2 T_1 \left[F_p + \frac{F_{p-1} + F_{p+1}}{2} \right]$$

Using this recursion relation to simplify the previous result leads to the following equation of motion:

$$\frac{dF_p}{dt} = \frac{n_p^{slow} e^{-t/T_1}}{T_1} = \frac{n_p - F_p}{T_1} \qquad (18)$$

Note that we have assumed $n(0) = n_u$ because we used $C_p(t,0) = n_p^{slow}(t)$ which only applies in that case (C_p is defined immediately below equation 15). More general initial conditions can however be taken (see appendix G).

Result (18) is intuitively sensible. For example when $t > T_1$, $F_p \approx n_p$ and we have a steady state saturation. It is clear that ϵ = constant (for $t > 0$) is necessary for such behaviour, and so it is explained why this constraint was needed in the preceeding derivation. For $t << T_1$ F_p is very small (see (17)) and $e^{-t/T_1} \approx 1$ so that $n_p = n_p^{slow}$, the slow absorber case, is approached.

From our intermediate results in this calculation it is now extremely easy to obtain a recursion formula for elimination of n_2 in the spirit of the method already developed in the slow absorber case. As already indicated, the closed system of equations to be given can apply only for the square pulse assumed in this section.

The resulting system is as follows (see Appendix G)

$$\frac{dF_1}{dt} = \frac{n_1 - F_1}{T_1} \qquad (19a)$$

$$\frac{d\bar{n}}{dt} = \frac{n_u - \bar{n}}{T_1} - 8\sigma\epsilon^2(\bar{n} + n_1) \qquad (19b)$$

$$\frac{dn_1}{dt} = \frac{-n_1}{T_1} \cdot\cdot 8\sigma\epsilon^2\left[n_1 + \frac{\bar{n} + n_2}{2}\right] \qquad (19c)$$

and, to close the system:

$$n_2 = \bar{n} + \frac{1}{4\sigma\epsilon^2}\left[\frac{n_1 - F_1}{t} + \frac{\bar{n} - n_u - n_1}{T_1}\right] \qquad (19d)$$

Compared with the slow absorber analysis there appears to be an extra equation (19a). This is used to supply F_1 which is now required in the recursion relation. In the slow absorber limit $t << T_1$ and we have said already that $F_p \approx 0$. Then $n_2 \approx \bar{n} + (n_1/4\sigma\epsilon^2 t)$ which is the same as (6) with $\epsilon^+ = \epsilon^- = \epsilon$.

Another case where F_1 is unnecessary is that of the fast absorber, for which we have

$$n_2 = \bar{n} + \frac{\bar{n} - n_u - n_1}{4\sigma\epsilon^2 T_1} .$$

This relationship is indeed satisfied by the Fourier components which were calculated in chapter 3.

To summarise, mathematically all that has been achieved by this example is to obtain differential equations for the time-dependent Fourier coefficients of the n(t) which is specified at the start of this section. In doing so, the interesting recursion relation 19d was discovered; it bridges the two limits normally assumed, for the special case of square pulses (of equal amplitude) from both directions.

CHAPTER 5

COMPUTER MODEL OF COLLIDING-PULSE MODE-LOCKING

5.1 Introduction

This chapter is concerned with a computer model of colliding-pulse mode-locking. The main advance over previous treatments of CPML is that it is no longer necessary to assume that the pulse-lengths are wide in comparison with the thickness of the saturable absorber jet. The two-way absorber theory of chapter 4 is used in the model.

Analytic predictions concerning CPML have been given [61] using Haus' model (see chapter 2) but the two-way absorber was assumed to be thin. The gain parabola then involves the approximate absorption term $n_u \sigma L\ [1 - 3J + 5J^2]$ which appeared in section 4.2 after a whole series of approximations had been made. The differences between conventional passive mode-locking, colliding-pulse mode-locking and contacted absorber [62] mode-locking have been studied in detail within the above context.

From the results given in chapter 2 we know that numerical simulations using rate equations with a bandwidth limiting element included do allow more realistic calculations of passive mode-locking to be carried out. The price, however, of the whole-cavity simulation approach (section 2.3) is that the main feature of mode-locking - which is the presence of pulses much shorter than the cavity transit time - is not included due to the very large number of meshpoints that would be required. In any event, since the two-way absorber theory takes on a simple form for the slow absorber, we do not wish to use a technique in which recovery has to be included in the material rate equations while the pulse propagates.

A partial-cavity simulation approach is introduced in this chapter. It is very close in spirit to the original "bouncing ball" approach: recovery between transits is calculated in one go. Special care has been taken to compute consistent values for the fields in the exponential wings of the pulse. This is important because, outside the compression zone, we found that a continuous injection signal (which an error in the boundary value would be like)

seriously affects the pulse-shape - we do not want to mask the two-way absorber performance under study. Note that the concern about boundary conditions stems from related work on mode-locking by synchronous pumping [65], where if there were not noise injected no steady state would even exist. This is not the case in passive mode-locking (section 2.8).

Recently Yoshizawa and Kobayashi [66] carried out the first computer simulations of CPML, improving upon the approximate treatments. They used a partial-cavity simulation and predicted that the pulses have steeper leading edges than trailing edges. It was still assumed in this work that the two-way absorber was thin.

In the sections to follow, we discuss the design of the computer model and present preliminary findings. A novel solution to the boundary condition problem has been to measure the slip of the entire pulse in local time in order to determine the trailing edge by the consistency technique which proved successful in section 2.8.

5.2 Treatment of colliding pulses

The two-way absorber (figure 1b) may be modelled using equations 7a - 7g as discussed in great detail in section 4.2. It is assumed that no recovery takes place during the interaction (slow absorber approximation). For this absorber, propagation effects and Bragg scattering from the induced grating are exactly taken into account. In the conventional case (figure 1a) the physical thickness of the element is not important (a "lumped" absorption coefficient appeared in section 2.3): apart from the transit time within the absorber, the effect is to multiply the incident field by $e^{-B(t)/2}$. This is not the case when there is a grating and therefore the thickness needs to be divided up by the numerical mesh. This would have been very difficult to implement without the new partial-cavity approach in which the mesh is only required in the vicinity of the pulse. The pulse width can be of the same order as the absorber thickness.

For convenience we shall assume that the colliding pulses are identical and meet exactly at the centre of the absorber. This is discussed in the next section. The hybrid absorber in figure 1c could not exist in practice but it exactly models one "channel" of the absorber in figure 1b. We shall not model the mirror-image channel because it is assumed to be identical. The advantage of making the absorber take this form is that the program will look similar when absorbers A and C are exchanged. Note that they are distinguishable even for a short pulse (compared with thickness d) which does not overlap with itself in C to produce a saturation grating. If it was important to study case B explicitly (for CPML with non-identical pulses) the program would not be difficult to expand.

We can speculate that the pulse-widths in a CPML simulation will scale not only with the bandwidth of the filter but also with the thickness of the absorber. Our program is the first to make this interesting possibility

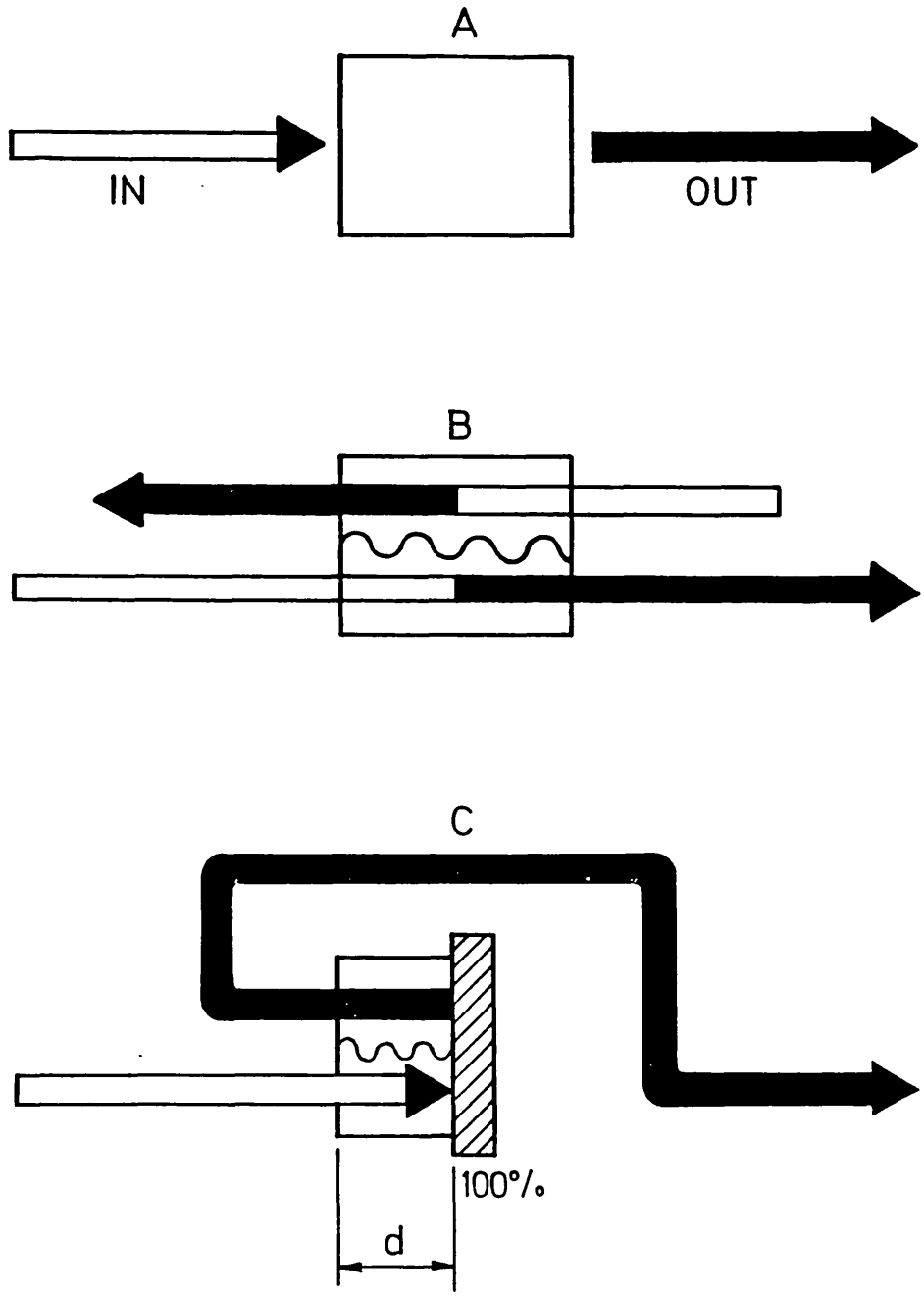

A Conventional (one-way) absorber
B Two-way absorber
C Model hybrid absorber using contacted mirror

FIGURE 1. SATURABLE ABSORBERS TO FIT IN THE RING CAVITY.

accessible for study. The compression zones may also be significantly perturbed away from the "bouncing ball" predictions.

5.3 Partial cavity simulations

Simulations commence from a hyperbolic secant pulse that is about five times shorter than the amount of local-time mesh provided (typically T_{MAX} = 100 meshpoints). It is assumed throughout the subsequent evolution that the edges of the frame are exactly exponential functions, but the logarithmic slopes are allowed to evolve.

At the start of a transit there are no existing field values inside the hybrid absorber. However since the earliest fields are not sufficiently intense to cause any saturation in the time taken to propagate through the element, the internal field values are passed into their positions as if the absorber were a linear element. Note that the fields inside the absorber are recorded in the program using a separate length of (equally spaced) numerical mesh in which both forward and backward propagating fields are stored (length typically 10 to 30 meshpoints): this is "invisible" to the main (unidirectional) mesh. Before collecting any output from the absorber its internal mesh is "filled" using points from the extreme leading edge of the pulse represented in the main mesh. They are all given equal amplification but only receive (varying) proportions of the full absorption depending on the point reached in the absorber mesh when the initialisation phase ends. In order that the pulse in the main mesh always keeps away from the edges (see below), only some of the leading edge is used to fill the absorber mesh. To initialise the fields between the point reached by the "filling" process and the output point of the absorber, backwards extrapolation is made by assuming that inputs before the start of the leading edge had the same exponential growth as that measured later on.

At the start of every cavity transit the main mesh is checked to see whether the peak of the pulse has slipped away from the centre of the frame. As well as the nonlinear slip there is always a delay of 2d which is the interval between input and output from the absorber element. The combined slip (SL) determines how many leading edge points may be used

in the absorber initialisation, discussed above. A simple choice of definition, that the output E[1] is the field at the ouput of the absorber even though the field at the input is E[SL], ensures that slip is fully compensated for on the next round trip. This prevents the pulse from moving far from the centre of the main mesh.

All the remaining input points are now passed through ampifier, absorber, linear loss and filter. The amplifier saturation and the stepping of difference equations within the absorber are carried out after each timestep. Due to the slip compensating definition, the final (trailing edge) input E[TMAX] is processed before the need for inputs has ceased. The remaining values are generated in a manner that hopefully does not prejudice the system's choice of trailing edge boundary condition. The method is to use the slip of the peak and the gain for the final input field (E[TMAX] → E[TMAX - SL]) to determine the exponential slope to use for extrapolation. As the steady state is gradually approached by the peak this will ensure that the consistent boundary condition is reached which we studied in chapter 2. The logarithmic slope is just ln(g')/SL where g' is taken here to include everything affecting the profile. The filter, for example, does not have to be considered separately. (The ratio g' is obviously <u>not</u> the same as the physical gain which determines stability and which is the one discussed up until now.)

The filter is implemented in the same way as in the whole-cavity work of section 2.3. The problem of finding the <u>first</u> output from the filter was solved in a similar way to that of "filling" the absorber: the analytic result for an exponential rising edge was used.

The specialised methodology described in this section and in appendix J (where the modular Pascal implementation is described) made possible the first realistic model of colliding pulse mode-locking, to be described next. Future work would benefit from more elegant formulations of the partial cavity approach, which perhaps will be found now that the present work has shown the principle to be good.

5.4 Computer model of colliding-pulse mode-locking

As mentioned in chapter 1, the positioning of the absorber jet in a ring cavity one quarter of the total perimeter away from the amplifier jet leads to counter-propagating mode-locked pulses timed to meet in the two-way absorber.

Figure 2 shows the locations of the cavity elements in the opened out ring. The times and distances are in cavity transit units. It is clear that the amplifier is crossed by a single pulse every half CPML cycle whereas the absorber is crossed by the colliding pulses once per cycle. Thus the maximum absorber saturation, but the least amplifier saturation (since recovery between pulses is allowed by the timing) affects the pulses.

The other (linear) losses in the ring (γ_1 and γ_2 in figure 2) determine whether both pulse trains are the same. Symmetry will allow the hybrid absorber to be used in a hypothetical unidirectional model (outlined by the dotted line in figure 2). One pulse, however, always sees $\gamma_1 \alpha\ \gamma_2$ where the other meets these elements in the reverse order - not equivalent, because the amplification α is saturable. We must assume that $\gamma_1 = \gamma_2$ to give identical pulse trains.

In the unidirectional computer model the amplifier (α) is handled in the normal way. It is not important that half way through the element attention is changed to the identical counter-propagating pulse that arrives half a cycle later, except that the perimeter of the model ring must be half that of the actual ring. In the diagram we see that the correct arrangement of the losses is now $\gamma_2 \alpha\ \gamma_2$, but in fact we have kept the arrangement $\gamma\alpha$ which is compatible with the computer simulation work on conventional mode-locking, although not so exact. The entire cavity losses γ and the bandwidth limiting Fabry-Perot filter are therefore included after the amplification (α) and two-way absorption (β).

The two ingredients essential for the development of the computer program (PMLFINAL) were the partial-cavity approach and the two-way absorber theory which have already been

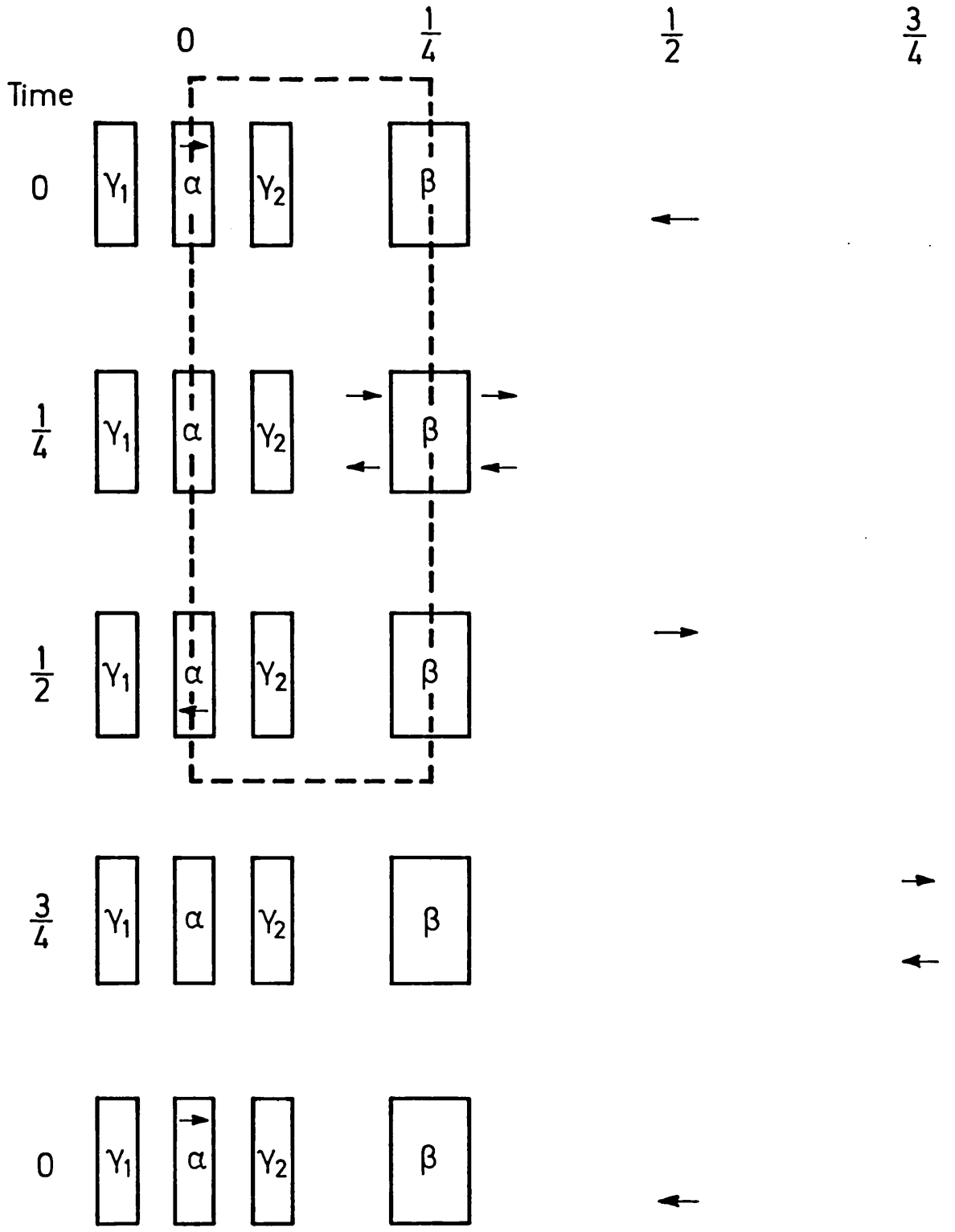

γ_1 γ_2 distributed linear losses

α amplifier jet

β saturable absorber jet

⇄ counter-propagating pulses

The computer modelling is done inside the dashed boundary.

FIGURE 2. EVENTS IN THE CPML CYCLE

discussed. An implementation using the structured programming language Pascal is described in appendix J. Further work is required to devise stringent checks that each procedure is correct, but some confidence was encouraged when the complete program ran successfully. The model shows the types of effect that it was written to study and the preliminary results will be discussed below.

5.5 Preliminary findings

Figures 3a-3c show the logarithmic flux profiles calculated for increasing values of the filter bandwidth whilst the absorber thickness (d = 12 meshpoints) and the other passive mode-locking parameters (α_u = 25, β_u = 0.2, γ = 0.4, Ξ_a = 1.1 and s = 1.667) are constant. Note that the total timescale studied (100 meshpoints) on each transit is so short compared with T_{1a} and T_{1b} that the slow absorber and slow amplifier assumptions apply exactly. (This regime could only be reached approximately by the whole-cavity simulations in chapter 2.) Each of the figures superimposes several transits (lettered A-I) beginning 22 transits after a seed pulse was injected (width = 26 meshpoints, j = 0.4).

The bandwidth is set as usual by the Fabry-Perot transmission, listed below together with the observed final pulse-widths and energies:

		TRANS	τ_{FWHM}	j
Figure-	3a	1.0	4	0.84
	3b	0.5	9	0.72
	3c	0.15	35	0.76

The higher energy of the short pulse is due to the lack of bandwidth limitation. It is not a steady state pulse, as is shown by the continued drop of the logarithmic wings during the evolution of figure 3a. In the presence of the filter (TRANS < 1), however, the development of a steady state is revealed by the fact that later curves partially cover the earlier curves in figures 3b and 3c. The broader pulse has the higher energy : this may be due to a reduced energy loss in saturating the two-way absorber for pulses longer than 2d (24 meshpoints).

The next step that must be taken with the computer program is to plot the events inside the hybrid absorber during the passage of the pulse. The detailed study of the properties of the model may lead to an improved understanding of colliding-pulse mode-locking.

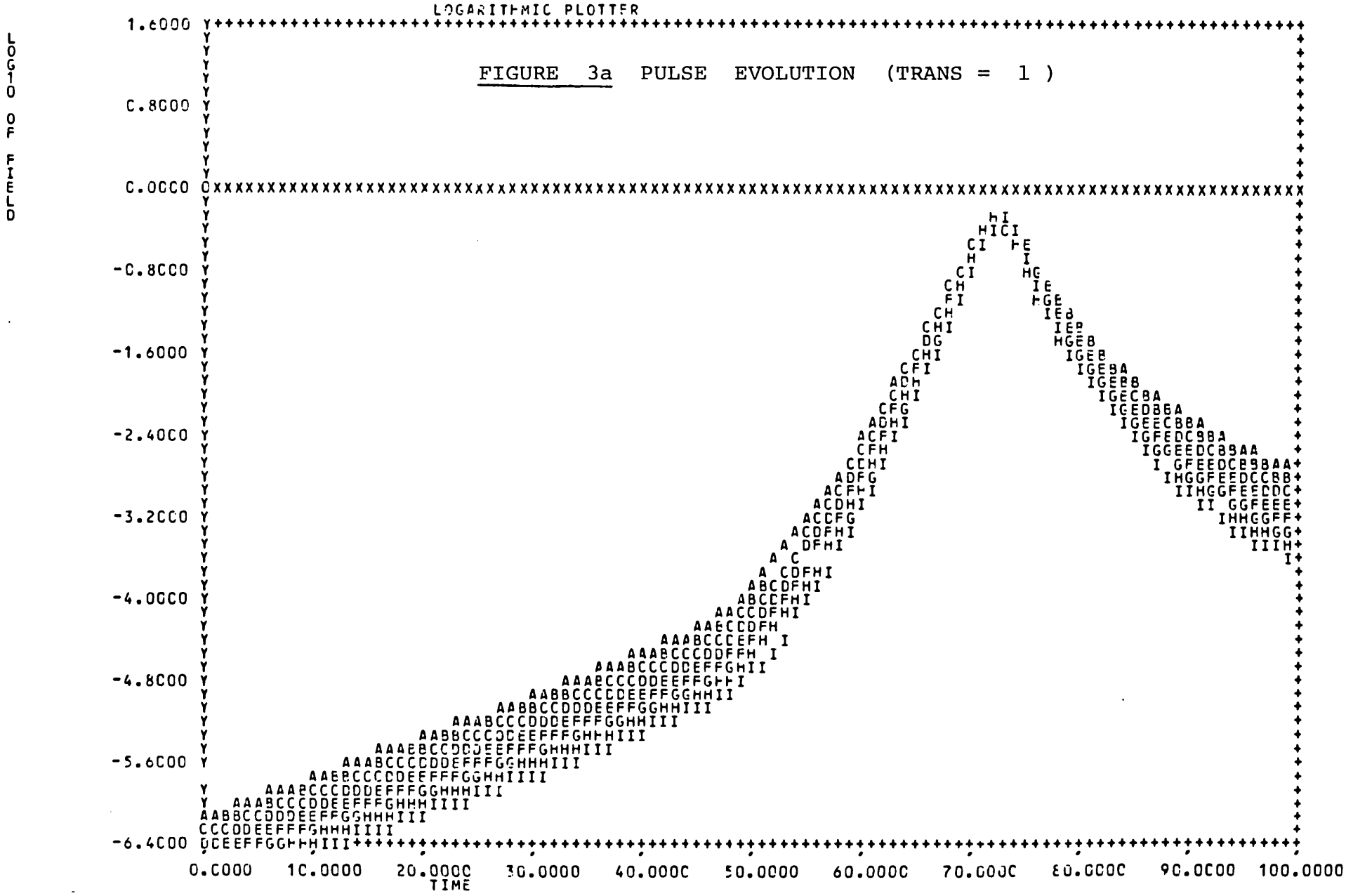
LOGARITHMIC PLOTTER
FIGURE 3a PULSE EVOLUTION (TRANS = 1)
LOG10 OF FIELD
1.6000
0.8000
0.0000
-0.8000
-1.6000
-2.4000
-3.2000
-4.0000
-4.8000
-5.6000
-6.4000
0.0000
10.0000
20.0000
30.0000
40.0000
50.0000
60.0000
70.0000
80.0000
90.0000
100.0000
TIME

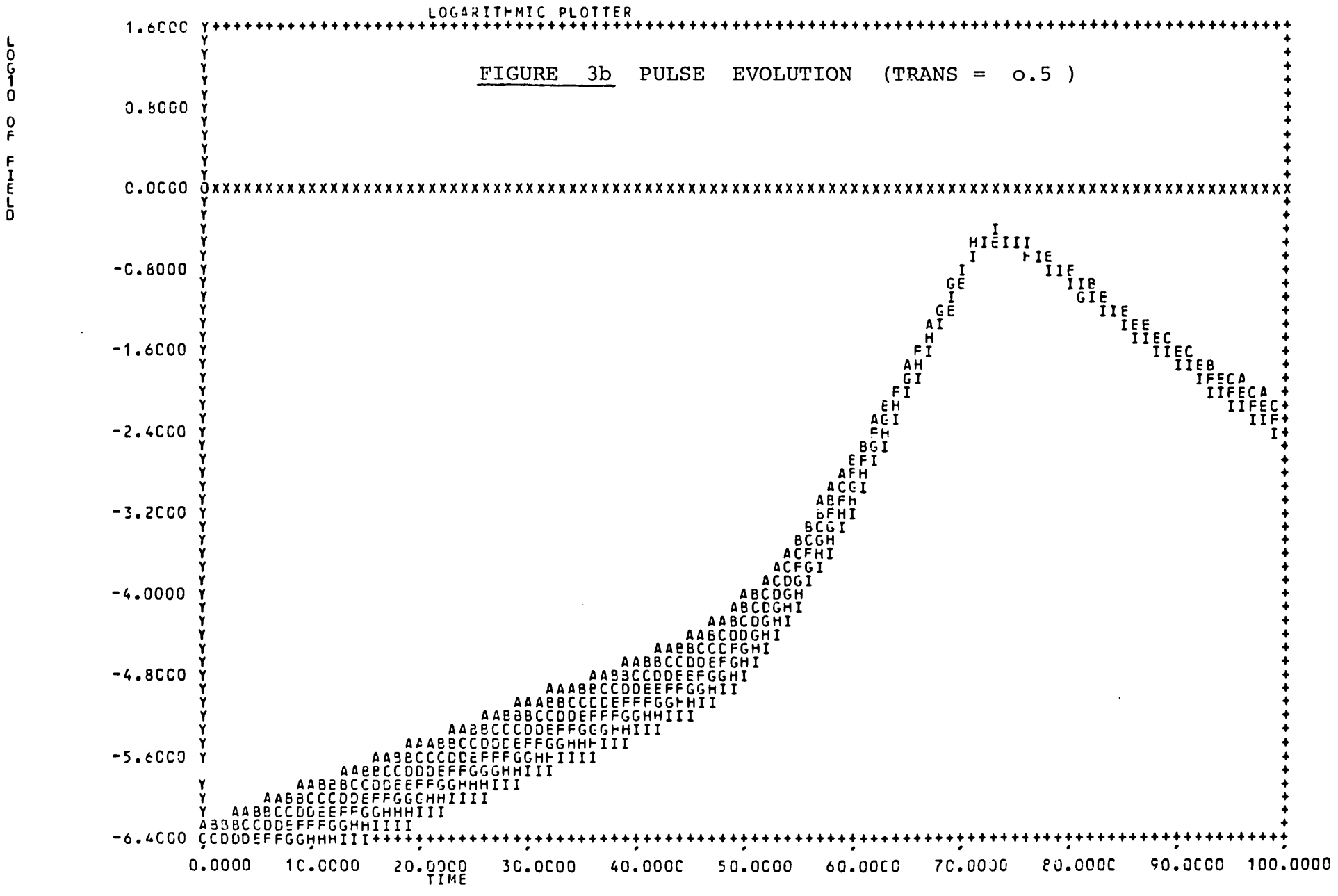

FIGURE 3b PULSE EVOLUTION (TRANS = 0.5)

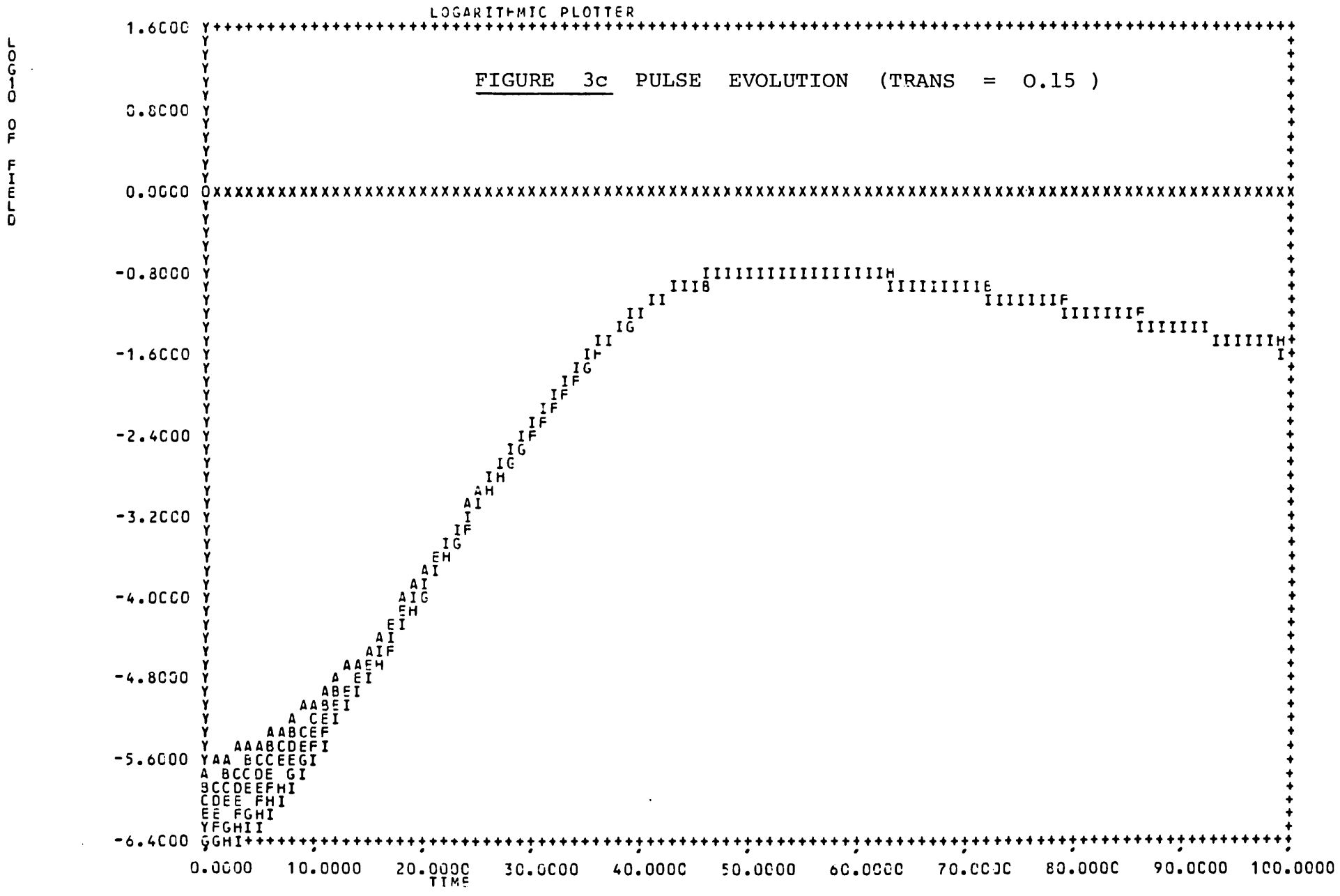

FIGURE 3c PULSE EVOLUTION (TRANS = 0.15)

5.6 Other CPML simulations and results

The theoretical evidence that a thin absorber jet may be necessary to produce ultrashort passively mode-locked laser pulses comes from a few studies which we shall now discuss. To make further progress we suggest the use of the partial-cavity computer simulation program developed here.

Diels et al. [67] first studied a linear cavity in which both absorber and amplifier dyes were mixed in a single jet. Bandwidth limitation was provided by the cavity mirrors. The mutual coupling between the two pulses which interfere in the jet could be artificially reduced for simulation purposes. It was found that steady state pulse widths were not affected by the induced gratings, but that the coupling did encourage the interwoven pulse trains to become identical (the shorter one becoming longer; the longer shorter). Separating the absorber jet from the gain jet, however, Diels et al. [68] subsequently simulated colliding-pulse mode-locking finding that in the absence of dispersion the pulse duration was limited by the jet thickness (35 fs pulses with a 10μ absorber dye jet were predicted). This suggests that we search for a regime where our model produces steady state pulses in the absence of the Fabry-Perot filter (by setting TRANS = 1.0), but so far this regime has not been located.

Stix and Ippen [41] have studied the passage of pulses through a two-way absorber thicker than the region of pulse overlap. Using approximate evolution equations for the population grating (based on the Fleck truncation discussed in chapter 3) they found that there is a reduced enhancement in pulse shortening velocity for such short pulses. When the pulses are much longer than the absorber thickness, the colliding pulse laser produces pulses up to three times shorter than an identical, but unidirectional, ring laser.

The influence of soliton shaping mechanisms in recent colliding-pulse mode-locked dye lasers [36] suggests that the use of a thin jet may also reduce the Kerr nonlinearities (arising from the solvent) that may be detrimental to achievement of the shortest pulses [69].

CHAPTER 6

CONCLUSIONS AND FURTHER WORK

6 Conclusions and further work

By studying evolving passively mode-locked pulses numerically, we have avoided making the restrictive assumptions that are necessary in analytic treatments. The intracavity Fabry-Perot etalon provided the bandwidth limitation required by Haus' analytic theory, which was also interpreted in terms of energy conservation in the "bouncing ball" model. The effect of noise and the connection between net gain and logarithmic slope for a steady state pulse were studied in detail for the first time.

In order to extend passive mode-locking theory to colliding pulse systems, the two-way saturable absorber was studied using a number of approaches. The techniques may also be relevant in other areas of quantum electronics where dynamic population gratings occur, such as optical bistability, the distributed feedback laser and phase conjugation (e.g. using the dye jet of a ring laser [70]). The most interesting result for passive mode-locking theory concerns the slow two-way absorber, for which a recursion relationship amongst the grating Fourier components was discovered. This allowed the unsatisfactory truncation of the Fleck hierarchy to be dispensed with.

The efficient partial-cavity simulation method was designed specifically to use the slow two-way absorber equations, using the experience gained already in whole-cavity simulations of conventional passive mode-locking. The new tool will allow a detailed numerical study of colliding-pulse mode-locking to be undertaken.

As a suggestion for further work, the effect of noise on the behaviour of a two-way absorber could be studied. Pulses with a reduced coherence length are not able to form the grating which reduces the energy loss in the absorber. This could mean that the noise component of the pulses is discriminated against in colliding-pulse lasers, by the absorption remaining at the minima of the standing-wave saturation field.

For an initial numerical study of soliton shaping effects in passive mode-locking, we suggest that a simplified numerical approach should be developed using the partial-cavity method for impementation on a microcomputer. It would be very easy to include group velocity dispersion in a manner similar to the use of the Fabry-Perot etalon which provided bandwidth limitation without leaving the time domain. The element that we would simulate is the Gires-Tournois interferometer [71,72,73]. Self phase modulation would be carried out by a further element with an intensity dependent refractive index. The recent theories based on hyperbolic secant pulses [34,69,74] could then be tested.

The analysis of wave packets containing many wavelengths simplifies optoelectronics [11] by allowing the slowly varying approximations to be used and also making it possible to use a scalar rather than a vector wave amplitude [71]. The approach to nearly carrier-free pulses may be extrapolated from the progress in mode-locking to date. This will lead to completely new physics, but it would also be interesting now to consider modelling passive mode-locking without the use of the sinusoidal carrier.

BIBLIOGRAPHY

1 Abraham N B,Lugiato L A and Narducci L M
J OPT SOC AM B2 (1985) p7 Overview of Instabilities in Laser Systems.

2 Casperson L W
J OPT SOC AM B2 (1985) p993 Spontaneous Coherent Pulsations in Ring-Laser Oscillators : Stability Criteria.

3 Kuizenga D J and Siegman A E
IEEE J QUANT EL QE6 (1970) p694 FM and AM Mode Locking of the Homogeneous Laser- Part I: Theory.

4 Kuizenga D J and Siegman A E
IEEE J QUANT EL QE6 (1970) p694 FM and AM Mode Locking of the Homogeneous Laser- Part II: Experimental Results in a Nd:YAG Laser With Internal FM Modulation.

5 Auston D H,Cheung K P,Valdmanis J A and Kleinman D A
PHYS REV LETT 53 (1984) p1555 Cherenkov Radiation from Femtosecond Optical Pulses in Electro-Optic Media.

6 Knox W H,Fork R L,Downer M C,Stolen R H,Shank C V and Valdmanis J A
APPL PHYS LETT 46 (1985) p1120 Optical Pulse Compression to 8 Fs at a 5-kHz Repetition Rate.

7 New G H C
OPT COMMUN 6 p188 Mode-Locking of Quasi-Continuous Lasers.

8 Haus H A
IEEE J QUANT EL QE11 (1975) p736 Theory of Mode Locking with a Slow Saturable Absorber.

9 M Sargent III,Scully M and Lamb W
"Laser Physics" Addison-Wesley (1974)

10 New G H C
REP PROG PHYS 46 (1983) p877 The Generation of Ultra-Short Laser Pulses.

11 Haus H A
"Waves and Fields in Optoelectronics" Prentice-Hall (1984)

12 Bradley D J
J PHYS CHEM 82 (1978) p2259 Generation and Measurement of Picosecond Pulses.

13 Ryan J P
LASER FOCUS June 1979 p74 Picosecond Techniques.

14 Ruddock I S
APPL OPT 18 (1979) p3212 Subpicosecond Pulse Generation in a Mode-Locked CW Dye Laser with a Slow Saturable Absorber.

15 Ruddock I S and Bradley D J
APPL PHYS LETT 29 (1976) p296 Bandwidth-Limited Subpicosecond Pulse Generation in Mode-Locked CW Dye Lasers.

16 Diels J C,Van Stryland E and Benedict G
OPT COMMUN 25 (1978) p93 Generation and Measurement of 200 Femtosecond Optical Pulses.

17 T Sizer II,Mourou G and Rice R R
OPT COMMUN 37 (1981) p207 Picosecond Dye Laser Pulses using a CW Frequency Doubled Nd:YAG as the Pumping Source.

18 T Sizer II,Kafka J D,Krisiloff A and Mourou G
OPT COMMUN 39 (1981) p259 Generation and Amplification of Sub-Picosecond Pulses using a Frequency Doubled Neodymium YAG Pumping Source.

19 Fork R L,Greene B I and Shank C V
APPL PHYS LETT 38 (1981) p671 Generation of Optical Pulses Shorter than 0.1 pSec by Colliding Pulse Mode Locking.

20 Cirkel H J and Schäfer F P
OPT COMMUN 5 (1972) p183 Passive Non-Reciprocal Element for Travelling Wave Ring-Lasers.

21 Siegman A E
IEEE J QUANT EL QE9 (1973) p247 An Antiresonant Ring Interferometer for Coupled Laser Cavities, Laser Output Coupling, Mode Locking, and Cavity Dumping.

22 Siegman A E and Vanherzeele H
PICOSECOND PHEN III, SPRINGER series in Chemical Physics 23 (1982) p14 New Picosecond Sources and Techniques.

23 Buchert J M,Basa D K,Tzu C and Alfano R R
J APPL PHYS 55 (1984) p683 Colliding Pulse Mode Locking for an Antiresonant Cavity of a Nd:Glass Laser.

24 Johnson A M,Stolen R H and Simpson W M
APPL PHYS LETT 44 (1984) p729 80x Single-Stage Compression of Frequency Doubled Nd:yttrium Aluminium Garnet Laser Pulses.

25 Johnson A M, Stolen R H and Simpson W M
ULTRAFAST PHEN IV, SPRINGER series in Chemical Physics 38 (1984) p16 Generation of 0.41-Picosecond Pulses by the Single-Stage Compression of Frequency Doubled Nd:YAG Laser Pulses.

26 Shank C V, Fork R L, Yen R, Stolen R H and Tomlinson W J
APPL PHYS LETT 40 (1982) p761 Compression of Femtosecond Optical Pulses.

27 Nikolaus B and Grischkowsky D
APPL PHYS LETT 42 (1983) p1 12x Pulse Compression Using Optical Fibers.

28 Mourou G A and T Sizer II
OPT COMMUN 41 (1982) p47 Generation of Pulses Shorter than 70 Fs with a Synchronously-Pumped CW Dye Laser.

29 Dietel W, Döpel E, KUhlke D and Wilhelmi B
OPT COMMUN 43 (1982) p433 Pulses in the Femtosecond Range from a CW Dye Ring Laser in the Colliding Pulse Mode-Locking (CPM) Regime with Down-Chirp.

30 Fontaine J J, Dietel W and Diels J C
IEEE J QUANT EL QE19 (1983) p1467 Chirp in a Mode-Locked Ring Dye Laser.

31 Dietel W, Fontaine J J and Diels J C
OPT LETT 8 (1983) p4 Intracavity Pulse Compression With Glass: a New Method of Generating Pulses Shorter Than 60 Fsec.

32 Jacobovitz G R, Brito Cruz C H and Scarparo M A
OPT COMMUN 57 (1986) p133 Pump Power and Saturable Absorber Effect on a Colliding Pulse-Modelocked Dye Laser Emitting Pulses Width 47 Fs.

33 Stix M S
OPT LETT 10 (1985) p279 Phase-Plane Analysis of Passively Mode-Locked Dye Lasers.

34 Martinez O E, Fork R L and Gordon J P
OPT LETT 9 (1984) p156 Theory of Passively Mode-Locked Lasers including Self-Phase Modulation and Group-Velocity Dispersion.

35 Mollenauer L F and Stolen R H
OPT LETT 9 (1984) p13 The Soliton Laser.

36 Valdmanis J A, Fork R L and Gordon J P
OPT LETT 10 (1985) p131 Generation of Optical Pulses as Short as 27 Femtoseconds Directly from a Laser Balancing Self-Phase Modulation, Group-Velocity Dispersion, Saturable Absorption, and Saturable Gain.

37 Fork R L,Martinez O E and Gordon J P
OPT LETT 9 (1984) p150 Negative Dispersion using Pairs of Prisms.

38 Salin F,Grangier P,Roger G and Brun A
PHYS REV LETT 56 (1986) p1132 Observation of High-Order Solitons Directly Produced by a Femtosecond Ring Laser.

39 Nuss M C,Leonhardt R and Zinth W
OPT LETT 10 (1985) p16 Stable Operation of a Synchronously Pumped Colliding-Pulse Mode-Locked Ring Dye Laser.

40 Cutler C C
PROC IRE 43 (1955) p140 The Regenerative Pulse Generator.

41 Stix M S and Ippen I P
IEEE J QUANT EL QE19 (1983) p520 Pulse Shaping in Passively Mode-Locked Ring Dye Lasers.

42 Frantz L M and Nodvik J S
J APPL PHYS 34 (1963) p2346 Theory of Pulse Propagation in a Laser Amplifier.

43 Bellman R,Birnbaum G and Wagner W G
J APPL PHYS 34 (1963) p780 Transmission of Monochromatic Radiation in a Two-Level Material.

44 Schulz-DuBois E O
B.S.T.J. 43 (1964) p625 Pulse Sharpening and Gain Saturation in Traveling-Wave Masers.

45 Macomber J D
J APPL PHYS 38 (1967) p3525 Theory of Pulse-Shaping by Saturable Optical Materials.

46 Kryukov P G and Letokhov V S
SOV PHYS USPEKHI 12 (1970) p641 Propagation of a Light Pulse in a Resonantly Amplifying (Absorbing) Medium.

47 Yasa Z A and Teschke O
OPT COMMUN 15 (1975) p169 Picosecond Pulse Generation in Synchronously Pumped Dye Lasers.

48 Bradley D J,Durrant A J F,O'Neill F and Sutherland B
PHYS LETT 30A (1969) p535 Picosecond Pulses from Mode-Locked Dye Lasers.

49 New G H C
IEEE J QUANT EL QE10 (1974) p115 Pulse Evolution in Mode-Locked Quasi-Continuous Lasers.

50 New G H C and Rea D H
J APPL PHYS 47 (1976) p3107 Rate-Equation Dynamics of Passively Mode-Locked Quasicontinuous Lasers : Perturbation Theory of a Ring Laser.

51 Haus H A,Shank C V and Ippen E P
OPT COMMUN 15 (1975) p29 Shape of Passively Mode-Locked Laser Pulses.

52 Fleck J A
J APPL PHYS 39 (1968) p3318 Origin of Short-Pulse Emission by Passively Switched Lasers.

53 Fleck J A
PHYS REV B1 (1970) p84 Ultrashort-Pulse Generation by Q-Switched Lasers.

54 Borisov V I,Kabaev N I,Lebedev V I and Yurevich V A
SOV J APPL SPECTR 34 (1981) p61 Certain Features of Opening (Lightening) of a Phototropic Valve by a Standing Light Wave.

55 Macomber J D and Kestner N R
J APPL PHYS 40 (1969) p3218 Theory of Saturable Reflection.

56 Gruneisen M T,Gaeta A L and Boyd R W
J OPT SOC AM B2 (1985) p1117 Exact Theory of Pump-Wave Propagation and its Effect on Degenerate Four-Wave Mixing in Saturable-Absorbing Media.

57 Ostrovskii L A and Yakubovich E I
SOV PHYS JETP 19 (1964) p656 Averaged Laser Equations and their Stationary Solutions.

58 Vinetskii V L,Kukhtarev N V,Odulov S G and Soskin M S
SOV PHYS USP 22 (1979) p742 Dynamic Self-Diffraction of Coherent Light Beams.

59 Bradley D J,New G H C and Caughey S J
OPT COMMUN 2 (1970) p41 Relationship Between Saturable Absorber Cell Length and Pulse Duration in Passively Mode-Locked Lasers.

60 Kühlke D,Rudolph W and Wilhelmi B
IEEE J QUANT EL QE19 (1983) p526 Calculation of the Colliding Pulse Mode Locking in CW Dye Ring Lasers.

61 Dietel W,KÜhlke D,Rudolph W and Wilhelmi B
SOV J QUANT EL 13 (1983) p44 Experimental and Theoretical Investigations of the Influence of a Saturation Grating in an Absorber on Pulse Generation in a Passively Mode-Locked Dye Laser.

62 Herrmann J,Weidner F and Wilhelmi B
APPL PHYS B26 (1981) p197 Theory of Passive Mode-Locking of CW Dye Lasers with Contacted and Non-Contacted Absorbers.

63 Arutunyan V M
SOV PHYS JETP 26 (1968) p125 Averaged Equations of a Nonstationary Resonant Medium.

64 Silberberg Y and Bar-Joseph I
IEEE J QUANT EL QE17 (1981) p1967 Transient Effects in Degenerate Four-Wave Mixing in Saturable Absorbers.

65 Catherall J M and New G H C
TO BE PUBLISHED: Role of Spontaneous Emission in the Dynamics of Mode-Locking by Synchronous Pumping.

66 Yoshizawa M and Kobayashi T
IEEE J QUANT EL QE20 (1984) p797 Experimental and Theoretical Studies on Colliding Pulse Mode Locking.

67 Diels J C,Fontaine J J,McMichael I C and Wang C Y
APPL PHYS LETT B28 (1982) p172 Experimental and Theoretical Study of the Mutual Interaction of Subpicosecond Pulses in Absorbing and Gain Media.

68 Diels J C,McMichael I C,Fontaine J J and Wang C Y
PICOSECOND PHEN III, SPRINGER series in Chemical Physics 23 (1982) p116 Subpicosecond Pulse Shape Measurement and Modeling of Passively Mode Locked Dye Lasers Including Saturation and Spatial Hole Burning.

69 Martinez O E,Fork R L and Gordon J P
J OPT SOC AM B2 (1985) p753 Theory of Passively Mode-Locked Lasers for the case of a Nonlinear Complex Propagation Coefficient.

70 Diels J C,McMichael I C and Vanherzeele H
IEEE J QUANT EL QE20 (1984) p630 Degenerate Four-Wave Mixing of Picosecond Pulses in the Saturable Amplification of a Dye Laser.

71 Froehly C,Colombeau B and Vampouille M
PROG OPT XX, North-Holland (1983) ed E Wolf Shaping and Analysis of Picosecond Light Pulses.

72 French P M W,Chen G F and Sibbett W
TO BE PUBLISHED: Tunable Group Velocity Dispersion Interferometer for Intracavity and Extracavity Applications.

73 Heppner J and Kuhl J
APPL PHYS LETT 47 (1985) p453 Intracavity Chirp Compensation in a Colliding Pulse Mode Locked Laser Using Thin-Film Interferometers.

74 Diels J C,Dietel W,Fontaine J J,Rudolph W and Wilhelmi B J OPT SOC AM B2 (1985) p680 Analysis of a Mode-Locked Ring Laser: Chirped-Solitary-Pulse Solutions.

75 Harrison R G,Key P,Little V I,Magyar G and Katzenstein J APPL PHYS LETT 13 (1968) p253 Bragg Reflection of Laser Light from a Phase Grating in a Q-Switching Liquid

76 Schwarz S E and Tan T Y
APPL PHYS LETT 10 (1967) p4 Wave Interactions in Saturable Absorbers.

77 Tocho J O,Sibbett W and Bradley D J
OPT COMMUN 37 (1981) p67 Thermal Effects in Phase-Conjugation in Saturable Absorbers with Picosecond Pulses.

78 Tocho J O,Sibbett W and Bradley D J
PICOSECOND PHEN II, SPRINGER series in Chemical Physics 14 (1980) p372 Picosecond Phase-Conjugation Reflection and Gain in Saturable Absorbers by Degenerate Four-Wave Mixing.

79 Lax M
J MATH PHYS 19 (1978) p2589 Analytic Solution of a Model Pulse Propagation Problem.

80 White J A
NATURE 201 (1964) p911 An Implication for Lasers of an Aspect of Interference at High Field Strengths.

81 M Sargent III
APPL PHYS 9 (1976) p127 Laser Saturation Grating Phenomena.

82 Kyrola E
PHYSICA SCRIPTA 23 (1981) p785 Probe Spectroscopy of Standing Wave Induced Saturation.

83 Garmire E M and Yariv A
IEEE J QUANT EL QE3 (1967) p222 Laser Mode-Locking with Saturable Absorbers.

84 Garmire E M and Yariv A
IEEE J QUANT EL QE3 (1967) p377 Correction.

85 Hermann J A
OPTICA ACTA 27 (1980) p159 Spatial Effects in Optical Bistability.

86 Hercher M
APPL OPT 6 (1967) p947 An Analysis of Saturable Absorbers.

87 Loudon R
"The Quantum Theory of Light" Problem 2.1
Clarendon Press, Oxford (1973)

88 Copson E T
ARCH RATL MECH ANAL 1 (1958) p324 On the Riemann-Green Function.

89 Courant R and Hilbert D
"Methods of Mathematical Physics" vol II Interscience (1962)

90 Abramowitz M and Stegun I A (eds.)
"Handbook of Mathematical Functions"
Dover Publications, New York (1972)

A C K N O W L E D G M E N T S

I am very grateful to my supervisor, Professor G.H.C. New for expert and patient help throughout this research.

In the Laser Group at Imperial College the stimulating contact with many experimental and theoretical colleagues was much appreciated. Essential mathematical and computational advice was received from Dr. P.M. Radmore and Mr. C. Penman.

Dr. L. Solymar kindly allowed me to take time off from my work in order to write up.

The S.E.R.C. generously provided a research studentship and also enabled me to attend the 23rd S.U.S.S.P. summer school on lasers at Heriot-Watt University. The Barber trust of the Institute of Physics helped with travel costs to the 12th International Quantum Electronics Conference.

Mrs. Alison Dygnas typed the thesis manuscript with great care and Mrs. J. Takacs drew the diagrams in chapter 5. The support of my friends is also happily acknowledged.

The greatest pleasure is to thank my parents for their continuous love and encouragement.

Appendix A Literature on spatial hole burning

Nonlinear optics with applied fields that interfere to produce a standing wave in an absorber were reported in 1968 by Harrison et al [75] who explained the observations that saturable absorber Q-switching and passive mode-locking in pulsed solid-state lasers could take place at relatively low laser intensity, by postulating the presence of a "Lippman plate". The new idea was that this grating (which selects cavity modes whose periodicity matches its own) exists because standing wave laser oscillation bleaches a spatially varying population into the absorber cell. This (homogeneous) process was described as 'spatial hole burning' because 'spectral hole burning' had been invoked previously as the mechanism allowing strong saturation on inhomogeneously broadened transitions [76].

Harrison et al proved the existence of a volume grating by Bragg reflecting an externally generated second harmonic probe beam off the Q-switching liquid of a Ruby laser. The greatest reflection occurred for a delayed probe and this could be explained by the growth of a thermal phase grating rather than a population grating. More recently, however, in an experiment on phase-conjugation with ps pulses, Tocho et al [77] found evidence of both thermal and population gratings in a saturable absorber that is used to mode-lock the cw dye laser (DODCI). When the dye cell [78] or jet [70] is placed inside the cavity of a laser it is possible that the population grating is enhanced relative to the thermal grating. It is the population grating which we consider in the present work.

In the theory of standing-wave laser oscillation population gratings were considered as early as 1964 [80]. Instead of temporal behaviour, most subsequent study of the nonlinear effects was in spectroscopy (see Sargent [81] for a review). As an example, the absorption of a probe at frequency ν' by a gas of two-level atoms where strong counter-running waves

saturate at frequency ν has been studied approximately by Kyrola [82]. In this work only a one-dimensional interaction is considered; if the probe beam entered at an angle then the geometry becomes that of phase conjugation where the theories are still not so complete as in one dimension.

Population gratings that influence the dynamics of passive mode-locking are one concern of this thesis. In the next pages we shall start from a description contained in the 1968 paper by Fleck [52].

Fleck's work is based on the rate equation approximation (REA) - see eqn (B6) - and surprisingly [81] this makes it more useful in its treatment of gratings than methods based on third order laser theory, which would only model final Bragg scattering off a ready-made grating (made by the waves that would have been present were scattering ignored).

For solid state lasers, mode-locking is now much better understood experimentally than it was when Harrison et al published their 1968 paper. The influence of population gratings in the contacted dye cell has been studied, for example, by Bradley, New and Caughey [59] who were able to match theory and experiment. Whereas Schwartz and Tan [76] had calculated the power removed from a c.w. standing wave by a saturable absorber cell, the appropriate quantity in a time-domain study of mode-locking is the energy which is removed from the short pulse [83 and 84]: that loss has to be minimised.

In the CPML dye laser population gratings again probably cause the large reductions in pulse-width obtainable, but this is not certain. A full treatment of population gratings is therefore very much needed.

Appendix B

SEMICLASSICAL THEORY AND THE RATE EQUATION APPROXIMATION

In a region free from currents Maxwell's equations for one dimensional electromagnetic waves state:

$$\left[\frac{\partial^2}{\partial z^2} - \frac{1}{c^2}\frac{\partial^2}{\partial t^2}\right] E = \mu_0 \frac{\partial^2 P}{\partial t^2} \tag{B1}$$

The polarization appearing on the right hand side of this classical equation is obtained by summing the contributions from individual atoms. The quantum mechanical side to the problem is to calculate the atomic response to the classical field; this response reacts on the field. The semiclassical theory is completed by setting $P = N\langle p\rangle$ where N is the atomic density, p the atomic dipole operator and the brackets cause the expectation value to be taken.

From the Liouville evolution equation for the 2 x 2 density matrix of two-level systems interacting with an electric field the (macroscopic) P may be derived. Including the damping terms as well, the required results are as follows:

$$P = N\langle p\rangle = N\mu\rho_{12} + c.c. \tag{B2}$$

$$\frac{\partial}{\partial t}(N\rho_{12}) + (-i\omega + T_2^{-1})N\rho_{12} = (i/\hbar)\mu nE \tag{B3}$$

$$\frac{\partial n}{\partial t} = \frac{n^o - n}{T_1} + \frac{2i}{\hbar} E(N\mu\rho_{12} - c.c.) \tag{B4}$$

where the real quantity $n = N(\rho_{22} - \rho_{11})$ is the population difference.

We express the field as the sum of two counter propagating plane waves,

$$E(z,t) = E^{+}(z,t)e^{i(\omega t-kz)} + E^{-}(z,t)e^{i(\omega t+kz)} + c.c. \quad (B5)$$

$$= E^{\omega}e^{i\omega t} + c.c.$$

and the off-diagonal matrix element as a single rotating "wave",

$$\rho_{12} = \rho'(z,t)\ e^{i\omega t}.$$

We shall assume that E^{+} and E^{-} vary slowly* with z and t but only specify ρ' and $n = N(\rho_{22} - \rho_{11})$ to vary slowly with t. In what follows, Fourier analysis of the remaining population gratings will be required.

The expression for ρ_{12} substituted into (B3) results in:

$$\frac{d\rho'}{dt} + \frac{\rho'}{T_2} = -(i/\hbar)\mu(\rho_{11} - \rho_{22})Ee^{-i\omega t}$$

For large T_2^{-1}compared with the derivative the RATE EQUATION APPROXIMATION allows the steady state solution to be used, which states:

$$N\rho_{12} = (i/\hbar)T_2\mu\ nE^{\omega}e^{i\omega t} \quad (B6)$$

In this approximation there are no dispersive effects.

---

*Therefore the optical fields in (B5) occupy a narrow bandwidth near the resonance (at ω) with the transition.

We can now combine (B6) with (B4) to obtain the rate equation

$$\frac{\partial n}{\partial t} = \frac{n_u - n}{T_1} - 2n\sigma F \qquad \text{(B7)}$$

where $\sigma = \omega\mu^2 T_2/\hbar c\epsilon_0$ is the absorption cross section and $F = \epsilon_0 E^2/\hbar k$ is the rate at which photons strike unit area. (The momentum per photon is $\hbar k$ and the energy per unit volume $\epsilon_0 E^2$ is "carried" by the total pressure $F\hbar k$).

Using (B5) and neglecting terms which oscillate at 2ω we replace E^2 (appearing in F) by the slowly time-varying term

$$2\left|E^+e^{-ikz} + E^-e^{+ikz}\right|^2 = 2(|E^+|^2 + |E^-|^2 + E^+E^{-*}e^{-2ikz} + E^{+*}E^-e^{+2ikz})$$

Equation (B6) with (B2) allows us to rewrite (B1) as follows

$$\left[\frac{\partial^2}{\partial z^2} - \frac{1}{c^2}\frac{\partial^2}{\partial t^2}\right](E^\omega e^{i\omega t} + \text{c.c.}) =$$

$$i\left[\frac{n\sigma c}{\omega}\right]\frac{1}{c^2}\frac{\partial^2}{\partial t^2}(E^\omega e^{i\omega t} - \text{c.c.})$$

but using the slowly varying approximation to neglect $\partial^2 E^\omega/\partial t^2$ and to match separately the coefficients of $e^{\pm i\omega t}$ gives:

$$\frac{\partial^2 E^\omega}{\partial z^2} = -k\left[1 + i\left\{\frac{n\sigma}{k}\right\}\right]\left[kE^\omega - 2i\frac{1}{c}\frac{\partial E^\omega}{\partial t}\right]$$

Applying the same approximations on the left hand side, where $E^\omega = E^+e^{-ikz} + E^-e^{+ikz}$ and we are neglecting the product term* on the right hand side which involves $(n\sigma/k)(\partial E^\omega/\partial t)$, the pair of resulting equations is:

$$\left[\frac{1}{c}\frac{\partial}{\partial t} \pm \frac{\partial}{\partial z}\right]E^{\pm} = \frac{\sigma}{2} \langle n\, e^{\pm ikz} E^{\omega} \rangle \qquad (B8)$$

The angular brackets remind that the spatial average is taken, since only driving terms that are phase-matched are taken in the slowly varying approximation - for the two-way absorber n itself is not slowly varying.

If we consider a one-way absorber ($E^{-} = 0$) then a single transport equation remains

$$\frac{\partial E^{+}}{\partial z} + \frac{1}{c}\frac{\partial E^{+}}{\partial t} = \frac{\sigma}{2} n E^{+}$$

$$\Rightarrow \frac{\partial F}{\partial z} + \frac{1}{c}\frac{\partial F}{\partial t} = n \sigma F \qquad (B9)$$

In general, however, we do <u>not</u> obtain this familiar equation which results in Beer's law. In order to evaluate the spatial averages we must express n(z,t) by the Fourier series:

$$n(z,t) = \bar{n} + \sum_{p=1}^{\infty} [n_p \exp\{-2pikz\} + c.c] \qquad (B10)$$

Then we obtain

$$\langle n e^{+ikz} E^{\omega} \rangle = \bar{n} E^{+} + n_1 E^{-}$$

$$\langle n e^{-ikz} E^{\omega} \rangle = \bar{n} E^{-} + n_1^{*} E^{+}$$

In the main text these results lead to the Fleck Hierarchy (Section 3.3).

---

*If E^{ω} really is slowly varying with z then the absorption over one wavelength ($n\sigma/k$) has to be small: the product term then vanishes at the same time as the second order derivatives.

The 2 appearing in equations (B4) and (B7) is absent when a four level scheme is used instead of the present two level system. Four level schemes apply to dye laser amplifiers (whereas we were considering saturable absorbers). Passive mode-locking theory uses rate equations of both types, however, and to resolve the notation we modify the σ cross section definition in the two-level case and write

$$\frac{\partial n_a}{\partial t} = \frac{n_{a0} - n_a}{T_{1a}} - n_a \sigma_a F \qquad \text{AMPLIFIER}$$

$$\frac{\partial n_b}{\partial t} = \frac{n_{b0} - n_b}{T_{1b}} - n_b \sigma_b F \qquad \text{ABSORBER}$$

The result is that the coefficients $A = n_a \sigma_a l$ and $B = -\frac{1}{2} n_b \sigma_b l$ of amplification and absorption also obey similar looking equations. We need to remember that their definitions differ, since the theory will be formulated not only in terms of A, B and a <u>normalised</u> intensity $\lambda_a = \sigma_a F$ or $\lambda_b = \sigma_b F$ but also will involve $s = \sigma_b / \sigma_a$ where σ_b is not the usual cross-section.

Note that the background refractive index (η) of the medium may be taken into account by replacing c by $v = c/\eta$ in all the equations of this appendix.

Appendix C

FORMAL SOLUTION OF THE FLECK EQUATIONS

This appendix contains details of the perturbative solution of the normalised equations of section 3.4. We replace A, B, a_0 and a_p ($p = 1,2,...$) everywhere in the equations by their expansions*, which are:

$$A = A_0 + \frac{1}{\alpha} A_1 + \frac{1}{\alpha^2} A_2 + ...$$

$$B = B_0 + \frac{1}{\alpha} B_1 + \frac{1}{\alpha^2} B_2 + ...$$

$$a_0 = -\alpha + a_{00} + \frac{1}{\alpha} a_{01} + \frac{1}{\alpha^2} a_{02} + ...$$

$$a_p = a_{p0} + \frac{1}{\alpha} a_{p1} + \frac{1}{\alpha^2} a_{p2} + ...$$

$(p = 1,2,...)$

This leads to the following field equations

---

*Notice that a_0 contains the leading coefficient $-\alpha$ since this is its unsaturated value, whereas the other a_p describe grating effects that only appear with saturation.

C1 $$\alpha\left\{\frac{\partial}{\partial T} + \frac{\partial}{\partial X}\right\}\left[A_0 + \frac{1}{\alpha}A_1 + \frac{1}{\alpha^2}A_2 + \ldots\right]$$

$$= (-\alpha + a_{00} + \frac{1}{\alpha}a_{01} + \ldots)\left[A_0 + \frac{1}{\alpha}A_1 + \frac{1}{\alpha^2}A_2 + \ldots\right]$$

$$+ (a_{10} + \frac{1}{\alpha}a_{11} + \ldots)\left[B_0 + \frac{1}{\alpha}B_1 + \ldots\right]$$

C2 $$\alpha\left\{\frac{\partial}{\partial T} - \frac{\partial}{\partial X}\right\}\left[B_0 + \frac{1}{\alpha}B_1 + \frac{1}{\alpha^2}B_2 + \ldots\right]$$

$$= (-\alpha + a_{00} + \frac{1}{\alpha}a_{01} + \ldots)\left[B_0 + \frac{1}{\alpha}B_1 + \frac{1}{\alpha^2}B_2 + \ldots\right]$$

$$+ (a^*_{10} + \frac{1}{\alpha}a^*_{11} + \ldots)\left[A_0 + \frac{1}{\alpha}A_1 + \ldots\right]$$

and now it is easy to extract simpler equations by equating the coefficients of α, 1, $\frac{1}{\alpha}$, $\frac{1}{\alpha^2}$ etc.

For example the $0(\alpha)$ and $0(1)$ problems are:

$0(\alpha)$ $$\left[\frac{\partial}{\partial T} + \frac{\partial}{\partial X}\right]A_0 = -A_0 \text{ and } \left[\frac{\partial}{\partial T} - \frac{\partial}{\partial X}\right]B_0 = -B_0$$

$0(1)$ $$\left[\frac{\partial}{\partial T} + \frac{\partial}{\partial X}\right]A_1 = -A_1 + a_{00}A_0 + a_{10}B_0$$

and $$\left[\frac{\partial}{\partial T} - \frac{\partial}{\partial X}\right]B_1 = -B_1 + a_{00}B_0 + a^*_{10}A_0$$

The solutions for A_0 and B_0 may be written down at once because no further population variables appear. The results are $A_0 = e^{-X}f(X - T)$; $B_0 = e^{X}g(X + T)$ where the functions f and g are entirely determined by the pulses entering at X = 0 and X = L. Outside the absorber A_0 and B_0 are zero. The partial differential equations for A_1 and B_1 are inhomogenous but linear: these equations are not coupled together because A_0, B_0 and also a_{00}, a_{10} are known (from $0(\alpha)$ results) driving terms by the time $0(1)$ contributions are evaluated. The results needed for a_{00} and a_{10} will be given later in this appendix. By employing characteristics u = T - X; v = T the A_1 equation (at constant u) becomes,

$$\frac{\partial}{\partial v} A_1 = -A_1 + a_{00}A_0 + a_{10}B_0$$

$$\Rightarrow \quad A_1 = e^{-v} \int_{\substack{\text{constant} \\ u}} e^{v} \left[a_{00}A_0 + a_{10}B_0\right] dv$$

$$\Rightarrow \quad A_1(X,T) = e^{-T} \int_0^T e^{T'} (a_{00}A_0 + a_{10}B_0)(X - T + T', T') dT'$$

where the constraint $T' - X' = T - X$ was used and the integration limits selected so that $A_1 = 0$ at $T = 0$. The evaluation of B_1 follows the same method, as does the field solution in all orders PROVIDED THAT THE DRIVING TERMS ARE KNOWN.

In order to evaluate all the driving terms, we next expand the population equations in exactly the same manner as the field equations above. From a_0 and a_p equations given on p64 the expansions are:

C3 $$\alpha\frac{\partial}{\partial T}\left(a_{p0} + \frac{1}{\alpha}a_{p1} + \ldots\right) + \left(a_{p0} + \ldots\right)$$

$$= -\Big[\left(a_{p-1,0} + \ldots\right)\left(A_0B_0^* + \ldots\right) + \left(a_{p,0} + \ldots\right)$$

$$\left[|A_0|^2 + |B_0|^2 + \ldots\right] + \left(a_{p+1,0} + \ldots\right)\left[A_0^*B_0 + \ldots\right]\Big]$$

$(p = 2,3,4\ldots.)$

C4 $$\alpha\frac{\partial}{\partial T}\left(a_{10} + \frac{1}{\alpha}a_{11} + \ldots\right) + \left(a_{10} + \ldots\right)$$

$$= -\Big[\left(-\alpha + a_{00} + \ldots\right)\left[A_0B_0^* + \frac{1}{\alpha}\left(A_0B_1^* + A_1B_0^*\right) + \ldots\right]$$

$$+ \left(a_{10} + \ldots\right)\Big[|A_0|^2 + |B_0|^2 + \ldots\Big]$$

$$+ \left(a_{20} + \ldots\right)\left[A_0^*B_0 + \ldots\right]\Big]$$

$(p = 1.)$

C5 $$\alpha\frac{\partial}{\partial T}\left(a_{00} + \frac{1}{\alpha}a_{01} + \ldots\right) + \left(a_{00} + \ldots\right)$$

$$= -\Big[\left(-\alpha + a_{00} + \ldots\right)\Big[|A_0|^2 + |B_0|^2 + \frac{1}{\alpha}$$

$$\left(A_0A_1^* + A_0^*A_1 + B_0B_1^* + B_0^*B_1\right) + \ldots\Big] + \left(a_{10} + \ldots\right)$$

$$\left[A_0^*B_0 + \ldots\right] + \left(a_{10}^* + \ldots\right)\left[A_0B_0^* + \ldots\right]\Big]$$

$(p = 0.)$

The coefficients whose evolution is given by equation (C3) do not enter into the expansions of a_0 and a_1 which are the only properties of the saturated absorber felt by the fields in C1 and C2. However, in order to use (C4) and (C5) we require knowledge of all these coefficients because $(a_{20} + \ldots)$ on the right hand side of (C4) represents a coupling that eventually brings in effects from all population grating harmonics. One important conclusion which we shall make upon equating coefficients of α in the present approach, is that truncating at $0(1/\alpha^{p-1})$ is similar to a truncation of the original Fleck hierarchy (page 64) at the a_p term. For sufficiently large α, therefore, higher order population Fourier components are not very significant.

To verify these statements we consider first the results of equating $0(\alpha)$ coefficients. With (C3-C5) we find:

$$\frac{\partial}{\partial T}\ a_{p0} = 0 \qquad (p = 2,3,4\ldots)$$

$$\frac{\partial}{\partial T}\ a_{10} = A_0 B_0^*$$

$$\frac{\partial}{\partial T}\ a_{00} = |A_0|^2 + |B_0|^2$$

From these equations we immediately obtain the integrals quoted on page 64. The coefficients a_{00} and a_{10} are the only ones that exist at this level. It also follows from (C3) that $a_{p1}\ldots\ldots\ a_{p,p-2}$ in turn remain zero just as a_{p0} does above.

The first non-zero term for the p^{th} Fourier component obeys:

$$\frac{\partial}{\partial T}\ a_{p,p-1} = a_{p-1,p-2}\ A_0 B_0^*$$

which occurs at $0(\ 1/\alpha^{p-2})$ in (C3).

If we stop the series for A, B, a_0, a_1 and a_2 after the $1/\alpha$ terms then there are only three more population equations to consider. They are:

C6 $$\frac{\partial}{\partial T} a_{21} = - a_{10} \frac{\partial}{\partial T} a_{10}$$

C7 $$\frac{\partial}{\partial T} a_{11} + a_{10} = A_0 B_1^* + A_1 B_0^* - \left[a_{00} \frac{\partial}{\partial T} a_{10} + a_{10} \frac{\partial}{\partial T} a_{00}\right]$$

C8 $$\frac{\partial}{\partial T} a_{01} + a_{00} = A_0 A_1^* + A_0^* A_1 + B_0 B_1^* + B_0^* B_1$$
$$- \left[a_{00} \frac{\partial}{\partial T} a_{00} + a_{10} \frac{\partial}{\partial T} a_{10}^* + a_{10}^* \frac{\partial}{\partial T} a_{10}\right]$$

These equations may be integrated explicitly because all the driving terms are known as a result of previous stages of the calculation. Then a_{01} and a_{11} may be used to improve upon the approximation to the fields A,B by evaluating A_2 and B_2. Notice that a_{21} is not redundant because it will appear if the calculation of a_{02} and a_{12} is carried out (to appear in A_3 and B_3).

Recovery of a_{00} and a_{10} was not contained in the $0(\alpha)$ calculation. However the structure of the left hand sides of C8 and C7 indicates that it is added in as part of the <u>next</u> term in the perturbation series

$$- \alpha + a_{00} + \frac{a_{01}}{\alpha} \qquad \text{or} \qquad a_{10} + \frac{a_{11}}{\alpha}.$$

Appendix D 'Conservation Law' analysis for Fast Absorber

Using normalised intensities, $U^{\pm} = 4\sigma T_1 (E^{\pm})^2$ we must solve

$$1. \quad \frac{dU^+}{dU^-} = \frac{U^+ + n_1/\bar{n} \; /U^+U^-}{U^- + n_1/\bar{n} \; /U^+U^-}$$

in order to obtain the conservation law. Here $\bar{n}$ and $\bar{n}/n_1$ have already been tabulated in terms of $x = 2/U^+U^-/a$ and $a = 1 + U^+ + U^-$ for the two cases where the Fleck truncation and the exact treatment applied. Using the formulae in table 1 we find:

$$2a. \quad \text{(EXACT)} \quad -\frac{dU^+}{dU^-} = \frac{2U^+ + \sqrt{(1 + U^+ + U^-)^2 - 4U^+U^-} - (1 + U^+ + U^-)}{2U^- + \sqrt{(1 + U^+ + U^-)^2 - 4U^+U^-} - (1 + U^+ + U^-)}$$

$$2b. \quad \text{(TRUNC)} \quad -\frac{dU^+}{dU^-} = \frac{U^+(1 + U^+)}{U^-(1 + U^-)}$$

Since (2a) is not separable we follow Hermann [85] in using variables $\theta = U^+ + U^-$, $\varphi = U^+ - U^-$, and readily obtain

$$\frac{d\theta}{d\varphi} = \frac{(dU^+/dU^-) + 1}{(dU^+/dU^-) - 1} = \frac{\varphi}{\sqrt{1 + 2\theta + \varphi^2} - 1}$$ which gives the unexpected explicit solution $\varphi^2 = (D + \theta)^2 - (1 + 2\theta)$. To see this is correct, use it to rewrite the differential equation above as $\varphi\frac{d\varphi}{d\theta} = (D + \theta) - 1$ which this solution automatically satisfies. Transforming back to the original physical variables the conservation law which results is:

$$3a. \quad (D + a - 1)^2 = (a/1 - x^2)^2$$

since $/1 + 2\theta + \varphi^2 = \sqrt{(1 + U^+ + U^-)^2 - 4U^+U^-} = a/1 - x^2$. This simplifies to give

$$4a. \quad \frac{\sqrt{1 - x^2} - 1}{x} = \frac{D - 1}{2/U^+U^-}$$

as quoted previously [(3) in sect. 3.5a].

For the truncated problem (2b) integration using separation of variables leads to $\frac{1 + U^+}{U^+} \quad \frac{1 + U^-}{U^-} = \frac{1 + C}{C}$, so

5b. $U^- = \frac{1 + U^+}{U^+ - C} \cdot C \qquad U^+ = \frac{1 + U^-}{U^- - C} \cdot C$

or alternatively

$$x = \frac{2 \sqrt{U^+U^-}}{1 + U^+ + U^-} = \frac{2C}{\sqrt{U^+U^-}}$$ as quoted in the main text.

The constants C or D contain information about the boundary conditions, which in normal cases would be split between two locations e.g. $E^+(0)$ and $E^-(L)$. Thus we can only 'guess' at the constants, solve the propagation equations over all locations and then see whether a plot of the fields has the "input fields" that were wanted. We shall now show that the propagation equations permit an analytic implicit solution of much use in such a calculation.

For this purpose we find it most convenient to continue by using the transformed variables θ, φ since the propagation equation for θ takes the simple form (see 1a, b)

$$\frac{d\theta}{dz} = - \sigma \bar{n} \quad \varphi$$

where

6. EXACT $\quad \bar{n} = \frac{n_u}{\sqrt{1 + 2\theta + \varphi^2}}$

or

FLECK TRUNCATION $\quad \bar{n} = \frac{n_u}{(1 + \theta)(1 - \frac{1}{2} x^2)}$

Since $\varphi^2 = (D + \theta)^2 - (1 + 2\theta)$ in the EXACT case the terms involving φ may be removed, leaving

$$\frac{d\theta}{dz} = - \sigma n_u \frac{\sqrt{(D + \theta - 1)^2 + 2(D - 1)}}{D + \theta}$$

$$\Rightarrow \quad \sigma n_u \, dz = \frac{-u \; du}{\sqrt{(u-1)^2 + 2(D-1)}}$$

with $u = (D + \theta)$ and this is a standard integral with which the implicit solution may be completed. In terms of φ one has

$$\text{EXACT} \qquad -\sigma n_u z = \varphi + \cosh^{-1}\left[1 + \frac{\varphi^2}{2(1-D)}\right] + \text{const.}$$

However the algebra becomes more complicated than this in the other example for $\bar{n}$. We therefore treat the Fleck truncation case using U^+ (or E^+) as the dependent variable.

From 1a,

$$\frac{dU^+}{dz} = -\sigma(\bar{n}\, U^+ + n_1 \sqrt{U^+U^-})$$

$$= -\sigma n_u \left(U^+ - \frac{U^+U^-}{a}\right) / a(1 - \tfrac{1}{2}x^2)$$

which, using (5b) expressed as $U^+U^- = Ca$,

$$= -\sigma n_u (U^+ - C)/a(1 - \tfrac{1}{2}x^2)$$

Now we write the denominator in terms of U^+:

$$a(1 - \tfrac{1}{2}x^2) = a - \sqrt{U^+U^-}\; x$$
$$= a - 2C$$

$$= 1 + U^+ + \frac{1 + U^+}{U^+ - C}.C \quad - 2C$$

$$= \frac{U^{+2} + (1 - 2C)U^+ + 2C^2}{U^+ - C}$$

Hence we arrive at the second of eqns (4):

$$\text{FLECK TRUNCATION} \qquad \frac{dU^+}{dz} = -\sigma n_u \frac{(U^+ - C)^2}{U^{+2} + (1 - 2C)U^+ + 2C^2}$$

$$\Rightarrow \quad -\sigma n_u dz = \frac{dU^+}{(U^+ - C)^2}\,[(U^+ - C)^2 + U^+ + C^2]$$

$$\Rightarrow \quad -\sigma n_u\, z = U^+ + \left\{\log(U^+ - C) - \frac{C}{U^+ - C}\right\} - \frac{C^2}{U^+ - C} + \text{const}$$

A solution in this form, without explicit mention of U^-, has the advantage that for $C \to 0$ it is already in the form of the well known one-way absorber solution (Hercher's fast saturable absorber [86] - a similar amplifier result is discussed in textbooks [87]), shown below:

$$-\sigma n_u z = U^+ + \log(U^+) + \text{const.}$$

The companion equation for the exact treatment (also quoted in (3)) of $\bar{n}$ and n_1 is obtained in just the same way, except that when the denominator $(a/1 - x^2)$ has to be simplified one needs to know that (4a) with a lot of algebra becomes

$$U^- = \frac{\frac{D+1}{2} + U^+}{U^+ - \frac{1-D}{2}} \cdot \frac{(1-D)}{2}.$$ Thus the solution to the propagation equation is found to be:

(8) EXACT $$-\sigma n_u z = U^+ + \left\{\log(U^+ - d) - \frac{d}{U^+ - d}\right\} + \text{const.}$$

where the constant d replaces $D = 1 - 2d$. In calculations of this type we conclude that nothing is ever gained by employing the truncation: (7) is in fact slightly more complicated than (8)!

From the definition $x = \frac{2\sqrt{U^+U^-}}{1 + U^+ + U^-}$ it transpires that x has an upper bound of 1 when $U^+ \approx U^- \approx U$ both become large. From (4a) we find $1 - 2U < D < 1$. Hence $(U^+ - d)$ remains positive even in a very extreme case.

Appendix E Solution of a partial differential equation for the slow absorber case.

In the 1958 paper by COPSON [88] the solutions to a number of second order partial differential equations are reviewed. In particular,

$$U_a = P_{-\frac{1}{2}+\frac{1}{2}i}\left[1 - 2\frac{(1-r)(s-a)}{(1+rs)(1+a)}\right]$$

is shown to be a particular solution of the equation

$$\frac{\partial^2 U}{\partial r \partial s} = \frac{1}{2}\frac{U}{(1+rs)^2}$$

which may be obtained from section 3.5b with $U = H$, $r = \xi$ and $s = \tau - 1$. P_α is the Legendre function.

The solution U_a satisfies the conditions $U = 1$ when $r = 1$ or $s = a$ rather than the required boundary conditions which are:

$$H = 0 \text{ when } s=0 \quad ; \quad H = h(s) \text{ when } r=\xi_R$$

In order to obtain the desired solution for $H(r,s)$ at $r=1$ one uses the Riemann-Green formula [88,89] which provides the expression

$$H(1, s) = 1/2\ h(s) + 1/2 \int_0^s \left[U_a(\xi_R, s)h'(a) - h(a)\frac{\partial U_a}{\partial a}(\xi_R, s) \right] da \qquad (E1)$$

If the strong wave enters the absorber, of length L, from the left at r=1 and the weak wave enters from the right at $r = \xi_R = e^{-\sigma n_u L}$ then the formulae above express $H_{LEFT}(\tau)$ (= H(1,s)) in terms of $H_{RIGHT}(\tau)$ (= h(s)) and $dH_{RIGHT}/d\tau$ (= h'(s)).

We now calculate $H_{RIGHT}(\tau)$ for the problem of interest. From section 3.5b :

$$\frac{dH_{RIGHT}}{d\tau} = \underset{\tau}{G}_{RIGHT}(\tau) = \frac{n_u \gamma (E_0)^2}{[\tau (\tau + \frac{1}{\xi_R} - 1)]^{1/2}}$$

The weak wave at the right hand of the absorber has amplitude γE_0 whilst the strong wave at the left hand end has amplitude E_0 (where $\gamma << 1$).

Assuming γ to be time-independent and using H=0 (no grating) when $\tau = 1$, we obtain

$$H_{RIGHT} = 2 n_u \gamma (E_0)^2 \ln \left[\frac{\tau^{1/2} + (\tau + \frac{1}{\xi_R} - 1)^{1/2}}{1 + (\frac{1}{\xi_R})^{1/2}} \right]$$

We shall only evaluate (E1) to first order in $1/\Delta$, where $\xi_R = 1 - 1/\Delta$.

In this approximation one finds:

$$U_a(\xi_R) \approx 1 - \frac{(e^{-p} - e^{-q})}{2\Delta}$$

$$h' \approx n_u \gamma (E_0)^2 \left[e^{-q} - \frac{e^{-2q}}{2\Delta} \right]$$

$$\partial U_a/\partial a = e^{-q}\ \partial U_a/\partial q \approx -\frac{e^{-2q}}{2\Delta}$$

$$h(q) \approx n_u\ \gamma\ (E_0)^2 \left[q - \tfrac{1}{2\Delta}(1 - e^{-p}) \right]$$

where $p = \ln (s+1) = \ln (\tau)$ and $q = \ln (a+1)$ are introduced in order to simplify the algebra below.

Finally, using (E1)

$$H_{LEFT}(p) = 1/2\ \ h(p) + 1/2 \int_0^p \left[U_a\ h' - h \frac{\partial U}{\partial a} \right]\ e^q\ dq$$

$$= n_u\ \gamma\ (E_0)^2 \left[p - \tfrac{1}{2\Delta}\ p\ e^{-p} \right] + O(\tfrac{1}{\Delta^2}) \qquad (E2)$$

This simple result is used in chapter 3. It may be possible to simplify the integrand in the exact case using the Riemann P functions and transformations given in Abramowitz and Stegun [90](article 15.6).

More work is required to find out whether the exact approach is useful. We agree with Lax [79] that an analytic result offers the best way to test a general numerical solution. Our two-way absorber procedure in the model of colliding-pulse mode-locking (chapter 5) can be tested in principle using E1.

Appendix F Generalised equation for thick absorber.

Here we confirm that the simplification used in 3.5c, corresponding to a thin absorber, may be lifted without great complications.

Full inclusion of propagation effects means that $-\frac{\partial \epsilon^-}{\partial z}$ is replaced by $\left[2\,\frac{\eta}{c}\,\frac{\partial}{\partial t} - \frac{\partial}{\partial z}\right]\epsilon^-$ for the left side of equation (4) on page 74, but that the ϵ^+ equation is unchanged because z,t are to be taken now as the "local-time" transformed coordinates for the '+' direction of propagation.

Instead of the result in the main text we have:

$$(F1)\quad 2\,\frac{\eta}{c}\,\frac{\partial G}{\partial t} - \frac{\partial G}{\partial z} = n_u\left[-n_1\,\frac{\sigma}{2}\,(\epsilon^+)^2 + 2\,\frac{\eta}{c}\,\epsilon^-\,\frac{\partial \epsilon^+}{\partial t}\right]$$

where $G = n_u \epsilon^+ \epsilon^-$ as before, and (2) and (4) were used as modified above together with the rule for differentiation of a product.

From section 3.5b,

$$\frac{1}{\epsilon^+}\,\frac{\partial \epsilon^+}{\partial \tau} = \frac{1}{2}\left[\frac{1}{\tau} - \frac{\xi}{1 + \xi(\tau - 1)}\right] + \text{term in } \frac{dE_0}{d\tau}$$

and using $\frac{\partial}{\partial t} = 4\,\sigma\tau E_0^{\,2}\,\frac{\partial}{\partial \tau}$ results, after some simplification, in:

$$(F2)\quad n_u \epsilon^-\,\frac{\partial \epsilon^+}{\partial t} = 4\,\sigma\tau E_0^{\,2}\,.\,G\,.\,\frac{1}{2}\left[\frac{1}{\tau} - \frac{\xi}{1 + \xi(\tau - 1)}\right]$$

The equation which occurs for G is therefore

$$2\,\frac{\eta}{c}\left[4\,\sigma\,E_0^{\,2}\tau\,\frac{\partial G}{\partial \tau}\right] + \sigma n_u \xi\,\frac{\partial G}{\partial \xi} = \sigma n_u\,.\,\frac{1}{2}H\,\frac{\tau}{[1 + \xi(\tau - 1)^2]}$$
$$+ \frac{\eta}{c}\,4\sigma E_0^{\,2}\,.\,G\,.\left[1 - \frac{\xi\tau}{1 + \xi(\tau - 1)}\right]$$

It is certainly possible to eliminate G from this equation using the $\partial H/\partial \tau$ equation which is unchanged. The linear

p.d.e. in H which results is more complicated than that solved in appendix E, but it is possible that it can still be solved e.g. by the techniques in [89]. Without pursuing this further, it will simply be noted that an approximate solution to the equation in H could also be obtained without great difficulty.

Appendix G

Recursion formula for saturation by a square pulse

Here we use the general theory of chapter 4 to obtain results mentioned in section 4.4.

As $n_p = n_p^{slow} e^{-t/T_1} + F_p$, the known slow absorber recursion relation provides information about $e^{t/T_1}(n_p - F_p)$ in the present case.

Substituting in (6) for n_p^{slow} and dividing by e^{t/T_1} gives, for p = 1:

$$(G1)\quad (\bar{n} - F_0) - (n_2 - F_2) = \frac{-1}{4\sigma\epsilon^2 t}(n_1 - F_1)$$

In order to use this formula to obtain n_2 it is essential to eliminate F_2, whose evolution (eqn. 18) depends on the same n_2. This is achieved through the recursion relation found previously by integration of equation (17). We shall make use of the first two such relations, which are

$$(G2)\quad F_0 = n_u - \frac{n_u}{n(0)}\left[\bar{n} - F_0\right] - 8\sigma\epsilon^2 T_1 \left\{F_0 + F_1\right\}$$

$$(G3)\quad F_1 = - \frac{n_u}{n(0)}\left[n_1 - F_1\right] - 8\sigma\epsilon^2 T_1 \left\{F_1 + \frac{F_0 + F_2}{2}\right\}$$

These results are slightly more general than those in the main text since n(0) is not necessarily equal to n_u. Consequently they apply when an absorber is first saturated by ϵ^+ alone with no standing wave and subsequently by $\epsilon^+ = \epsilon^- = \epsilon$ together, as in the case of regions some distance away from the mirror at the end of a contacted absorber.

We rearrange (G1) to yield

$$n_2 = \bar{n} + (F_0 + 2F_1 + F_2) - 2(F_0 + F_1) + \frac{1}{4\sigma\epsilon^2}\left[\frac{n_1 - F_1}{t}\right]$$

Substituting for both the combinations of F from G2, G3 gives:

$$(G4)\quad n_2 = \bar{n} + \frac{1}{4\sigma\epsilon^2}\left[\frac{n_1 - F_1}{t} + \frac{(1 - n_u/n(0))\{(F_0 - \bar{n}) - (F_1 - n_1)\}}{T_1}\right.$$

$$\left. + \frac{\bar{n} - n_u - n_1}{T_1}\right]$$

For $n_u = n(0)$ this reduces to 19d as required. The presence of F_0 as well as F_1 in the second term can be overcome using G2. In the form given here it is easy to see that this term vanishes for the slow ($T_1 \to \infty$) and fast ($F_0 \to \bar{n}$, $F_1 \to n_1$) extremes; furthermore it is straightforward to monitor the evolution of both F_0 and F_1 using the result

$$\frac{dF_p}{dt} = \frac{n_u}{n(0)}(n_p - F_p)$$

which is the generalisation of (18).

Appendix H

An inductive proof of equation (15)

Applying an analogous description to (16) but covering the previous timestep we write

$$n_{p-r}(t-\Delta t) = \left\{ \sum_{s=-\infty}^{\infty} n_{p-r-s}(t-2\Delta t) \cdot \left[\frac{1}{n_u} C_s(t-\Delta t, t-2\Delta t) \right] \right\} \times$$

$$\times e^{-\Delta t/T_1} + \delta_{o(p-r)} n_u \frac{\Delta t}{T_1}$$

Using this result (16) itself becomes,

$$n_p(t) = \sum_{r=-\infty}^{\infty} \left[\sum_{s=-\infty}^{\infty} n_{p-r-s}(t-2\Delta t) \cdot \left\{ \frac{1}{n_u} C_s(t-\Delta t, t-2\Delta t) \right\} e^{-\Delta t/T_1} \right.$$

$$\left. + \delta_{o(p-r)} n_u \frac{\Delta t}{T_1} \right] \left[\frac{1}{n_u} C_r(t, t-\Delta t) e^{-\Delta t/T_1} \right] + \delta_{op} n_u \frac{\Delta t}{T_1}$$

$$= \left\{ \sum_{u=-\infty}^{\infty} n_{p-u}(t-2\Delta t) \cdot \left[\frac{1}{n_u} \sum_{r=-\infty}^{\infty} \frac{1}{n_u} C_{u-r}(t-\Delta t, t-2\Delta t) \times \right. \right.$$

$$\left. \left. \times C_r(t, t-\Delta t) \right] \right\} \cdot e^{\frac{-2\Delta t}{T_1}} + \delta_{op} n_u \frac{\Delta t}{T_1} + \frac{\Delta t}{T_1} e^{\frac{-\Delta t}{T_1}} C_p(t, t-\Delta t)$$

(having set $u = r + s$ and noting $\sum_{r=-\infty}^{\infty} \delta_{o(p-r)} C_r = C_p$)

$$= \left\{ \sum_{u=-\infty}^{\infty} n_{p-u}(t-2\Delta t) \cdot \left[\frac{1}{n_u} C_u(t, t-2\Delta t) \right] \right\} e^{-2\Delta t/T_1}$$

$$+ \delta_{op} n_u \frac{\Delta t}{T_1} + \frac{\Delta t}{T_1} C_p(t, t-\Delta t) e^{-\Delta t/T_1} \qquad \text{(H1)}$$

Comparing with (16) we note that the expressions are very similar (setting the step to $2\Delta t$) apart from the residue

$(\Delta t/T_1)\ C_p(t,t-\Delta t)e^{-\Delta t/T_1}$. This suggests that we will find that this process may be repeated in order to obtain the same form of result for $3\Delta t$ etc. with further extra terms of exactly the same type e.g. $(2\Delta t/T_1)\ C_p(t,t-2\Delta t)e^{-2\Delta t/T_1}$. The proof in this appendix will work for every case, so that by induction the following discrete version of (15) is generated:

$$(H2)\quad n_p(t) = \left\{ \sum_{r=-\infty}^{\infty} n_{p-r}\big|_0 \cdot \left[\frac{1}{n_u} C_r(t,0)\right]\right\} e^{-t/T_1}$$

$$+ \delta_{op} n_u \frac{\Delta t}{T_1} + \sum_{k=1}^{N-1} \frac{\Delta t}{T_1} C_p(t,t-k\Delta t)e^{-k\Delta t/T_1}$$

The first term is equivalent to the first term in the general result derived in the normal fashion in section 4.3. The second term vanishes in the limit $\Delta t \to 0$ ($N\Delta t$ = constant,t) and the residual sum in (H2) tends to the integral

$$\frac{1}{T_1} \int_0^t C_p(t,t'')e^{-(t-t'')/T_1}\, dt''$$

required in (15).

It is clear now that this integral accounts for the special behaviour of $\bar{n}$ during recovery ($p = 0$ in (16) picks out extra term involving n_u) and the consequent cumulative effects which feed through to the other grating components.

Appendix I Connection between net gain and Logarithmic slope profile.

As explained in section 2.8, the effects of net gain g(t) and the Fabry-Perot transmission must add together to produce a common slip throughout the reproduced pulse-profile which we refer to as the self-reproducing pulse.

If the self-reproducing pulse embarking on the round trip is denoted by $E(\tau)$ this is subsequently "processed" to become $E(\tau-\tau_{SHIFT})$ which requires:

$$g^{1/2}\ (1-R)\ \left\{E(\tau) + R\ E(\tau-t_M) + R^2E(\tau-2t_M) + \ldots\right\} = E(\tau-\tau_{SHIFT}) \qquad (I1)$$

where t_M is the mesh spacing. The etalon, as in section 2.3, has plate spacing $t_M/2$ and power reflectivity R for each plate.

The logarithmic slope, k, is now used to evaluate the field at times other than τ in terms of $E(\tau)$:

$$E(\tau-\epsilon) = E(\tau)\ e^{-(k/2)\ \epsilon} \qquad (I2)$$

Substituting I2 into I1, treating k and g as if they were time invariant we obtain the relation

$$g^{1/2}\ (1-R)\ \left[\frac{1}{1 - R\ e^{-kt_M/2}}\right] = e^{-k\tau_{SHIFT}/2}$$

This result was used to predict the graph of g versus $k\tau_{SHIFT}$ in section 2.8. (The range of calculation, the slip value $\tau_{SHIFT}/\ t_M$ and the value of R were all known.)

Near the peak of the pulse our approach fails, for it clearly predicts g=1. The formulae of section 2.5 give us an alternative approach if Haus' approximations are adopted. With some algebra one finds the following parabola for the coefficient G as a function of $k = d \ln|V^2| / dt$:

$$G = \left(\tfrac{1}{4}z\right)^2 \left(1 - 2\left[\frac{k}{k_\infty}\right]^2\right) + \left(\tfrac{1}{4}z\right)\left(\frac{\delta T}{t_F}\right)\left[\frac{k}{|k_\infty|}\right]$$

The exponential wings of Haus' solution have the logarithmic slopes $k = \pm |k_\infty|$ where k_∞ can be deduced from the sech pulse formula in section 2.5. It is not for the wings, but in the neighbourhood of the peak where the parabola now proves to be a useful tool. The gain at the peak of the pulse can be predicted, namely:

$$G(k=0) = \left(\tfrac{1}{4}z\right)^2 \qquad (I3)$$

This is the most direct way to fit the z parameter to the data in figure 5b. The net gains when $k_\pm = \pm|k_\infty| / \sqrt{2}$ satisfy :

$$G(k=k_\pm) = \pm \frac{z}{4\sqrt{2}} \frac{\delta T}{t_F}$$

This result may prove useful as an empirical definition for k_∞. The combined influences of gain (G), filter (t_F) and slip (δT) are all summarised in this approximate formula (exact for a sech pulse).

Appendix J Design of Pascal program PMLFINAL.

The Pascal modular diagram (figure J1) shows the overall structure of the colliding-pulse mode-locking simulation program PMLFINAL. Routines at any level in the diagram are accessible only to the next routine to the left, which is identified by the bracketing. For example the program PMLFINAL uses the three procedures TABULATE, RECONFIGURE and PML.

In this section we shall describe each routine shown in figure J1. (The advantage of the modular approach is that complexity is dealt with at the earliest design stages possible, with the result that the final coding is kept simple enough to be done very accurately at all the levels.)

The total length of the program is under five hundred lines, and there is scope for simplification of several procedures which will result in a compact and readable second version if required. It is inappropriate to document the program completely here, but it is hoped that the information which does follow provides insight.

Since STEP and FIRSTSTEP constitute the kernel of the computer model we shall describe them first. Their use is to compute one output sample of a pulse from an input sample, taking into account circulation of the laser cavity once.

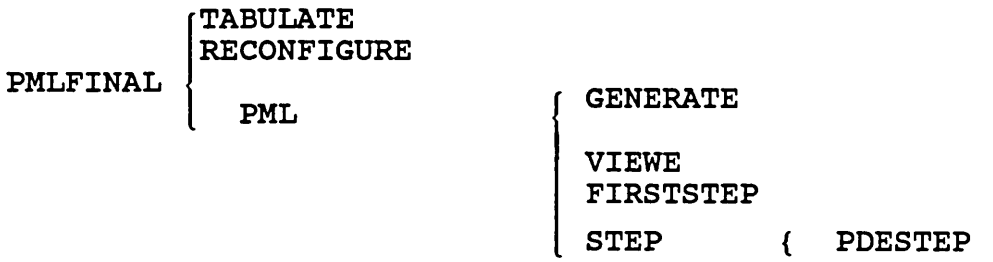

Figure J1 Modular program design.

EXPLANATION OF STEP:

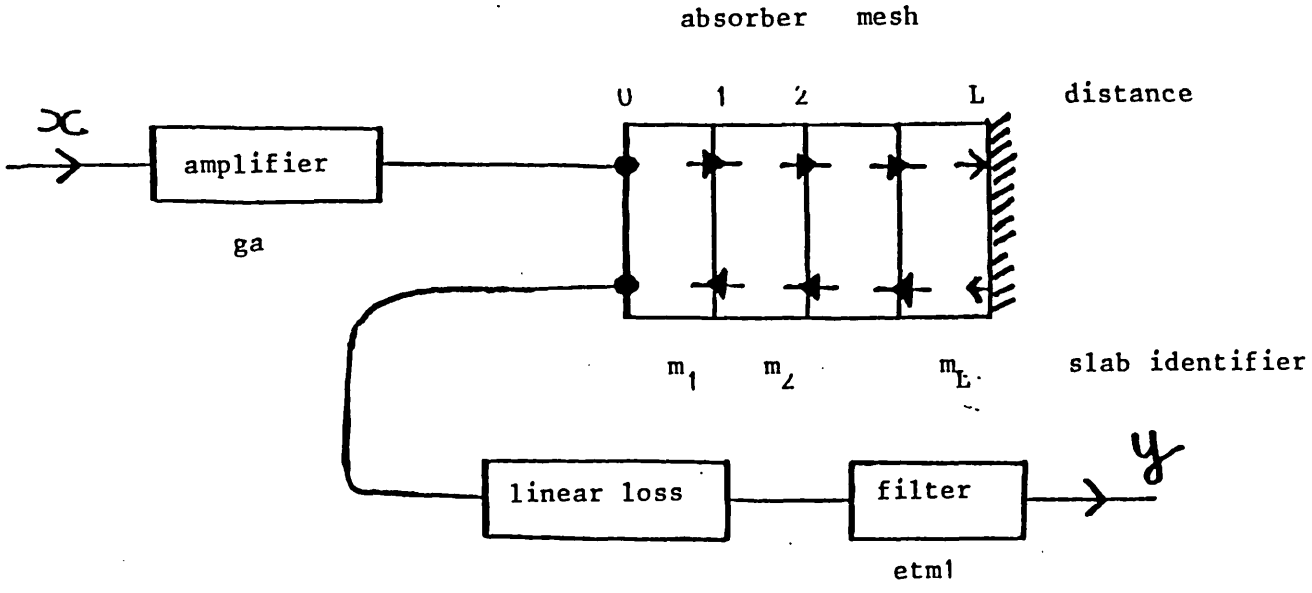

Figure J2 STEP procedure.

The figure above shows how the instruction STEP(y,x) would use an input field sample x and supply an output y.

The input boundary field in the absorber is called PL[0]. It is calculated by amplifying x, as follows:

```
PL[0] := /s * /ga * x ;
ga := ga * ( 1 - [ga-1] x^2/2 ) ;
```

Note that x is normalised so that saturation of ga takes this simple form. The s parameter, discussed in chapter 2, is needed in the (more saturable) absorber mesh.

It was decided to use the simplest possible first order scheme to carry out the step in the absorber. PDESTEP is responsible for the implementation of the required finite difference equations.

PDESTEP updates the fields stored in the absorber, PL[0] to PL[L] and MI[0] to MI[L] by using equations 7a and 7b of section 4.2. Then it updates the slab data m_1 to m_L which consist of the values of $\bar{n}$, $|n_1|$, $|b|$, $\cos(\theta-\Delta)$ and $\sin(\theta-\Delta)$ for which the evolution equations are also given in the same section. Note that the grating is not taken into account until $|b| > 0.01$, to avoid an attempt at division by zero in these equations.

Finally STEP is able to compute an output field y in terms of the field at the exit of the two-way absorber MI[0]. The linear loss and the filter operation are performed at this stage. The formulae governing this process are:

```
y := R * etm1 + T * /γ * MI[0] / /s ;
etm1 := y ;
```

where etm1 "remembers" the previous y, γ is the (intensity) loss factor and R,T are the Fabry-Perot etalon reflectance and transmission.

EXPLANATION OF FIRSTSTEP:

The FIRSTSTEP circulation "machinery" is the same as in figure J2, but the initialisation of ga, m_1 to m_L, etm1, PL[0] to PL[L] and MI[0] to MI[L] must take place before x comes in.

The gain (ga) is set with the recovery law for the depleted value at the end of the previous transit:

$$ga := \exp(\Xi * \ln(ga) + (1-\Xi) * A_u)$$

(This is equivalent to equation 6 in section 2.2, because the "bouncing ball" model represents our partial-cavity method exactly.)

The absorber slabs are given a complete recovery and do not saturate at all during FIRSTSTEP, but the fields in the

absorber mesh (and etml) still need to be provided. FIRSTSTEP looks at the leading edge logarithmic slope of the input pulse and sets up the required fields as if an exponential edge with that slope had been applied since $t = -\infty$. FIRSTSTEP also applies (prior to arrival of x) the leading portion of the pulse (E[0] to E[SL]) to figure J2, which means that most of the samples propagated into the absorber mesh do not depend on the extrapolation just mentioned. SL is a deliberate slip of the partial-cavity "window" to keep it centred on the pulse.

Only when E[SL] reaches the input "terminal" is y computed. The output formula is the same as in STEP.

EXPLANATION OF PML:

PML uses GENERATE to provide a starting pulse which is then subjected to a specified number of round trips of the cavity. Each such round trip involves calling FIRSTSTEP once and STEP repeatedly (when the "machinery" has been primed). The partial-cavity approach requires that FIRSTSTEP takes care of amplifier and (total) two-way absorber recovery at the start of every trip.

Because the local procedures used by PML are powerful, its main block is kept simple. It includes the slip-compensating feature mentioned in section 5.3, which is designed to keep the pulse near the centre of the calculation's "window".

A typical round trip (not the first) involves the code shown in figure J3. Notice the use of the steady state constraint to supply missing inputs necessary because of slip compensation (section 5.3).

```
THE PURPOSE OF THE FOLLOWING CODE IS TO UPDATE PARTIAL CAVITY  E[0]...E[SLIP]

begin

viewe( SLIP ) ;                                    { measure the pulse }


{ E[SLIP] goes round cavity first ; E[0] comes out] }
firststep( E[0], E[SLIP] ) ;

for m := ( SLIP + 1 ) to estop
  do step( E[M-SLIP], E[M] ) ;

slope := LN( fullGT ) / SLIP ;                     { steady state constraint }

for q := ( estop - SLIP + 1 ) to estop
  do step( E[q], Etrailing * EXP(-slope * ( SLIP + q - estop ) ) ) ;
{ E[estop] is last out }


Etrailing := E[estop]

end ;
```

fullGT is set by step(y, x) as the ratio y/x.

FIGURE J3 Pulse round-trip within the procedure PML.

EXPLANATIONS OF VIEWE, TABULATE, RECONFIGURE AND GENERATE:

These routines need little description. VIEWE records details of the pulse between round trips, such as energy and width. The slip (SL) of the peak of the pulse in the partial-cavity "window", required elsewhere in the program, is also measured. TABULATE is a routine which makes PML repeat automatically with changing laser parameter values (absorber length or Ξ for example) to explore trends in the model. RECONFIGURE allows the interactive user to change preset parameters and to control lineprinter graphics.

GENERATE provides the start pulse that evolves in PML for a specified number of round trips.